

Editorial corner – a personal view

Polymers are bound to save the world

*J. Seppälä**

Faculty of Chemistry and Materials Sciences, Department of Biotechnology and Chemical Technology,
Polymer Technology Research Group, Helsinki University of Technology, P.O. Box 6100, FI-02015 TKK, Finland

One of the hottest topics in today's polymer research is the research and development of biopolymers. Biopolymers can be based on renewable resources or synthetic raw materials. The term biopolymer covers not only biodegradable polymers that degrade in the environment (compost) but also bioresorbable polymers that are used in medical and pharmaceutical applications where they are eliminated by the body. Biopolymers used in medical applications are biocompatible and sometimes even bioactive, promoting cell proliferation on the polymeric scaffold material.

Increasing crude oil prices have boosted the search for sustainable material solutions. Important motivation in the search for novel biopolymers is the need to exploit renewable resources and labor force locally around the world, not only in the oil-rich countries.

In the biomedical sector, the polymers may offer giant leaps in the applications that benefit both patients and the entire society. Already today polymer/bioactive glass composites are in clinical use. In future, polymers for tissue engineering enable not only healing of traumas and tissue defects, but also cultivation of new tissue based on patients' own cells or stem cells. In this development the role of polymer based bioactive scaffolds is of highest importance.

Polymer based active agent release is another emerging sector in biomedical field. More precise, targeted and time-controlled drug or active agent delivery devices will revolutionize therapies of several diseases. First breakthroughs using either biostable or bioresorbable polymers in these areas already exist, and more is to come. Although the first truly bioactive polymers and composites are already in clinical studies, a new challenge is to meet all the demands in various sectors of clinical practices.

The above mentioned are some of the emerging areas where sophisticated level polymer science and its' advances are of key significance.

Polymers are bound to save the world!



Prof. Dr. Jukka Seppälä
Member of International Advisory Board

*Corresponding author, e-mail: jukka.seppala@tkk.fi
© BME-PT and GTE

Pharmaceutical significance of cellulose: A review

S. Kamel^{1,3*}, N. Ali¹, K. Jahangir¹, S. M. Shah¹, A. A. El-Gendy²

¹Pharmacy Department, University of Malakand, Chakdara, N.W.F.P., Pakistan

²Cellulose and Paper Department, National Research Center, Dokki, Cairo, Egypt

³Permanent address: Cellulose and Paper Department, National Research Center, El-Tahrir St., Dokki, Cairo, P.O. 12622, Egypt

Received 25 April 2008; accepted in revised form 16 July 2008

Abstract. The amalgamation of polymer and pharmaceutical sciences led to the introduction of polymer in the design and development of drug delivery systems. Polymeric delivery systems are mainly intended to achieve controlled or sustained drug delivery. Polysaccharides fabricated into hydrophilic matrices remain popular biomaterials for controlled-release dosage forms and the most abundant naturally occurring biopolymer is cellulose; so hydroxypropylmethyl cellulose, hydroxypropyl cellulose, microcrystalline cellulose and hydroxyethyl cellulose can be used for production of time controlled delivery systems. Additionally microcrystalline cellulose, sodium carboxymethyl cellulose, hydroxypropylmethyl cellulose, hydroxyethyl cellulose as well as hydroxypropyl cellulose are used to coat tablets. Cellulose acetate phthalate and hydroxymethyl cellulose phthalate are also used for enteric coating of tablets. Targeting of drugs to the colon following oral administration has also been accomplished by using polysaccharides such as hydroxypropylmethyl cellulose and hydroxypropyl cellulose in hydrated form; also they act as binders that swell when hydrated by gastric media and delay absorption. This paper assembles the current knowledge on the structure and chemistry of cellulose, and in the development of innovative cellulose esters and ethers for pharmaceuticals.

Keywords: *biopolymers, cellulose derivatives, drug delivery*

1. Introduction

For many years pharmacists have been employing polymers in every aspect of their work; polystyrene vials, rubber closures, rubber and plastic tubing for injection sets, and polyvinylchloride flexible bags to hold blood and intravenous solutions are all examples of such polymers. The initial use was often restricted to packaging rather than drug delivery. Subsequently, the amalgamation of polymer and pharmaceutical sciences led to the introduction of polymer in the design and development of drug delivery systems.

1.1. Drug delivery

Drug delivery is highly innovative in terms of materials to assist delivery, excipients, and technology which allow fast or slow release of drugs. For example analgesics, which often involve as much as five or six tablets a day, can be reduced to a single dose by using appropriate excipients, based on carbohydrate polymers. Polymers are classified in several ways; the simplest classification used for pharmaceutical purposes is into natural and synthetic polymers.

Polysaccharides, natural polymers, fabricated into hydrophilic matrices remain popular biomaterials for controlled-release dosage forms and uses of a hydrophilic polymer matrix is one of the most pop-

*Corresponding author, e-mail: samirki@yahoo.com
© BME-PT and GTE

ular approaches in formulating an extended-release dosage forms [1–3]. This is due to the fact that these formulations are relatively flexible and a well designed system usually gives reproducible release profiles.

Since drug release is the process by which a drug leaves a drug product and is subjected to absorption, distribution, metabolism, and excretion (ADME), eventually becoming available for pharmacologic action, hence drug release is described in several ways as follows:

- a) Immediate release refers to the instantaneous availability of drug for absorption or pharmacologic action in which drug products allow drugs to dissolve with no intention of delaying or prolonging dissolution or absorption of the drug.
- b) Modified-release dosage forms include both delayed and extended-release drug products. Delayed release is defined as the release of a drug at a time other than immediately following administration, while extended release products are formulated to make the drug available over an extended period after administration.
- c) Controlled release includes extended-release and pulsatile-release products. Pulsatile release involves the release of finite amounts (or pulses) of drug at distinct intervals that are programmed into the drug product.

One of the most commonly used methods of modulating tablet drug release is to include it in a matrix system. The classification of matrix systems is based on matrix structure, release kinetics, controlled release properties (diffusion, erosion, swelling), and the chemical nature and properties of employed materials. Matrix systems are usually classified in three main groups: hydrophilic, inert, and lipidic [4]. In addition, the drug release is a function of many factors, including the chemical nature of the membrane, geometry and its thickness, and the particle surface area of the drug device, the physico-chemical nature of the active substance and the interaction between the membrane and the permeating fluids are also important [5–7]. In fact, the mechanism probably varies from membrane to membrane, depending on the membrane structure as well as on the nature of the permeating solution. It is believed that several different mechanisms are involved in the drug release through a non-disintegrating polymer coat [8]:

- a) Permeation through water-filled pores; in this mechanistic model, the release of the drug involves transfer of the dissolved molecule through water-filled pores. The coating membrane is not homogeneous. The pores can be created by the incorporation of leachable components, such as sugars or incompatible water-soluble polymers into the original coating material [9] or can be produced by an appropriate production process.
- b) Permeation through membrane material; in this mechanism, the release process involves the consecutive process of drug partition between the core formulation and the membrane. The drug molecules are dissolved in the membrane at the inner face of the coat, representing equilibrium between a saturated drug solution and the membrane material. The transport of drug across the coat is then driven by the concentration gradient in the membrane. Outside the membrane, the drug is dissolved in an aqueous environment.
- c) Osmotic pumping; this release mechanism is driven by a difference in osmotic pressure between the drug solution and the environment outside the formulation.

In addition to the above, controlled release of drug from the matrix is dependent on particle size and type of the polymer wetting, polymer hydration, polymer dissolution, and drug: polymer ratio [10–13]. The hydration rate depends on the nature of the constituents, such as the molecular structure and the degree of substitution. The viscosity of the aqueous solution can be increased by increasing the average molecular weight of the polymer, the concentration of the polymer or decreasing the temperature of the solution [1, 14]. So, the factors associated with polymers, such as molecular weight type (nominal viscosity), concentration, degree of substitution, and particle size [15–22]; have been shown to have a significant influence on drug release. For example, in tablet formulations containing hydrophilic polymers like HPMC, the release of active drug is controlled by the rate of formation of a partially hydrated gel layer of the tablet surface formed upon contact with aqueous gastric media following ingestion and the continuous formation of additional gel layers. In addition to this, process variables like method of granulation, amount of binder added during granulation,

use of high or low shear mixer, granule size distribution, compression force during tableting, etc., are also important for extended-release [23–33].

1.2. Cellulose and cellulotics

Cellulose is the most abundant naturally occurring biopolymer [34, 35]. Various natural fibers such as cotton and higher plants have cellulose as their main constituent [36, 37]. It consists of long chains of anhydro-D-glucopyranose units (AGU) with each cellulose molecule having three hydroxyl groups per AGU, with the exception of the terminal ends (Figure 1). Cellulose is insoluble in water and most common solvents [35]; the poor solubility is attributed primarily to the strong intramolecular and intermolecular hydrogen bonding between the individual chains [34]. In spite of its poor solubility characteristics, cellulose is used in a wide range of applications including composites, netting, upholstery, coatings, packing, paper, etc. Chemical modification of cellulose is performed to improve process ability and to produce cellulose derivatives (cellulotics) which can be tailored for specific industrial applications [38]. Cellulotics are in general strong, reproducible, recyclable and biocompatible [39], being used in various biomedical applications such as blood purification membranes and the like. Thus, through derivatization, cellu-

losics have opened a window of opportunity and have broadened the use of cellulotics.

As shown in the molecular structure represented in Figure 1, the hydroxy groups of β -1,4-glucan cellulose are placed at positions C₂ and C₃ (secondary, equatorial) as well as C₆ (primary). The CH₂OH side group is arranged in a trans-gauche (*t_g*) position relative to the O₅–C₅ and C₄–C₅ bonds. As a result of the supramolecular structure of cellulose, the solid state is represented by areas of both high order (crystalline) and low order (amorphous). The degree of crystallinity (DP) of cellulose (usually in the range of 40 to 60%) covers a wide range and depends on the origin and pretreatment of the sample (Table 1). The morphology of cellulose has a profound effect on its reactivity, the hydroxyl groups located in the amorphous regions are highly accessible and react readily, whereas those in crystalline regions with close packing and strong inter-chain bonding can be completely inaccessible [40]. Cellulose that is produced by plants is referred to as native cellulose, which is found in two crystalline forms, cellulose I and cellulose II [41]. Cellulose II, generally occurring in marine algae, is a crystalline form that is formed when cellulose I is treated with aqueous sodium hydroxide [42–44]. Among the four different crystalline polymorphs cellulose I, II, III, and IV, cellulose I is thermodynamically less stable while cellulose II is the most

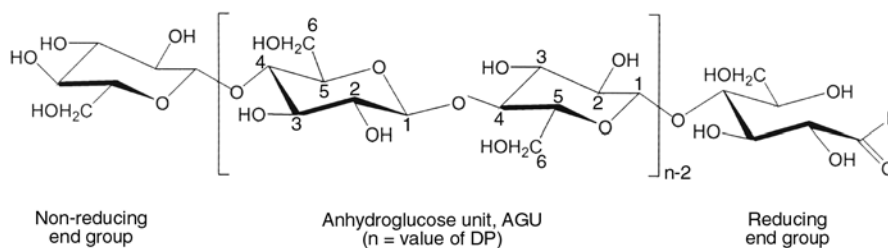


Figure 1. Molecular structure of cellulose

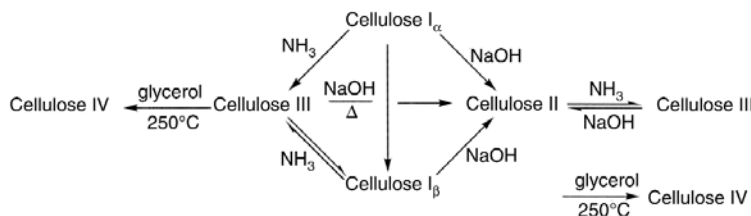


Figure 2. Transformation of cellulose into its various polymorphs

Table 1. Average DP of cellulose obtained from different sources. (Reprinted from reference [39].)

Source	Wood	Valonia	Cotton	Acetobacter xylinum	Cotton linters	Flax	Pulp	Kapok	Ramie
*DP _w (10 ³)	8–9	25–27	8–15	2–6	1–5	7–8	2.1	9.5	9–11

*DP_w weight average DP determined by viscometric methods

stable structure. A liquid ammonia treatment of cellulose I and cellulose II gives crystalline cellulose III form [45-47], and the heating of cellulose III generates cellulose IV crystalline form [48]. Figure 2 shows the transformation of cellulose into its various polymorphs [49].

2. Chemical modification of cellulose

The typical modifications of cellulose are esterifications and etherifications at the hydroxyl groups of cellulose. Most water-soluble and organic solvent-soluble cellulose derivatives are prepared by these substitution reactions, and drastic changes in the original properties of cellulose can usually be achieved by these chemical modifications. Others are ionic and radical grafting, acetalation, deoxyhalogenation, and oxidation. Figure 3 shows schematic representation of position in cellulose structure for chemical modifications [38].

2.1. Oxidation

Oxidized celluloses (or oxycelluloses) are water insoluble materials produced by reacting cellulose

with an oxidant such as gaseous chlorine, hydrogen peroxide, peracetic acid, chlorine dioxide, nitrogen dioxide (dinitrogen tetraoxide), persulfates, permanganate, dichromate-sulfuric acid, hypochlorous acid, hypohalites or periodates. These oxidized celluloses may contain carboxylic, aldehyde, and/or ketone functionalities, in addition to the hydroxyl groups, depending on the nature of the oxidant and the reaction conditions used in their preparation [50].

It is well known that primary alcohol groups of cellulose are partly converted to carboxyl ones by oxidation with N_2O_4 in chloroform. Recently a new water-soluble reagent, 2,2,6,6-tetramethylpiperidine-1-oxyl radical (TEMP) can oxidize primary alcohol groups of water soluble polysaccharides such as starch to carboxyl ones with good yields and selectivity in the presences of an oxidizing agent at pH 9–11 [51]. The TEMPO-NaBr-NaClO system was first applied to native cellulose by Chang and Robyt [52] but did not give water-soluble cello-uronic acid. By oxidation of cellulose under various condition and using regenerated and mercerized celluloses as starting materials, small amounts of carboxyl groups were introduced into

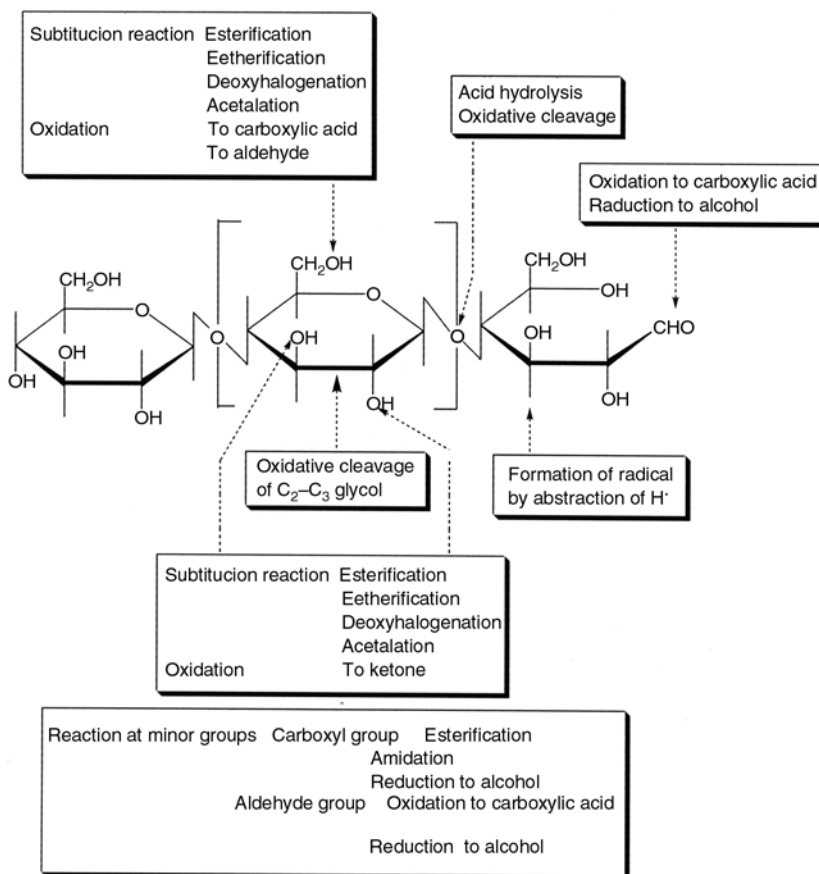


Figure 3. Position in cellulose structure for chemical modifications

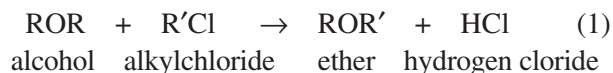
cellulose by this oxidation and water soluble cello-urionic acid sodium salts were obtained [53]. On the other hand, the periodate oxidation is used to prepare dialdehyde cellulose at laboratory levels which proceeded homogeneously in the aqueous solution, and almost completely oxidized dialdehyde cellulose was obtained within 20 h [54]. This dialdehyde cellulose can be oxidized to the corresponding dicarboxyl cellulose with sodium chlorite, or reduced to the corresponding dialcohol cellulose with sodium borohydride [55, 56].

2.2. Microcrystallization

Purified microcrystalline cellulose is partially depolymerized cellulose prepared by treating α -cellulose, obtained as a pulp from fibrous plant material, with mineral acids. The degree of polymerization is typically less than 400. Traditionally, MCC has been prepared from bamboo [57, 58], wood pulp [59], viscose rayon [60] and cotton [61]. Attempts have also been made to produce MCC from other sources such as newsprint waste [62], hosiery waste [63], and corncobs [64], as well as from fast-growing plants including sesbania sesban, sroxburghii, crotalaria juncea [65], bagasse, rice straw, as well as cotton stalks bleached pulps [66]. When cellulose reacts with acid, the $\beta(1-4)$ glycoside bond is attacked and the acetal linkage is broken resulting in the hydrolysis of the chain, thus the degree of polymerization decreases [67]. On the other hand, oxidizing agents have an impacting effect on the cellulose chain and the hydroxyl groups react to form carbonyl and carboxyl groups. So, the oxidation reaction of cellulose shortens the average length of the cellulose chain and using of HNO_3 or N_2O_4 , each of which transfer cellulose into MCC with carboxyl groups [68].

2.3. Etherification

The presence of hydroxyl groups readily suggested to chemists that cellulose might be converted to useful derivatives by etherification. This reaction is expressed by the Equation (1):



where R' is an organic radical such as the methyl (CH_3-), ethyl (C_2H_5-), or a more complex structure. The alcohol, ROH, represents one of the three OH groups in an AGU. Cellulose ethers can be prepared by treating alkali cellulose with a number of various reagents including alkyl or aryl halides (or sulfates), alkene oxides, and unsaturated compounds activated by electron-attracting groups. For example methyl and ethylcellulose ethers can be prepared by the action of methyl and ethyl chlorides or methyl and ethyl sulfates, respectively, on cellulose that has been treated with alkali. Purification is accomplished by washing the reaction product with hot water. The degree of methylation or ethylation can be controlled to yield products that vary in their viscosities when they are in solution. If mixed ether such as ethylhydroxyethyl cellulose is to be produced, the two reagents, ethyl chloride and ethylene oxide, can be added either consecutively or as a mixture. The nature of the resultant product is dependent upon the molar ratio of the two etherifying agents (the ratio of the number of molecules of one to the other) and on the method of their addition. Table 2 provides a list of some typical reagents, co-products, and by-products.

On the other hand, cellulose ethers of moderate to high molecular weight are insoluble in water. As a rule, as the DS increases, the polymers gradually pass through a stage of solubility in dilute alkali

Table 2. Etherifying agents, co-products, and by-products from the production of cellulose ethers

Cellulose ether	Etherifying agent	Co-product	By-product	
			Name	Formula
Methyl (MC)	methyl chloride	NaCl	methanol dimethyl ether	CH_3OH CH_3OCH_3
Ethyl (EC)	ethyl chloride	NaCl	ethanol diethyl ether	$\text{C}_2\text{H}_5\text{OH}$ $\text{C}_2\text{H}_5\text{OC}_2\text{H}_5$
Hydroxyethyl (HEC)	ethylene oxide	none	ethylene glycol and polymers thereof	$\text{CH}_2\text{OHCH}_2\text{OH}$
Hydroxypropyl (HPC)	propylene oxide	none	propylene glycol and polymers thereof	$\text{CH}_3\text{CH}_2\text{OHCH}_2\text{OH}$
Carboxymethyl (CMC)	chloroacetic acid	NaCl	glycolic acid	$\text{HO}-\text{CH}_2-\text{COOH}$

Table 3. Solubility of cellulose ether (organic solvent is a mixture of chloroform or methylene chloride and methanol or ethanol)

Cellulose ether	DS	Solubility
MC	0.1–1.1	soluble in 6–8% NaOH
	1.4–2.0	soluble in H ₂ O
	2.4–2.8	soluble in organic solvents
EC	0.8–1.7	soluble in H ₂ O
	2.4–2.8	soluble in organic solvents
NaCMC	0.1–3.0	soluble in H ₂ O
CMC	0.05–0.25	soluble in 6–8% NaOH
HEC	0.11–0.31	soluble in 6–8% NaOH
	0.66–1.66	soluble in H ₂ O
HPC	0.15–0.35	soluble in 6–8% NaOH
	3.5–4.5	soluble in H ₂ O
EHEC [70]	0.68 (ethyl) and 0.87 (hydroxyethyl)	soluble in H ₂ O
	1.9–2.2 (ethyl) and 0.35–0.65 (hydroxyethyl)	soluble in organic solvents
	1.33 (ethyl) and 0.51 (hydroxyethyl)	soluble in both H ₂ O and organic solvents

(those with a DS of up to about 1.0), then through a water soluble stage (about DS 1.0–2.3), and finally attain an organic-solvent-soluble stage (DS 2.3–3.0) such DS ranges are, of course, only approximate. Also, the trend toward organic solvent solubility is gradual and differs for individual ethers. The ionic character of CMC, for example, makes its behavior exceptional. Moreover, the uniformity of substitution along the cellulose chain can have a major influence on solubility [69]. Solubility of some typical cellulose ether is summarized in Table 3. The ranges of DS cited in these examples are only approximate because solubility is influenced by the distribution of molecular weights of various fractions in a given product and by the extent and uniformity of substitution within particular products or molecular weight fractions. The water-soluble cellulose ethers should not be regarded simply as water-soluble forms of cellulose. The ethers are derivatives of cellulose, containing only a fraction of the original cellulose structure in their molecular make-up [70].

2.4. Esterification

The esterification can be considered as a typical equilibrium reaction in which an alcohol and acid react to form ester and water. Cellulose is esterified with certain acids such as acetic acid, nitric acid, sulfuric acid, and phosphoric acid. A prerequisite is that the acid used can bring about a strong swelling thus penetrating throughout the cellulose structure. Esterification of cellulose to give cellulose trinitrate was discovered by Schonbein in 1846 using a

mixture of sulfuric and nitric acids. The resultant compound was so flammable that its first use was as smokeless gunpowder. By the end of the nineteenth century, cellulose nitrates had been prepared with a lower DS, and they could safely be used for other purposes. All cellulose nitrates are prepared by Schonbein's method, in which aqueous slurry of cellulose is reacted with nitric acid in the presence of sulfuric acid. The reaction is in equilibrium and thus the removal of water during the reaction forces the reaction to completion and the relative concentrations of the reacting species determine the ultimate DS [71].

The discovery that cellulose esters could be prepared with organic substituents led to the development of cellulose derivatives that had decreased flammability compared to that of cellulose nitrate. The most important organic ester is cellulose acetate which prepared by the reaction of acetic anhydride with cellulose in the presence of sulfuric acid. Acetic acid is used as the solvent and the reaction is carried out for about 8 h to yield the triester (defined as having a DS greater than 2.75). The derivatives with lower DS values are obtained by the hydrolysis of the triester by hydrochloric acid to yield the desired substitution.

3. Pharmaceutical uses of cellulose and cellulose derivatives

3.1. Oxycellulose

Oxidized cellulose (oxycellulose) is cellulose in which some of the terminal primary alcohol groups of the glucose residues have been converted to car-

boxyl groups. Therefore, the product is possibly a synthetic polyanhydrocellobiuronide and that contain 25% carboxyl groups are too brittle (friable) and too readily soluble to be of use. Those products that have lower carboxyl contents are the most desirable.

The oxidized cellulose fabric, such as gauze or cotton, resembles the parent substance; it is insoluble in water and acids but soluble in dilute alkalis. In weakly alkaline solutions, it swells and becomes translucent and gelatinous. When wet with blood, it becomes slightly sticky and swells, forming a dark brown gelatinous mass. So, it is used in various surgical procedures, by direct application to the oozing surface except when used for homeostasis, it is not recommended as a surface dressing for open wounds [72].

The oxidized cellulose product readily disperses in water and forms thixotropic dispersions. Such suspensions/dispersions, which may be optionally combined with other pharmaceutical and cosmetic adjuvants, can be used for producing novel film-forming systems. A wide variety of solid (crystalline or amorphous) and liquid (volatile or non-volatile) acidic, neutral, and basic bioactive compounds can be entrapped/loaded in such systems, thereby producing substantive controlled and/or sustained release formulations, having unique applications in the development of variety of cosmetic, pharmaceutical, agricultural, and consumer products. Topical formulations (cream, lotion, or spray) prepared using the oxidized cellulose material, are bioadhesive, can be applied on the human skin or hair, can be included in cosmetics [73]. Oxidized cellulose dispersion uses in anti-acne cream, anti-acne lotion, sunscreen spray, anti-fungal cream also.

For using oxidized cellulose as a direct compression excipient Banker and Kumar grounded it and prepared tablets by mixing the ingredients by ratio of 20, 79 and 1% for oxidized cellulose, lactose NF (Fast-Flo), magnesium stearate respectively, each tablet weighed 500 ± 10 mg. The hardness, the disintegration times and water penetration rate were 5.17 kg, 30 sec and 10.49 mg/sec respectively [73].

3.2. Microcrystalline cellulose

Since its introduction in the 1960s, MCC has offered great advantages in the formulation of solid

dosage forms, but some characteristics have limited its application, such as relatively low bulk density, moderate flowability, loss of compactibility after wet granulation, and sensitivity to lubricants. Silicification of MCC improves the functionality of MCC with such properties as enhanced density, low moisture content, flowability, lubricity, larger particle size, compactibility and compressibility. Silicified MCC (SMCC) is manufactured by co-drying a suspension of MCC particles and colloidal silicon dioxide such that the dried finished product contains 2% colloidal silicon dioxide [74]. Silicon dioxide simply adheres to the surface of MCC and occurs mainly on the surface of MCC particles; only a small amount was detected in the internal regions of the particles. So, SMCC shows higher bulk density than the common types of MCC [75]. Also, tensile strength of compacts of SMCC is greater than that of the respective MCC [76] and it is most probably a consequence of intersurface interactions of silicon dioxide and MCC [77].

Tableting studies have suggested that SMCC has enhanced compactibility, even after wet granulation, and reduced lubricant sensitivity, compared to the regular grade of MCC.

For example, Sherwood and Becker [78] have compared the direct-compression tableting performance of SMCC 90 with a regular grade of MCC (Avicel PH102) that has similar particle size and density. They found that, SMCC 90 was 10–40% more compactable than regular MCC in the absence of drug. The SMCC 90 also showed a lower lubricant sensitivity and retained, two to three times the compactibility in tableting of the comparable MCC grade in a blending time study. Also, Guo and Augsburg compared SMCC's performance to that of other excipients commonly used in hard gelatin capsule direct-fill formulations such as anhydrous lactose (direct tableting grade), pregelatinized starch (PGS), and MCC. The study revealed that SMCC exhibited relatively higher compactibility under the low compression force of a donator capsule filling than either PGS or lactose. Products formulated with the SMCC materials exhibited faster dissolution rates than those formulated with PGS and anhydrous lactose when loaded with 5% piroxicam, 30 and 50% acetaminophen. Such higher compactibility and fast dissolution rates suggest that SMCC could be a suitable alternative excipient for direct- fill formulations for hard shell

capsules [79]. In another study, comparison of the compaction force versus tablet tensile strength showed that SMCC was approximately 20% more compactible than regular MCC. Stronger tablets manufactured from SMCC were easier to coat further also, the size and weight of individual tablets were decreased, which increases patients' compliance [80]. SMCC possesses further advantages, decreasing the hygroscopicity of the active ingredient (increased stability of tablets). Due to a decreased size, higher compressibility, and better flow properties (lower sensitivity to the rate of tableting); a larger number of tablets in one batch can be achieved, which makes their manufacture substantially cheaper [81].

In contrast to routinely used SMCC, the high-density degree showed further improvement in flow properties and lesser sensitivity to the rate of tableting. Muzíková and Nováková compare the tensile strength and disintegration time of compacts from two types of SMCC, Prosolv SMCC 90, and Prosolv HD 90 high density SMCC [82]. The used lubricants were magnesium stearate and sodium stearyl fumarate in a concentration of 0.5%, while ascorbic acid and acetylsalicylic acid in a concentration of 50% were used as active ingredients. They found that; SMCC proved to be better compatible than high density SMCC; the compacts were of higher strength, which was markedly increased with increasing compression force. High density SMCC was more sensitive to additions of lubricants, and a greater decrease in strength was recorded due to the influence of sodium stearyl fumarate. The disintegration time of compacts from high density SMCC without as well as with lubricants was shorter than that of those from SMCC and was increasing with increasing compression force.

3.3. Cellulose ether

Cellulose ethers are widely used as important excipients for designing matrix tablets. On contact with water, the cellulose ethers start to swell and the hydrogel layer starts to grow around the dry core of the tablet. The hydrogel presents a diffusional barrier for water molecules penetrating into the polymer matrix and the drug molecules being released [83–87].

3.3.1. Sodium carboxymethyl cellulose

It is a low-cost commercial soluble and polyanionic polysaccharide derivative of cellulose that has been employed in medicine, as an emulsifying agent in pharmaceuticals, and in cosmetics [88]. The many important functions provided by this polymer make it a preferred thickener, suspending aid, stabilizer, binder, and film-former in a wide variety of uses. A representative listing of the many applications for NaCMC is given below in Table 4 [89].

In biomedicine it has been employed for preventing postsurgical soft tissue and epidural scar adhesions. Sanino *et al.* have proposed the use of CMC and HEC-based gels as water absorbents in treating edemas [90]. It can also be used for the therapeutic application of the superoxide dismutase enzyme (SOD), presented as hydrogels of CMC carrying the enzyme for its controlled release [91]. Therapeutic use of SOD enzyme is limited by its fast clearance from the bloodstream and inactivation by its own reaction product, i.e. hydrogen peroxide. The SOD enzyme was adsorbed into the hydrogel for its controlled release, rendering two formulations: SOD-CMC conjugates and SOD-CMC hydrogels [92]. Both formulations were chemically and biologically characterized, the resulting showed that up to 50% of the SOD was released from the

Table 4. Applications for NaCMC

Specific applications	Properties utilized
Ointments, creams, lotions	emulsion, stabilizer, thickener, film-former
Jellies, salves	thickener, gelling agent, protective colloid, film-former
Tablet binder, granulation aid	high-strength binder
Sustained release	thickener, diffusion barrier
Tablet coating	film-former
Bulk laxatives	physiologically inert, high water-binding capacity
Syrups, suspensions	thickener, suspending aid
Toothpaste	thickener, flavor stabilizer, suspending aid, binder
Shampoos, foamed products	suspending aid, thickener, foam stabilizer, high water-binding capacity
Denture adhesives	wet tack, long-lasting adhesion

SOD-CMC hydrogel after 72 h, indicating a controlled release kinetic [93].

In a double-blind trial in patients suffering from Sjogren's syndrome, a CMC-containing substitute and a glycerine mouthwash used as a control were tested. Nocturnal oral discomfort was the only symptom which was relieved more by the CMC-containing substitute [94]. And in comparing the lubricating properties of two saliva substitutes, one containing mucin and the other CMC both showed almost the same objective effects, with changed friction values of about 15 min which was more than twice as long as for water. Both water and the two saliva substitutes relieved the symptoms of dry mouth to some extent but they did not have a sufficiently long lasting effect [95].

Also, NaCMC can be used in preparation of semi-interpenetrating polymer network microspheres by using glutaraldehyde as a crosslinker. Ketorolac tromethamine, an anti-inflammatory and analgesic agent, was successfully encapsulated into these microspheres and drug encapsulation of up to 67% was achieved. The diffusion coefficients decreased with increasing crosslinking as well as increasing content of NaCMC in the matrix and in vitro release studies indicated a dependence of release rate on both the extent of crosslinking and the amount of NaCMC used to produce microspheres [96]. Another nonsteroidal anti-inflammatory agent indomethacin, has a short biological half-life of 2.6–11.2 h [97], the usual oral dosage for adults is 25 or 50 mg, 2 to 3 times a day. Controlled release preparations of this drug are to increase patient compliance and to reduce adverse effects, fluctuation in plasma concentration and dosing frequency. Waree and Garnpimol prepared a complex of chitosan and CMC and crosslinked by glutaraldehyde to control the release of indomethacin from microcapsule [98]. The membrane of microcapsules was formed by electrostatic interaction between positive charged amine on the chitosan chain and the negative charged hydroxyl group on the CMC chain, the concentration of CMC affect on the formability of chitosan-CMC microcapsules [99]. Glutaraldehyde reacted with hydroxyl group in CMC chain to form acetal and reacted with amino group in chitosan to form Schiff base. The crosslinking provided dense and rigid surface of microcapsule and reduced the degree of swelling and the rate of drug release microcapsule. In the

drug release study, the mechanism of drug release was prominently diffusion controlled through wall membrane and pore. The release of drug from microcapsule could be governed by optimizing the pH of chitosan solution, the hardening time and the glutaraldehyde content [100–103].

Esterification of NaCMC with acryloyl chloride improves the swelling properties such as the degree of swelling of the esterified product changes as the pH is varied. At pH 9.4 the swelling % is quite high compared to that at pH 1.4 and 5.4 so; it can be used as a pH responsive polymer for various biomedical applications. Since this polymer swells at high pH and collapses at low pH values so; this polymer can be used in oral delivery, in which the polymer will retard drug release at low pH values in the stomach while releasing the same at high pH values in the small intestine [104]. Hence this polymer can be used for pH-sensitive drug delivery system like aspirin, indomethacin, diclofenac etc. in the intestine and as a wound dressing material [105].

3.3.2. Methylcellulose

MC resembles cotton in appearance and is neutral, odorless, tasteless, and inert. It swells in water and reproduces a clear to opalescent, viscous, colloidal solution and it is insoluble in most of the common organic solvents. However, aqueous solutions of MC can be diluted with ethanol. MC solutions are stable over a wide range of pH (2 to 12) with no apparent change in viscosity. They can be used as bulk laxatives, so it can be used to treat constipation, and in nose drops, ophthalmic preparations, burn preparations ointments, and like preparations. Although MC when used as a bulk laxative takes up water quite uniformly, tablets of MC have caused fecal impaction and intestinal obstruction [72]. As we mention before; it dissolves in cold water but higher DS-values result in lower solubility, because the polar hydroxyl groups are masked so; the expected questions are, how drug works and how it is given? MC absorbs water, which expands in the intestines, when eaten MC is not absorbed by the intestines but passes through the digestive tract undisturbed. It attracts large amounts of water into the colon, producing a softer and bulkier stool so; it is used to treat constipation, diverticulosis, hemorrhoids and irritable bowel syndrome. It should be taken with sufficient amounts of fluid to prevent

dehydration. The common side effect is nausea and the less common side effects are vomiting and cramp [106].

On the other hand, solid dispersion, in which compounds are dispersed into water-soluble carriers, has been generally used to improve the dissolution properties and the bioavailability of drugs that are poorly soluble in water [107–111]. MC has the hydroxyl group in a structure and is interactive with the carboxylic acid of carboxyvinyl polymer (CP), as well as poly(ethylene oxide) (PEO). Ozeki *et al.* examined the controlled release of antipyretic phenacetin (PHE) from solid dispersion by the formation of an interpolymer complex between MC and CP. They found that, the rate of PHE release from the solid dispersion granules was lower than from the PHE powder. The PHE release profiles from the solid dispersion granules varied depending on the MC/CP ratio, and the rate of release was the lowest at a MC/CP ratio of 50:50. Also the rate of PHE release decreased as the molecular weight of MC increased. By studying the effect of the molecular weight of MC on the time required to release half of PHE (T_{50}). The T_{50} of the MC-CP solid dispersion increased as the molecular weight of the MC increased, and it essentially leveled off when the molecular weight of MC was 180 000 (Figure 4). So, from this study it is feasible to control the release of PHE from MC-CP polymer solid dispersion granules by modulating complex formation between MC and CP, which can be accomplished by altering the MC/CP ratio and the molecular weight of MC [112].

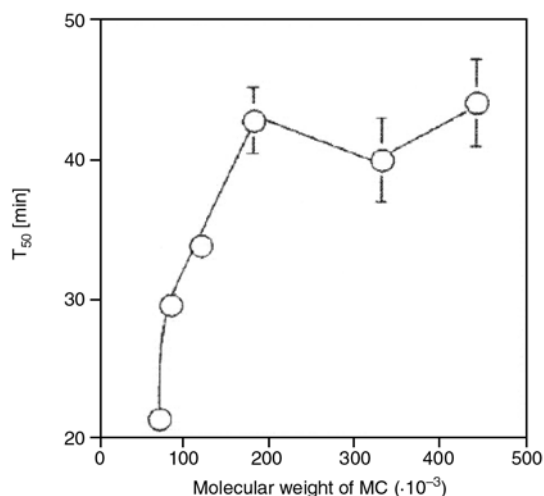


Figure 4. T_{50} for PHE release from MC-CP solid dispersion using various molecular weights of MC

3.3.3. Ethylcellulose

It is the non-ionic, pH insensitive cellulose ether and insoluble in water but soluble in many polar organic solvents. It is used as;

- A non-swelling, insoluble component in matrix or coating systems.
- When water-soluble binders cannot be used in dosage processing because of water sensitivity of the active ingredient, EC is often chosen.
- It can be used to coat one or more active ingredients of a tablet to prevent them from reacting with other materials or with one another.
- It can prevent discoloration of easily oxidizable substances such as ascorbic acid.
- Allowing granulations for easily compressed tablets and other dosage forms.
- It can also be used on its own or in combination with water-soluble polymers to prepare sustained release film coatings that are frequently used for the coating of micro-particles, pellets and tablets.

In addition to EC, HEC is also non-ionic water-soluble cellulose ether, easily dispersed in cold or hot water to give solutions of varying viscosities and desired properties, yet it is insoluble in organic solvents. It is used as a modified release tablet matrix, a film former and a thickener, stabilizer and suspending agent for oral and topical applications when a non-ionic material is desired. Many researchers like Mura *et al.* [113] Friedman and Golomb [114] Soskolne *et al.* [115] have demonstrated the ability of EC to sustain the release of drugs.

3.3.4. Hydroxypropyl cellulose

It is non-ionic water-soluble and pH insensitive cellulose ether. It can be used as thickening agent, tablet binding, modified release and film coating. By using solid dispersions containing a polymer blend, such as HPC and EC, it is possible to precisely control the rate of release of an extremely water soluble drug, such as oxprenolol hydrochloride [116–120] In this case, the water-soluble HPC swells in water and is trapped in the water-insoluble EC so that the release of the drug is slowed. These studies have shown that there is a linear relationship between the rate of release of the water insoluble drug and its interaction with the polymer [121–123]. On the other hand, Buccal delivery formulations containing HPC and polyacrylic acid



Figure 5. Treatment of a 12-year-old male patient with the bioadhesive tablet. (a) 7 mm diameter aphthous lesion on the mucosal membrane. (b) 15 minutes after placement of tablet onto the canker sore. (c) After 36 h.

have been in use for many years [124–128], with various ratios of the two polymers. Whereas mucoadhesive delivery systems have been reported for several different drugs [129–131], there have been only a few reports about their use in the treatment of oral mucosal disorders such as canker sores. Adhesive tablets were prepared by compression molding of mixed powders of crosslinked polyacrylic acid and HPC, absorbed with citrus oil and magnesium salt. Tablets adhere well to the mucosal tissue and gradually erode for 8 h releasing the citrus oil whereas the magnesium is released during a period of 2 h. Both experimental and plain tablets were effective in reducing pain and decreasing healing time without adverse side effects, and the tablets loaded with active agents were more effective [132]. Figure 5 shows a male who had recurrent aphthous stomatitis, with a 7 mm diameter canker sore in the left lip before, during, and after treatment with the mucoadhesive tablet.

To obtain a new biocompatible polymeric materials of high molecular weight with a range of hydrophilic and swelling properties, as well as chemical and mechanical ones [133] hydroxypropyl methacrylate was grafted onto hydroxypropyl starch and HPC by Ce(IV) redox initiation method and crosslinked by different amounts of ethyleneglycol dimethacrylate. The graft copolymers can be considered of great interest as direct compression excipients due to their different chemical structure and composition; they showed differences in viscoelastic properties that revealed an interesting range of possibilities for use in drug delivery for-

mulations [134]. Although no crosslinked polymer was suitable as a direct compression excipient, rheological studies suggested that the use of this kind of graft copolymer in a formulation could improve the controlled release properties. Furthermore, non-crosslinked graft copolymers of hydroxypropyl methacrylate on both hydroxypropyl starch and HPC offer interesting characteristics as controlled release matrices. Gon *et al.* observed that when excipients were added, performance (compressional and tablet parameters and dissolution tests) of the tablets was negatively affected. Therefore, graft copolymers can stand alone as an effective matrix for tablets designed for drug delivery systems [135].

3.3.5. Hydroxypropyl methyl cellulose

HPMC is water soluble cellulose ether and it can be used as hydrophilic polymer for the preparation of controlled release tablets. Water penetrates the matrix and hydrating the polymer chains which eventually disentangle from the matrix. Since it is generally recognized that drug release from HPMC matrices follows two mechanisms, drug diffusion through the swelling gel layer and release by matrix erosion of the swollen layer [136–139], therefore, quantifying the percent contribution of diffusion and erosion to the overall drug release is important. Several authors [140–142] have attempted to model the erosion mechanism of swellable polymeric matrices. Reynolds *et al.* found that; drug release resulting from polymer erosion was linear versus

time and was found to be a function of the number average molecular weight of the polymer (HPMC). In contrast, by comparing the diffusional release rates of HPMC of different molecular weight, they found that, they were independent of number average molecular weight of the polymers studied. The erosion study indicated that polymer diffusion of the HPMC polymer chains through the aqueous diffusion layer was the rate-limiting step for polymer erosion and in general polymer erosion was found to be inversely related to the polymer number average molecular weight [143]. In addition, surface area/volume is one of the key variables in controlling drug release from HPMC matrix tablets. It can be utilized to duplicate drug release profiles for tablets having different sizes, shapes, and dose levels. Tablets having the same surface area but different surface area/volume values did not result in similar drug release; tablets with larger surface area/volume values had faster release profiles [144].

Another variable in controlling drug release is the viscosity of HPMC. Ifat Katzhendler *et al.* studied the effect of molecular weight of HPMC on the mechanism of drug release of naproxen sodium (NS) and naproxen (N) [145]. The study showed that matrices composed of various viscosity grades of HPMC are characterized by similar microviscosity values in spite of the difference in their molecular weight. pH measurements revealed that incorporation of N to HPMC matrix led to lower internal pH value inside the hydrated tablet compared with NS. This behavior led to lower solubility of N which dictates its surface erosion mechanism, compared with NS matrix that was characterized by higher internal pH value and higher drug solubility. These properties of HPMC/NS increased chain hydration and stability, and led to drug release by the diffusion mechanism.

Also there have been many studies demonstrating that the drug release profile from a hydrophilic matrix tablet is influenced by the viscosity of the gel layer formed due to its polymer hydration [146, 147]. However, little work has been done to study the influence of lot-to-lot apparent viscosity difference on in vitro dissolution. Also, not much has been done to compare the effect of using a single grade of HPMC versus a mixture of two different grades of HPMC on drug release [148]. The current apparent viscosity range specification for HPMC

given by the manufacturer is 11,250–21,000 cps [149] and two lots of this polymer may differ widely from each other in terms of apparent viscosity. Khanvilkar *et al.* studied the effects of a mixture of two different grades of HPMC and apparent viscosity on drug release profiles of extended-release matrix tablets. The study showed that lower and higher viscosity grades of HPMC can be mixed uniformly in definite proportions to get the desired apparent viscosity. Incorporating a low viscosity grade of HPMC in the formulation would lead to a significantly shorter t_{lag} (*lag time, the time taken by the matrix tablet edges to get hydrated and achieve a state of quasi equilibrium before erosion and the advance of solvent front through the matrix occur*) however, it imposes minimal impact on the overall dissolution profile. Also the drug release from an HPMC matrix tablet prepared by dry blend and direct compression approach is independent of tablet hardness, is diffusion-controlled, and depends mostly on the viscosity of the gel layer formed [150]. Moreover by studying the distribution of HPMC within the tablet matrix Ye *et al.* found that manufacturing process has a significant impact in determining the dissolution characteristics of HPMC matrix tablets. When HPMC matrix tablets were prepared by wet-granulation approach, the tablet hardness, distribution of HPMC within the tablet (intergranular and intragranular), and the amount of water added in the wet granulation step all have a significant impact on dissolution. By incorporating partial amount of HPMC intergranularly in the dry-blend step, drug-release profiles could be made much less sensitive to the manufacturing process [151]. Liu *et al.* used alginate as the gelling agent in combination with HPMC which acted as a viscosity-enhancing agent in release of gatifloxacin. The rheological behaviors were not affected by the incorporation of gatifloxacin. Both in vitro release and in vivo pre-corneal retention studies indicated that the alginate/HPMC solution retained the drug better than the alginate or HPMC solutions alone. These results demonstrate that the alginate/HPMC mixture can be used as an in situ gelling vehicle to enhance ocular bioavailability and patient compliance [152].

Owing to the hydration and gel forming properties of HPMC, it can be used to prolong the release of active compound like yahom, yahom is a well-known traditional remedy/medicine for treatment

of nausea, vomiting, flatulent and unconscious in Thailand [153]. The yahom buccal tablet had antimicrobial activities that could be able to cure the oral microbial infection and aid the wound healing but the addition of polyvinyl pyrrolidone (PVP) combined with HPMC could promote the bioadhesive of yahom tablet [154]. Chantana *et al.* found that, the disintegration time of tablet was longer as the amount of polymer was increased or the higher amount of HPMC was enhanced, while the water sorption and erosion of tablet containing yahom: polymer mixture 50:50, which the polymer mixture containing PVP: HPMC 1:2 was lower than that of tablet containing these polymers at ratio of 1:1 and 2:1 respectively. This indicated that PVP had the higher water sorption and erosion, whereas HPMC could prolong the erosion of tablet. So, the tablet containing yahom 50%, that had the polymer mixture of PVP: HPMC 1:2 was suitable to use as the buccal tablet since it had the low water sorption and erosion [155]. On the other hand, the combination of two or more excipients is frequently used in drug formulation to improve the tableting and release properties of the materials. In addition to the cellulose derivatives, crosslinked high amylose starch (CLA), has been successfully used as a controlled release excipient for the preparation of solid dosage forms [156]. Rahmouni *et al.* characterized the gel matrix properties of binary mixtures of CLA/HPMC, and evaluated the effect of incorporated HPMC on the release kinetics of three model drugs of different solubilities such as pseudoephedrine sulfate (very soluble), sodium diclofenac (sparingly soluble), and prednisone (very slightly soluble) [157]. Swelling characteristics and erosion of granulated crosslinked high amylose starch (CLAgr)/HPMC tablets were found to increase with HPMC concentration and incubation time. The equilibrium swelling and weight loss of CLAgr tablets were reached after 6 h, whereas HPMC tablets continued to swell and erode even after 24 h. HPMC is known to hydrate more rapidly than CLA, and forms a gel layer upon contact with aqueous medium. When the gel layer is sufficiently hydrated, the polymeric network begins to disintegrate and dissolve in the medium, resulting in matrix weight loss. Since CLA is a natural polysaccharide derivative, which does not much differ from HPMC, the same mechanism of hydration and erosion is expected for

CLA matrices. However, in this case, extensive swelling is restrained by the physical crosslinks, which limit tablet expansion and disintegration, the limited erosion observed with CLA tablets is probably related to the release of non-crosslinked amylose chains. The drug release experiments revealed that, in the absence of α -amylase, both pseudoephedrine and sodium diclofenac were released more rapidly from CLAgr, CLAgr/HPMC and granulated CLA/HPMC tablets than HPMC matrices. Release of pseudoephedrine and sodium diclofenac was completed in approximately 12 and 22 h, respectively, whereas only 30–35% prednisone was released after 24 h and all three drugs were probably released mainly by diffusion. The addition of α -amylase to the dissolution medium increased substantially the release rate. It has been demonstrated that α -amylase degrades CLA tablets into water-soluble degradation products, resulting in surface tablet erosion which enhances the release kinetics of poorly water soluble drugs [158, 159]. Introducing HPMC into CLA tablets at a concentration of 10% may reduce the enzymatic hydrolysis by slowing down the diffusion of the enzyme in the substrate. However, this decrease in release rate was less significant for highly water soluble drugs, such as pseudoephedrine, which rapidly diffuses out of the matrix. So, swelling and erosion of the matrices increased with HPMC content and incubation time. In addition CLA formed stronger gels than HPMC or CLA/HPMC mixture and the presence of HPMC in CLA tablets at concentration 10% protected CLA against α -amylase hydrolysis and reduced the release rate of poorly and moderately water-soluble drugs. The release of the highly water soluble model drug was rapid both in the presence or absence of HPMC, and occurred mainly by diffusion.

In another study the effect of the concentration of HPMC on naproxen release rate was studied, the dissolution results showed that an increased amount of HPMC resulted in reduced drug release. The inclusion of buffers to increase the dissolution and to decrease the gastric irritation of weak acid drugs, such as naproxen in the HPMC matrix tablets enhanced naproxen release. Naproxen is a weak acid, so it is more soluble in alkaline media. The inclusion of sodium bicarbonate and calcium carbonate in the HPMC matrix improved the

naproxen dissolution; however, including sodium citrate did not produce any effect on naproxen dissolution [160].

The drug release for extended duration, particularly for highly water-soluble drugs, using a hydrophilic matrix system is restricted due to rapid diffusion of the dissolved drug through the hydrophilic gel network. For such drugs with high water solubility, hydrophobic polymers (waxes) are suitable as matrix forming agents for developing sustained-release dosage forms [161]. Hydrophobic polymers provide several advantages, ranging from good stability at varying pH values and moisture levels to well-established safe applications. Tramadol, which is a synthetic opioid of the aminocyclohexanol group, is freely soluble in water and hence judicious selection of release retarding excipients is necessary to achieve a constant *in vivo* input rate of the drug [162]. Sandip *et al.* studied the effect of concentration of hydrophilic (HPMC) and hydrophobic polymers (hydrogenated castor oil [HCO] and EC) on the release rate of tramadol [163]. The results showed that hydrophobic matrix tablets resulted in sustained *in vitro* drug release (>20 h) as compared with hydrophilic matrix tablets (<14 h). Figure 6 depicts the effect of HPMC on the tramadol release from hydrophilic matrices. Increasing the concentration of HPMC in the matrix did not alter the drug release profile significantly. Figure 7 shows the effect of EC on tramadol release

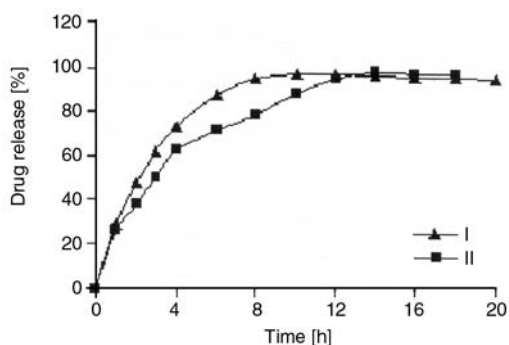


Figure 6. Effect of HPMC on tramadol release from hydrophilic matrix system prepared by wet granulation as per Table 5

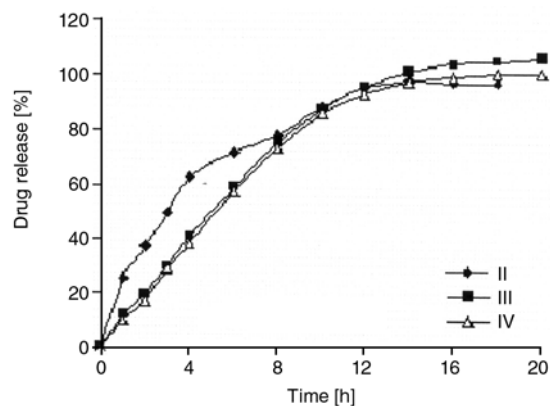


Figure 7. Effect of EC on tramadol release from hydrophilic matrix system prepared by wet granulation as per Table 5

from hydrophilic matrix system. The tablets formulations as in Table 5.

In another study the release kinetic profiles of naproxen (NP) from microcapsule compressed as well as matrix tablets using a combination of water insoluble materials (like bees wax (BW), cetyl alcohol (CA) and stearic acid (SA)) with hydrophilic polymers was investigated. The EC/HPMC combinations, contributing an increase in hydrophilic part of blend system rationally increased the release rate, kinetic constant and diffusion co-efficient thereby whereas HPMC/BW, HPMC/CA and HPMC/SA combinations, contributing an increase in hydrophobic part of the blend system caused a substantial reduction of release [164].

Also, Vueba *et al.* studied the influence of cellulose ether derivatives on ibuprofen release from matrix tablets formulations containing mixtures of polymers with both low and high viscosity grades MC or HPC, and HPMC, respectively were prepared by a direct compression method using 20, 25, and 30% of either MC or HPC [165]. The results obtained in this study illustrated that both low and high viscosity grade cellulose ether polymers can be mixed uniformly, in different proportions, in order to produce matrices with modulated drug release properties. On the other hand, the swelling experiments showed that the water uptake increases until the

Table 5. Tramadol HCl 200 mg tablet formulations

Excipients	mg/Tablet							
	I	II	III	IV	VI	VII	VIII	IX
Hydrogenated castor oil	0	0	0	0	200	200	200	200
Ethylcellulose	0	0	10	20	0	5	10	20
HPMC K100	150	200	110	110	0	0	0	0
PVP K 90	10	10	10	10	0	0	0	0

low viscosity polymer content reaches 25%. At higher concentrations, the swelling behavior changes drastically, suggesting a gradual degradation of the matrices and the dissolution of ibuprofen from mixtures of MC/HPMC or HPC/HPMC matrices was found to be more effective when either the MC or HPC content was increased.

3.4. Cellulose esters

Cellulose acetate phthalate is a partial acetate ester of cellulose that has been reacted with phthalic anhydride. One carboxyl of the phthalic acid is esterified with the cellulose acetate. The finished product contains about 20% acetyl groups and about 35% phthalyl groups. In the acid form, it is soluble in organic solvents and insoluble in water. The salt formed is readily soluble in water. This combination of properties makes it useful in enteric coating of tablets because it is resistant to the acid condition of the stomach but soluble in the more alkaline environment of the intestinal tract [72].

4. Conclusions

Chemical modification of cellulose is performed to produce cellulose derivatives (cellulosics) which are in general strong, low cost, reproducible, recyclable and biocompatible, so they can be tailored for pharmaceutical applications.

Cellulose derivatives are often used to modify the release of drugs in tablet and capsule formulations and also as tablet binding, thickening and rheology control agents, for film formation, water retention, improving adhesive strength, for suspending and emulsifying.

MCC is used as diluent and disintegrating agent for release oral solid dosage. HEC and HPC are used in hydrophilic matrix systems, while EC can be used in hydrophobic matrix system. Also, liquid and semi-solid pharmaceutical dosage forms are important physicochemical systems for medical treatment which require rheological control and stabilizing excipients as essential additives, CMC can be used to adjust the viscosity of syrups.

References

- [1] Alderman D. A. A.: Review of cellulose ethers in hydrophilic matrices for oral controlled-release dosage forms. *International Journal of Pharmaceutical Technology and Product Manufacture*, **5**, 1–9 (1984).
- [2] Heller J.: Use of polymers in controlled release of active agents. in 'Controlled Drug Delivery. Fundamentals and Applications' (eds.: Robinson J. R., Lee V. H. L.) Marcel Dekker, New York, 179–212 (1987).
- [3] Longer M. A., Robinson J. R.: Sustained-release drug delivery systems. in 'Remington's Pharmaceutical Sciences' (Ed.: Remington J. P.) Mack Publishing, Easton, 1676–1693 (1990).
- [4] Sandip B. T., Ali R.: Extended-release oral drug delivery technologies: monolithic matrix systems. *Methods of Molecular Biology*, **437**, 217–243 (2008).
- [5] Liu J., Lin S., Li L., Liu E.: Releases of theophylline from polymer blend hydrogels. *International Journal of Pharmaceutics*, **298**, 117–125 (2005).
- [6] Prokop A., Kozlov E., Carlesso G., Davidson J. M.: Hydrogel-based colloidal polymeric system for protein and drug delivery: physical and chemical characterization, permeability control and applications. *Advances in Polymer Science*, **160**, 119–173 (2002).
- [7] Zaikov G. E., Iordanskii A. P., Markin V. S.: Diffusion of electrolytes in polymers. VSP Science Press, Utrecht (1988).
- [8] George S. C., Thomas S.: Transport phenomena through polymeric system. *Progress in Polymer Science*, **26**, 985–1017 (2001).
- [9] Lindholm T., Juslin M.: Controlled release tablets 3: Ethylcellulose coats containing surfactant and powdered matter. *Pharmaceutical Industry*, **44**, 937–941 (1982).
- [10] Rodriguez C. F., Bruneau N., Barra J., Alfonso D., Doelker E.: Hydrophilic cellulose derivatives as drug delivery carriers: Influence of substitution type on the properties of compressed matrix tablets. in 'Handbook of Pharmaceutical Controlled Release Technology' (ed.: Wise D. L.) Marcel Dekker, New York, 1–30 (2000).
- [11] Lapidus H., Lord N. G.: Drug release from compressed hydrophilic matrices. *Journal of Pharmaceutical Sciences*, **57**, 1292–1301 (1968).
- [12] Bettini R., Colombo P., Massimo G., Catellani P. L., Vitali T.: Swelling and drug release in hydrogel matrices: Polymer viscosity and matrix porosity effects. *The European Journal of Pharmaceutical Sciences*, **2**, 213–219 (1994).
- [13] Campos-Aldrete M. E., Villafuerte-Robles L.: Influence of the viscosity grade and the particle size of HPMC on metronidazole release from matrix tablets. *European Journal of Pharmaceutics and Biopharmaceutics*, **43**, 173–178 (1997).

- [14] Amaral H. M., Lobo S. J. M., Ferreira D. C.: Effect of hydroxypropyl methylcellulose and hydrogenated castor oil on naproxen release from sustained-release tablets. *AAPS Pharmaceutical Science Technology*, **2**, 14–21 (2001).
- [15] Ford J. L., Rubinstein M. H., Hogan J. E.: Formulation of sustained release promethazine hydrochloride tablets using hydroxypropyl methylcellulose matrices. *International Journal of Pharmaceutics*, **24**, 327–338 (1985).
- [16] Cheong L. W. S., Heng P. W. S., Wong L. F.: Relationship between polymer viscosity and drug release from a matrix system. *Pharmaceutical Research*, **9**, 1510–1514 (1992).
- [17] Tahara K., Yamamoto K., Nishihata T.: Overall mechanism behind matrix sustained release (SR) tablets prepared with hydroxypropyl methylcellulose. *Journal of Controlled Release*, **35**, 59–66 (1995).
- [18] Krögel I., Bodmeier R.: Development of a multifunctional matrix drug delivery system surrounded by an impermeable cylinder. *Journal of Controlled Release*, **61**, 43–50 (1999).
- [19] Shah N., Zhang G., Apelian V., Zeng F., Infield M. H., Malick A. W.: Prediction of drug release from hydroxypropyl methylcellulose (HPMC) matrices: Effect of polymer concentration. *Pharmaceutical Research*, **10**, 1693–1695 (1993).
- [20] Xu G., Sunada H.: Influence of formulation change on drug release kinetics from hydroxypropyl methylcellulose matrix tablets. *Chemical and Pharmaceutical Bulletin*, **43**, 483–487 (1995).
- [21] Velasco M. V., Ford J. L., Rowe P., Rajabi-Siahboomi A. R.: Influence of drug: Hydroxypropyl methylcellulose ratio, drug and polymer particle size and compression force on the release of diclofenac sodium from HPMC tablets. *Journal of Controlled Release*, **57**, 75–85 (1999).
- [22] Mitchell K., Ford J. L., Armstrong D. J., Elliot P. N. C., Hogan J. E., Rostron C.: The influence of substitution type on the performance of methyl cellulose and hydroxypropyl methylcellulose in gels and matrices. *European Journal of Pharmaceutics and Biopharmaceutics*, **100**, 143–154 (1993).
- [23] Sheskey P. J., Williams D. M.: Comparison of low-shear and high-shear wet granulation techniques and the influence of percent water addition in the preparation of a controlled-release matrix tablet containing HPMC and a highdose, highly water-soluble drug. *Pharmaceutical Technology*, **20**, 81–92 (1996).
- [24] Bettini R., Colombo P., Massimo G., Catellani P. L., Vitali T.: Swelling and drug release in hydrogel matrices: Polymer viscosity and matrix porosity effects. *The European Journal of Pharmaceutical Sciences*, **2**, 213–219 (1994).
- [25] Ford J. L., Rubinstein M. H., Hogan J. E.: Formulation of sustained release promethazine hydrochloride tablets using hydroxypropyl methylcellulose matrices. *International Journal of Pharmaceutics*, **24**, 327–338 (1985).
- [26] Selkirk A. B., Ganderton D.: The influence of wet and dry granulation methods on the pore structure of lactose tablets. *Journal of Pharmaceutical and Pharmacology*, **22**, 86S–94S (1970).
- [27] Huber H. E., Christenson G. L.: Utilisation of hydrophilic gums for the control of drug substance release from tablet formulations II. Influence of tablet hardness and density on dissolution behavior. *Journal of Pharmaceutical Sciences*, **57**, 164–166 (1968).
- [28] Genc L., Bilac H., Güler E.: Studies on controlled release dimenhydrinate from matrix tablet formulations. *Pharmaceutical Acta Helvetiae*, **74**, 43–49 (1999).
- [29] Chalmers A. A., Elworthy P. H.: Oxytetracycline tablet formulations: The influence of excipients and the method of granulation. *Journal of Pharmaceutical and Pharmacology*, **28**, 234–238 (1976).
- [30] Chowhan Z. T., Yang I-C.: Effect of intergranular versus intragranular corn starch on tablet friability and in vitro dissolution. *Journal of Pharmaceutical Sciences*, **72**, 983–988 (1983).
- [31] Khattab I., Menon A., Sakr A.: Effect of mode of incorporation of disintegrants on the characteristics of fluid-bed wet-granulated tablets. *Journal of Pharmaceutical and Pharmacology*, **45**, 687–691 (1993).
- [32] Li J. Z., Rekhi G. S., Augsburg L. L., Shangraw R. F.: The role of intra- and extragranular microcrystalline cellulose in tablet dissolution. *Pharmaceutical Development and Technology*, **1**, 343–355 (1996).
- [33] Zhang Y. E., Tchao R., Schwartz J. B.: Effect of processing methods and heat treatment on the formation of wax matrix tablets for sustained drug release. *Pharmaceutical Development and Technology*, **6**, 131–144 (2001).
- [34] Hinterstoisser B., Salmen L.: Application of dynamic 2D FTIR to cellulose. *Vibrational Spectroscopy*, **22**, 111–118 (2000).
- [35] Bocek A. M.: Effect of hydrogen bonding on cellulose solubility in aqueous and nonaqueous solvents. *Russian Journal of Applied Chemistry*, **76**, 1711–1719 (2003).
- [36] Myasoedova V. V.: Physical chemistry of non-aqueous solutions of cellulose and its derivatives. John Wiley and Sons, Chirchester (2000).
- [37] Gross R. A., Scholz C.: Biopolymers from polysaccharides and agropoteins. American Chemical Society, Washington (2000).
- [38] Akira I.: Chemical modification of cellulose. in ‘Wood and Cellulosic Chemistry’ (eds.: Hon D. N-S., Shiraishi N.) Marcel Dekker, New York, 599–626 (2001).
- [39] Conner A. H.: Size exclusion chromatography of cellulose and cellulose derivatives. in ‘Handbook of Size Exclusion Chromatography’ (ed.: Wu C-S.) Marcel Dekker, New York, 331–352 (1995).
- [40] Sjöstrom E.: Wood chemistry, fundamentals and applications. Academic Press, New York (1993).

- [41] Kuga S., Brown R. M. Jr.: Silver labeling of the reducing ends of bacterial cellulose. *Carbohydrate Research*, **180**, 345–350 (1988).
- [42] Saxena I. M., Bown R. M.: Cellulose biosynthesis: Current views and evolving concepts. *Annals of Botany*, **96**, 9–21 (2005).
- [43] Kolpak F. J., Blackwell J.: Determination of the structure of cellulose II. *Macromolecules*, **9**, 273–278 (1976).
- [44] Langan P., Nishiyama Y., Chanzy H.: A revised structure and hydrogen-bonding system in cellulose II. From a neutron fiber diffraction analysis. *Journal of American Chemical Society*, **121**, 9940–9946 (1999).
- [45] Wada M., Heux L., Isogai A., Nishiyama Y., Chanzy H., Sugiyama J.: Improved structural data of cellulose III_I prepared in supercritical ammonia. *Macromolecules*, **34**, 1237–1243 (2001).
- [46] Sarko A., Southwick J., Hayashi J.: Packing analysis of carbohydrates and polysaccharides. 7. crystal structure of cellulose III_I and its relationship to other cellulose polymorphs. *Macromolecules*, **9**, 857–863 (1976).
- [47] Chanzy H., Vincendon M., Henrissat B., Tanner S. F., Belton P. S.: Solid state ¹³C-NMR and electron microscopy study on the reversible transformation cellulose I-cellulose III_I in Valonia. *Carbohydrate Research*, **160**, 1–11 (1987).
- [48] Buleon A., Chanzy H.: Single crystals of cellulose IV_{II}. Preparation and properties. *Journal of Polymer Science: Polymer Physics Edition*, **18**, 1209–1217 (1980).
- [49] Klemm D., Heublein B., Fink H-P. Bonn A.: Cellulose: Fascinating biopolymer and sustainable raw material. *Angewandte Chemie, International Edition*, **44**, 3358–3393 (2005).
- [50] Nabar G. M., Padmanabhan C. V.: Studies in oxycellulose. *Proceedings of the Indian Academy of Sciences: A*, **31**, 371–80 (1950).
- [51] Da Silva Perez D., Montanari S., Vignon M. R.: TEMPO-mediated oxidation of cellulose III. *Bio-macromolecules*, **4**, 1525–1425 (2003).
- [52] Chang P. S., Robyt J. F.: Oxidation of primary alcohol groups of naturally occurring polysaccharides with 2,2,6,6-tetramethyl-1-piperidine oxoammonium ion. *Journal of Carbohydrate Chemistry*, **15**, 819–830 (1996).
- [53] Manderson K., Pinart M., Tuohy K. M., Grace W. E., Hotchkiss A. T., Widmer W., Yadhav M. P., Gibson G. R., Rastall R. A.: In vitro determination of prebiotic properties of oligosaccharides derived from an orange juice manufacturing by-product stream. *Applied and Environmental Microbiology*, **71**, 8383–8389 (2005).
- [54] Kim U-J., Kuga S., Wada M., Okano T., Kondo T.: Periodate oxidation of crystalline cellulose. *Bio-macromolecules*, **1**, 488–492 (2000).
- [55] Bogaard J., Morris H. R., Whitmore P. M.: A method for the aqueous deacidification of oxidized paper. *Journal of the American Institute for Conservation*, **44**, 63–74 (2005).
- [56] Lichtenthal F. W.: *Ullmann's encyclopedia of industrial chemistry*. 6th edition: Carbohydrates. Wiley-VCH, Weinheim (2002).
- [57] Sun Y., Lin L., Deng H., Li J., He B., Sun R., Ouyang P.: Structural changes of bamboo cellulose in formic acid. *Bioresources*, **3**, 297–315 (2008).
- [58] Reier C. E., Shangraw R. F.: Microcrystalline cellulose in tableting. *Journal of Pharmaceutical Sciences*, **55**, 510–515 (1966).
- [59] Durand H. W., Fleck E. J., Raynor G. E.: Microcrystalline cellulose compositions Co-dried with hydrocelluloses. US patent 3 537 058, USA (1970).
- [60] Battista O. A., Smith P. A.: Microcrystalline cellulose. *Industrial and Engineering Chemistry*, **54**, 20–29 (1962).
- [61] Baruah P. P., Bhattacharya G. C., Chaliha B. P.: Microcrystalline cellulose from cotton. *Indian Pulp and Paper*, 971–976 (2000).
- [62] Bhimte N. A., Tayade P. T.: Evaluation of microcrystalline cellulose prepared from sisal fibers as a tablet excipient: A technical note. *AAPS Pharmaceutical Science and Technology*, **8**, 1–6 (2007).
- [63] Anand S. M., Chawla J. S.: Microcrystalline cellulose from hosiery waste. *Research and Industry*, **26**, 227–235 (1981).
- [64] Nagavi B. G., Mithal B. M., Chawla J. S.: Microcrystalline cellulose from corncobs. *Research Industry*, **28**, 277–280 (1989).
- [65] Jain A. K., Dixit V. K., Varma K. C.: Preparation of microcrystalline cellulose from cereal straw and its evaluation as a tablet excipient. *Industrial Journal of Pharmaceutical Science*, **3**, 83–85 (1983).
- [66] El-Sakhawy M., Hassan M. L.: Physical and mechanical properties of microcrystalline cellulose prepared from agricultural residues. *Carbohydrate Polymers*, **67**, 1–10 (2007).
- [67] Hakansson H., Ahlgren P.: Acid hydrolysis of some industrial pulps: Effect of hydrolysis. *Cellulose*, **12**, 177–183 (2005).
- [68] Kaputskii F. N., Gert E. V., Torgashov V. I., Zubets O. V.: Hydrogels for medical applications fabricated by oxidative-hydrolytic modification of cellulose. *Fiber Chemistry*, **37**, 485–489 (2005).
- [69] Kirk R., Othmer D.: *Encyclopedia of chemical technology*. John Wiley, New York (1968).
- [70] Cohen S. G., Haas H. C., Farney L., Valle C. Jr.: Preparation and properties of some ether and ester derivatives of hydroxyethylcellulose. *Industrial and Engineering Chemistry*, **45**, 200–203 (1953).
- [71] Wadworth L. C., Daponte D.: Cellulose esters. in 'Cellulose Chemistry and its Applications' (eds.: Nevell T. P., Zeronian S. H.) Ellis Horwood, Chichester, 349–362 (1985).

- [72] Delgado J. N., William A.: Wilson and Gisvold's textbook of organic medicinal and pharmaceutical chemistry. Lippincott-Raven Publishers, Wickford (1998).
- [73] Banker G. S., Kumar V.: Microfibrillated oxycellulose. US patent 5405953, USA (1995).
- [74] Kibbe A. H.: Handbook of pharmaceutical excipients: Cellulose, silicified microcrystalline. American Public Health Association, Washington (2000).
- [75] Luukkonen P., Schaefer T., Hellen J., Juppo A. M., Yliruusi J.: Rheological characterization of microcrystalline cellulose and silicified microcrystalline cellulose wet masses using a mixer torque rheometer. *International Journal of Pharmaceutics*, **188**, 181–192 (1999).
- [76] Edge S., Steele F., Chen A., Tobyn M., Staniforth J. N.: The mechanical properties of compacts of microcrystalline cellulose and silicified microcrystalline cellulose. *International Journal of Pharmaceutics*, **200**, 67–72 (2000).
- [77] Van Veen B., Bolhuis G. K., Wu Y. S., Zuurman K., Frijlink H. W.: Compaction mechanism and tablet strength of unlubricated and lubricated (silicified) microcrystalline cellulose. *European Journal of Pharmaceutics and Biopharmaceutics*, **59**, 133–138 (2005).
- [78] Sherwood B. E., Becker J. W.: A new class of high functionality excipients: Silicified microcrystalline cellulose. *Pharmaceutical Technology*, **22**, 78–88 (1998).
- [79] Guo M., Augsburg L. L.: Potential application of silicified microcrystalline cellulose in direct-fill formulations for automatic capsule-filling machines. *Pharmaceutical Development and Technology*, **8**, 47–59 (2003).
- [80] Zografi G., Kontny M. J., Yang A. Y. S., Brenner G. S.: Surface area and water vapor sorption of microcrystalline cellulose. *International Journal of Pharmaceutics*, **18**, 99–116 (1984).
- [81] Hwang R.-C., Peck G. R.: A systematic evaluation of the compression and tablets characteristics of various types of microcrystalline cellulose. *Pharmaceutical Technology*, **24**, 112–132 (2001).
- [82] Muzíková J., Nováková P.: A study of the properties of compacts from silicified microcrystalline celluloses. *Drug Development and Industrial Pharmacy*, **33**, 775–781 (2007).
- [83] Siepmann J., Kranz H., Bodmeier R., Peppas N. A.: HPMC-matrices for controlled drug delivery: a new model combining diffusion, swelling, and dissolution mechanisms and predicting the release kinetics. *Pharmaceutical Research*, **16**, 1748–1756 (1999).
- [84] Colombo P., Bettini R., Peppas N. A.: Observation of swelling process and diffusion front position during swelling in hydroxypropylmethyl cellulose (HPMC) matrices containing a soluble drug. *Journal of Controlled Release*, **61**, 83–91 (1999).
- [85] Lowman A. M., Peppas N. A.: Hydrogels. in 'Encyclopedia of Controlled Drug Delivery' (ed.: Mathiowitz E.) Wiley, New York, 397–417 (2000).
- [86] Le Neel T., Morlet-Renaud C., Lipart C., Gouyette A., Truchaud A., Merle C.: Image analysis as a new technique for the study of water uptake in tablets. *STP Pharma Sciences*, **7**, 117–122 (1997).
- [87] Baumgartner S., Šmid-Korbar J., Vreèer F., Kristl J.: Physical and technological parameters influencing floating properties of matrix tablets based on cellulose ethers. *STP Pharmaceutical Sciences*, **8**, 182–187 (1998).
- [88] Arion H.: Carboxymethyl cellulose hydrogel-filled breast implants. Our experience in 15 years (in French). *Annales de Chirurgie Plastique et Esthétique*, **46**, 55–59 (2001).
- [89] Hercules Incorporated, Aqualon Division: <http://www.aqualon.com> (16.07.2008).
- [90] Sannino A., Madaghiele M., Conversano F., Mele G., Maffezzoli A., Netti P. A., Ambrosio L., Nicolais L.: Cellulose derivative-hyaluronic acid-based microporous hydrogels crosslinked through divinyl sulfone (DVS) to modulate equilibrium sorption capacity and network stability. *Biomacromolecules*, **5**, 92–673 (2004).
- [91] Valeriani M., Mezzana P., Madonna S., Terracina F.: Carboxy-methyl-cellulose hydrogel mammary implants: Our experience. *Acta Chirurgiae Plasticae*, **44**, 71–76 (2002).
- [92] Domínguez A., Valdivia A., Hernández J., Villalonga R.: Biocompatibilidad in vitro de Superóxido dismutasa interactuando con polímero e hidrogeles de carboximetilcelulosa ensayado con fibroblastos humanos. *Revista de Biotecnología Aplicada*, **21**, 218–2381 (2004).
- [93] Domínguez A.: Modifying superoxide dismutase for improved biopharmaceutical properties. *Biotecnología Aplicada*, **23**, 17–21 (2006).
- [94] Klestov A. C., Webb J., Latt D., Schiller G., McNamara K., Young D. Y., Hobbes J., Fetherston J.: Treatment of xerostomia: A double-blind trial in 108 patients with Sjögren's syndrome. *Oral Surgery Oral Medicine and Oral Pathology*, **51**, 594–599 (1981).
- [95] Olsson H., Axell T.: Objective and subjective efficacy of saliva substitutes containing mucin and carboxymethyl cellulose. *Scandinavian Journal of Dental Research*, **99**, 316–319 (1991).
- [96] Rokhade A. P., Agnihotri S. A., Patil S. A., Mallikarjuna N. N., Kulkarni P. V., Aminabhavi T. M.: Semi-interpenetrating polymer network microspheres of gelatin and sodium carboxymethyl cellulose for controlled release of ketorolac tromethamine. *Carbohydrate Polymers*, **65**, 243–252 (2006).
- [97] Flower R. J., Moncada S., Vane J. R.: Indomethacin. in 'Goodman and Gilman's the Pharmacological Basis of Therapeutics' (eds.: Hardman J. G., Limbird L. E.) Macmillan Publishing, New York, 695–697 (1990).

- [98] Waree T., Garnpimol C. R.: Development of indomethacin sustained release microcapsules using chitosan-carboxymethyl cellulose complex coacervation. *Songklanakarin Journal of Science Technology*, **25**, 245–254 (2003).
- [99] Ritthidej G. C., Tiyaboonchai W.: Formulation and drug entrapment of microcapsules prepared from chitosan-carboxymethylcellulose complex coacervation. *Thai Journal of Pharmaceutical Sciences*, **21**, 137–144 (1997).
- [100] Hou W. M., Miyasaki S., Takada M., Komai T.: Sustained release of indomethacin from chitosan granules. *Chemical and Pharmaceutical Bulletin*, **33**, 3986–3992 (1985).
- [101] Thanoo B. C., Sunny M. C., Jayakrishnan A.: Cross-linked chitosan microspheres: Preparation and evaluation as a matrix for the controlled release of pharmaceuticals. *Journal of Pharmacy and Pharmacology*, **44**, 283–286 (1992).
- [102] Polk A., Amsden B., De Yao K., Peng T., Goosen M. F.: Controlled release of albumin from chitosan-alginate microcapsules. *Journal of Pharmaceutical Sciences*, **83**, 178–195 (1994).
- [103] Remunan-Lopez C., Bodmeier R.: Effect of formulation and processing variables on the formation of chitosan-gelatin coacervates. *International Journal of Pharmaceutics*, **135**, 63–72 (1996).
- [104] Kunal P., Banthia A. K., Majumdar D. K.: Esterification of carboxymethyl cellulose with acrylic acid for targeted drug delivery system. *Trends in Biomaterials and Artificial Organs*, **19**, 12–14 (2005).
- [105] Kunal P., Banthia A. K., Majumdar D. K.: Development of carboxymethyl cellulose acrylate for various biomedical applications. *Biomedical Materials*, **1**, 85–91 (2006).
- [106] Wilkes G. M.: *Consumers guide to cancer drugs* (American Cancer Society). Jones and Bartlett Publishers, Sudbury (2004).
- [107] Keiji S., Noboru O.: Studies on absorption of eutectic mixture. I. A comparison of the behavior of eutectic mixture of sulfathiazole and that of ordinary sulfathiazole in man. *Chemical and Pharmaceutical Bulletin*, **9**, 866–872 (1961).
- [108] Chiou W. L., Riegelman S.: Oral absorption of griseofulvin in dogs. Increased absorption via solid dispersion in polyethylene glycol 6000. *Journal of Pharmaceutical Sciences*, **59**, 937–942 (1970).
- [109] Sugimoto I., Kuchiki A., Nakagawa H., Tohgo A., Kondo S., Iwane I., Takahashi K.: Dissolution and absorption of nifedipine from nifedipine-polyvinylpyrrolidone coprecipitate. *Drug Development and Industrial Pharmacy*, **6**, 137–160 (1980).
- [110] Takeuchi H., Handa T., Kawashima Y.: Spherical solid dispersion containing amorphous tolbutamide embedded in enteric coating polymers or colloidal silica prepared by spray-drying technique. *Chemical and Pharmaceutical Bulletin*, **35**, 3800–3806 (1987).
- [111] Suzuki H., Sunada H.: Influence of water-soluble polymers on the dissolution of nifedipine solid dispersions with combined carriers. *Chemical and Pharmaceutical Bulletin*, **46**, 482–487 (1998).
- [112] Ozeki T., Yuasa H., Okada H.: Controlled release of drug via methylcellulose-carboxyvinyl polymer interpolymer complex solid dispersion. *AAPS Pharmaceutical Science and Technology*, **6**, 231–236 (2005).
- [113] Mura P., Fauci M. T., Manderioli A., Bramanti G., Parrini P.: Thermal behavior and dissolution properties of naproxen from binary and ternary solid dispersion. *Drug Development and Industrial Pharmacy*, **25**, 257–264 (1999).
- [114] Friedman M., Golomb G.: New sustained release dosage form of chlorhexidine for dental use. *Journal of Periodontal Research*, **17**, 323–328 (1982).
- [115] Soskolne W. A., Golomb G., Friedman M., Sela M. N.: New sustained release dosage form of chlorhexidine for dental use. *Journal of Periodontal Research*, **18**, 330–336 (1983).
- [116] Yuasa H., Ozeki T., Kanaya Y., Oishi K., Oyake T.: Application of the solid dispersion method to the controlled release of medicine. I. Controlled release of water soluble medicine by using solid dispersion. *Chemical and Pharmaceutical Bulletin*, **39**, 465–467 (1991).
- [117] Yuasa H., Ozeki T., Kanaya Y., Oishi K.: Application of the solid dispersion method to the controlled release of medicine. II. Sustained release tablet using solid dispersion granule and the medicine release mechanism. *Chemical and Pharmaceutical Bulletin*, **40**, 1592–1596 (1992).
- [118] Ozeki T., Yuasa H., Kanaya Y., Oishi K.: Application of the solid dispersion method to the controlled release of medicine. V. Suppression mechanism of the medicine release rate in the three-component solid dispersion system. *Chemical and Pharmaceutical Bulletin*, **42**, 337–343 (1994).
- [119] Ozeki T., Yuasa H., Kanaya Y., Oishi K.: Application of the solid dispersion method to the controlled release of medicine. VII. Release mechanism of a highly water-soluble medicine from solid dispersion with different molecular weight of polymer. *Chemical and Pharmaceutical Bulletin*, **43**, 660–665 (1995).
- [120] Ozeki T., Yuasa H., Kanaya Y., Oishi K.: Application of the solid dispersion method to the controlled release of medicine. VIII. Medicine release and viscosity of the hydrogel of a water-soluble polymer in a three-component solid dispersion system. *Chemical and Pharmaceutical Bulletin*, **43**, 1574–1579 (1995).
- [121] Yuasa H., Takahashi H., Ozeki T., Kanaya Y., Ueno M.: Application of the solid dispersion method to the controlled release of medicine. III. Control of the release rate of slightly water soluble medicine from solid dispersion granules. *Chemical and Pharmaceutical Bulletin*, **41**, 397–399 (1993).

- [122] Yuasa H., Ozeki T., Takahashi H., Kanaya Y., Ueno M.: Application of the solid dispersion method to the controlled release of medicine. VI. Release mechanism of slightly water soluble medicine and interaction between flurbiprofen and hydroxypropyl cellulose in solid dispersion. *Chemical and Pharmaceutical Bulletin*, **42**, 354–358 (1994).
- [123] Ozeki T., Yuasa H., Kanaya Y.: Application of the solid dispersion method to the controlled release of medicine. IX. Difference in the release of flurbiprofen from solid dispersions with poly(ethylene oxide) and hydroxypropylcellulose and interaction between medicine and polymers. *International Journal of Pharmaceutics*, **115**, 209–217 (1997).
- [124] Nagai T., Machida Y.: Advances in drug delivery: Mucosal adhesive dosage forms. *Pharmaceutical International*, **6**, 196–200 (1985).
- [125] Satoh K., Takayama K., Machida Y., Suzuki Y., Nakagaki M., Nagai T.: Factors affecting the bioadhesive property of tablets consisting of hydroxypropyl cellulose and carboxyvinyl polymer. *Chemical and Pharmaceutical Bulletin*, **37**, 1366–1368 (1989).
- [126] Han R-Y., Fang J-Y., Sung K. C., Hu O. Y. P.: Mucoadhesive buccal disks for novel nalbuphine pro-drug controlled delivery: Effect of formulation variables on drug release and mucoadhesive performance. *International Journal of Pharmaceutics*, **177**, 201–209 (1999).
- [127] Chen W-G., Hwang G. C-C.: Adhesive and in vitro release characteristics of propranolol bioadhesive disc system. *International Journal of Pharmaceutics*, **82**, 61–66 (1992).
- [128] Park C. R., Munday D. L.: Development and evaluation of a biphasic buccal adhesive tablet for nicotine replacement therapy. *International Journal of Pharmaceutics*, **237**, 215–226 (2002).
- [129] Lo Muzio L., Della Valle A., Mignogna M. D., Pannone G., Bucci P., Bucci E., Sciubba J.: The treatment of oral aphthous ulceration or erosive lichen planus with topical clobetasol propionate in three preparations: A clinical and pilot study on 54 patients. *Journal of Oral Pathology and Medicine*, **30**, 611–617 (2001).
- [130] Senel S., Hincal A. A.: Drug permeation enhancement via buccal route: Possibilities and limitations. *Journal of Controlled Release*, **72**, 133–144 (2001).
- [131] Okamoto H., Nakamori T., Arakawa Y., Iida K., Danjo K.: Development of polymer film dosage forms of lidocaine for buccal administration. II. Comparison of preparation methods. *Journal of Pharmaceutical Sciences*, **91**, 2424–2432 (2002).
- [132] Mizrahi B., Golenser J., Wolnerman J. S., Domb A. J.: Adhesive tablet effective for treating canker sores in humans. *Journal of Pharmaceutical Sciences*, **93**, 2927–2935 (2004).
- [133] Gurruchaga M., Goñi I., Valero M., Guzmán G. M.: Graft polymerisation of acrylic monomers onto starch fractions. I. Effect of reaction time on grafting MMA onto amylopectin. *Journal of Polymer Science, Part A: Polymer Chemistry*, **21**, 2573–2580 (1983).
- [134] Gander B., Gurny R., Doelker E., Peppas N. A.: Crosslinked poly(alkylene oxides) for the preparation of controlled release micromatrices. *Journal of Controlled Release*, **5**, 271–283 (1988).
- [135] Gon M. C., Ferrero R. M., Jimenez C., Gurruchaga M.: Synthesis of hydroxypropyl methacrylate/ polysaccharide graft copolymers as matrices for controlled release tablets. *Drug Development and Industrial Pharmacy*, **28**, 1101–1115 (2002).
- [136] Tahara K., Yamamoto K., Nishihata T.: Overall mechanism behind matrix sustained release (SR) tablets prepared with hydroxypropylmethyl cellulose. *Journal of Controlled Release*, **35**, 59–66 (1995).
- [137] Skoug J. W., Mikelsons M. V., Vigneron C. N., Stemm N. L.: Qualitative evaluation of the mechanism of release of matrix sustained release dosage forms by measurement of polymer release. *Journal of Controlled Release*, **27**, 227–245 (1993).
- [138] Ford J. L., Rubinstein M. H., McCaul F., Hogan J. E., Edgar P. J.: Importance of drug type, tablet shape and added diluents on drug release kinetics from hydroxypropylmethyl cellulose matrix tablets. *International Journal of Pharmaceutics*, **40**, 223–234 (1987).
- [139] Ranga Rao K V., Padmalatha D., Buri P.: Influence of molecular size and water solubility of the solute on its release from swelling and erosion controlled polymeric matrices. *Journal of Controlled Release*, **12**, 133–141 (1990).
- [140] Harland R. S., Gazzaniga A., Sangalli M. E., Colombo P., Peppas N. A.: Drug/polymer matrix swelling and dissolution. *Pharmaceutical Research*, **5**, 488–494 (1988).
- [141] Lee P. I.: Diffusional release of a solute from a polymeric matrix-approximate analytical solution. *Journal of Membrane Science*, **7**, 255–275 (1980).
- [142] Lee P. I., Peppas N. A.: Prediction of polymer dissolution in swellable controlled-release systems. *Journal of Controlled Release*, **6**, 207–215 (1987).
- [143] Reynolds T. D., Gehrke S. H., Hussain A. S., Shenouda S. L.: Polymer erosion and drug release characterization of hydroxypropylmethyl cellulose matrices. *Journal of Pharmaceutical Sciences*, **87**, 1115–1123 (1998).
- [144] Reynolds T. D., Mitchell S. A., Balwinski K. M.: Investigation of the effect of tablet surface area/volume on drug release from hydroxypropylmethylcellulose controlled-release matrix tablets. *Drug Development and Industrial Pharmacy*, **28**, 457–466 (2002).
- [145] Katzhendler I., Mader K., Friedman M.: Structure and hydration properties of hydroxypropyl methylcellulose matrices containing naproxen and naproxen sodium. *International Journal of Pharmaceutics*, **200**, 161–179 (2000).

- [146] Lee P. I.: Kinetics of drug release from hydrogel matrices. *Journal of Controlled Release*, **2**, 277–288 (1985).
- [147] Colombo P.: Swelling-controlled release in hydrogel matrices for oral route. *Advanced Drug Delivery Reviews*, **11**, 37–57 (1993).
- [148] Vazquez M.-J., Casalderrey M., Duro R., Gómez-Amoza J.-L., Martínez-Pacheco R., Souto C., Concheiro A.: Atenolol release from hydrophilic matrix tablets with hydroxypropylmethylcellulose (HPMC) mixtures as gelling agent: Effects of the viscosity of the HPMC mixture. *The European Journal of Pharmaceutical Sciences*, **4**, 39–48 (1996).
- [149] Alvarez-Lorenzo C., Duro R., Gomez-Amoza J. L., Martínez-Pacheco R., Souto C., Concheiro A.: Influence of polymer structure on the rheological behavior of hydroxypropylmethylcellulose-sodium carboxymethylcellulose dispersions. *Colloid and Polymer Science*, **279**, 1045–1057 (2001).
- [150] Khanvilkar K. H., Ye H., Moore A. D.: Influence of hydroxypropyl methylcellulose mixture, apparent viscosity, and tablet hardness on drug release using a 2³ full factorial design. *Drug Development and Industrial Pharmacy*, **28**, 601–608 (2002).
- [151] Ye H., Khanvilkar K. H., Moore A. D., Hilliard-Lott M.: Effects of manufacturing process variables on in vitro dissolution characteristics of extended-release tablets formulated with hydroxypropylmethyl cellulose. *Drug Development and Industrial Pharmacy*, **29**, 79–88 (2003).
- [152] Liu Z., Li J., Nie S., Liu H., Ding P., Pan W.: Study of an alginate/HPMC-based in situ gelling ophthalmic delivery system for gatifloxacin. *International Journal of Pharmaceutics*, **315**, 12–17 (2006).
- [153] Suvitayavat W., Tunlert S., Thirawarapan S. S., Bunyapraphatsara N.: Effects of Ya-hom on blood pressure in rats. *Journal of Ethnopharmacology*, **97**, 503–508 (2005).
- [154] Phaechamu T., Vesapun C., Kraisit P.: Ya Hom in dosage form of buccal tablet. in 'Proceedings of the 10th World Congress on Clinical Nutrition. Phuket, Thailand' 193–198 (2004).
- [155] Chantana V., Juree C., Thawatchaj P.: Effect of hydroxypropylmethyl cellulose and polyvinyl pyrrolidone on physical properties of Yahoo buccal tablets and the antimicrobial activity of Yahoo. in 'The 4th Thailand Materials Science Technology Conference. Khong Wan, Thailand' PP01/1–PP01/3 (2006).
- [156] Lenaerts V., Dumoulin Y., Mateescu M. A.: Controlled release of theophylline from cross-linked amylose tablets. *Journal of Controlled Release*, **15**, 39–46 (1991).
- [157] Rahmouni M., Lenaerts V., Massuelle D., Doelker E., Johnson M., Leroux J.-C.: Characterization of binary mixtures consisting of cross-linked high amylose starch and hydroxypropylmethyl cellulose used in the preparation of controlled release tablets. *Pharmaceutical Development and Technology*, **8**, 335–348 (2003).
- [158] Rahmouni M., Chouinard F., Nekka F., Lenaerts V., Leroux J.-C.: Enzymatic degradation of crosslinked high amylose starch tablets and its effect on in vitro release of sodium diclofenac. *European Journal of Pharmaceutics and Biopharmaceutics*, **51**, 191–198 (2001).
- [159] Chowhan Z. T.: Role of binder in moisture-induced hardness increase in compressed tablets and its effect on in vitro disintegration and dissolution. *Journal of Pharmaceutical Sciences*, **69**, 1–4 (1980).
- [160] Amaral M. H., Sousa Lobo J. M., Ferreira D. C.: Effect of hydroxypropylmethyl cellulose and hydrogenated castor oil on naproxen release from sustained-release tablets. *APS Pharmaceutical Science and Technology*, **2**, 1–8 (2001).
- [161] Liu J., Zhang F., McGinity J. W.: Properties of lipophilic matrix tablets containing phenylpropanolamine hydrochloride prepared by hot-melt extrusion. *European Journal of Pharmaceutics and Biopharmaceutics*, **52**, 181–190 (2001).
- [162] Salsa T., Veiga F., Pina M. E.: Oral controlled-release dosage forms. I. Cellulose ether polymers in hydrophilic matrices. *Drug Development and Industrial Pharmacy*, **23**, 929–938 (1997).
- [163] Sandip B., Tiwari T., Krishna M., Raveendra Pai M., Pavak R. M., Pasula B. C.: Controlled release formulation of tramadol hydrochloride using hydrophilic and hydrophobic matrix system. *AAPS Pharmaceutical Science and Technology*, **4**, 1–6 (2003).
- [164] Molla M. A. K., Shaheen S. M., Rashid M., Hossain A. K. M. M.: Rate controlled release of naproxen from HPMC Based sustained release dosage form, I. Microcapsule compressed tablet and matrices. *Dhaka University Journal of Pharmaceutical Sciences*, **4**, (2005).
- [165] Vueba M. L., Batista de Carvalho L. A. E., Veiga F., Sousa J. J., Pina M. E.: Influence of cellulose ether mixtures on Ibuprofen release: MC25, HPC and HPMC K100M. *Pharmaceutical Development and Technology*, **11**, 213–228 (2006).

Poly(acrylic acid) surface grafted polypropylene films: Near surface and bulk mechanical response

L. A. Fasce¹, V. Costamagna², V. Pettarin¹, M. Strumia², P. M. Frontini^{1*}

¹Universidad Nacional de Mar del Plata, Instituto de Investigaciones en Ciencia y Tecnología de Materiales, INTEMA, J.B. Justo 4302 - B7608 FDQ - Mar del Plata, Argentina

²Departamento de Química Orgánica, Facultad de Ciencias Químicas, Universidad Nacional de Córdoba, Argentina

Received 19 August 2008; accepted in revised form 20 September 2008

Abstract. Radical photo-grafting polymerization constitutes a promising technique for introducing functional groups onto surfaces of polypropylene films. According to their final use, surface grafting should be done without affecting overall mechanical properties. In this work the tensile drawing, fracture and biaxial impact response of biaxially oriented polypropylene commercial films grafted with poly(acrylic acid) (PAA) were investigated in terms of film orientation and surface modification. The variations of surface roughness, elastic modulus, hardness and resistance to permanent deformation induced by the chemical treatment were assessed by depth sensing indentation. As a consequence of chemical modification the optical, transport and wettability properties of the films were successfully varied. The introduced chains generated a PAA-grafted layer, which is stiffer and harder than the neat polypropylene surface. Regardless of the surface changes, it was proven that this kind of grafting procedure does not detriment bulk mechanical properties of the PP film.

Keywords: *mechanical properties, depth sensing indentation, surface photo-grafting, polypropylene, films*

1. Introduction

Owing to its useful properties, easy workability and low manufacturing costs, polypropylene (PP) is widely used for the preparation of films, fibers, plates, injection-molded as well as blow molded parts [1]. Often, insufficient surface properties preclude its use in an application to which bulk mechanical properties may be well-suited. For example dyeability, printability, paintability, adhesion, biocompatibility, antifogging, and gas permeability of PP parts can be improved by surface modification [2–9].

Efforts have been made to develop polymer modifications processes which allow the surface properties to be tailored to meet a specific requirement while retaining beneficial mechanical properties. Surface modification can be accomplished by

increasing the polarity introducing special chemical functionalities like carboxylic groups, or by coating the surfaces with polar thin films, for example, poly(acrylic acid) (PAA). Surface grafting techniques including photo-initiated grafting [10–14], living radical grafting [15], ceric ion induced grafting [16], layer-by-layer ionic grafting [17] and plasma polymerization [18, 19] have proven to be effective to graft poly-functional monomers or polymers onto PP surfaces.

Among the methods to modify polymers, radical photo-grafting polymerisation appears as an attractive method to impart a variety of functional groups to a polymer [20, 21]. The advantages of photo-grafting over other available methods are: i) easy and controllable introduction of chains, ii) high density and exact localization of chains onto the

*Corresponding author, e-mail: pmfronti@fi.mdp.edu.ar
© BME-PT and GTE

surface, iii) covalent attachment of chains which avoids delamination and assures long-term chemical stability of introduced chains, in contrast to physically attached layers [1].

Low energy radiation, such as UV light, is frequently used to initiate surface modification. The ability of graft co-polymerization to quickly change the surface properties in a tunable fashion allows for the development of a product that can be adapted on-demand to a particular application.

Modification of PP films through grafting at relatively low amounts were previously demonstrated to be an effective approach to functionalize PP providing a defined, stable, organic foundation for subsequent surface modification of various types [22]. Costamagna *et al.* were able to modify exclusively the surface of bi-oriented PP films by grafting reaction of poly(acrylic acid) (PAA) [23]. They showed that values of the permeability coefficient of oxygen, nitrogen, carbon dioxide, carbon monoxide, argon, methane, ethane, ethylene, and propane across the grafted films undergo a marked drop. Their morphology investigations by Atomic Force Microscopy (AFM) suggested the initial formation of PAA brushes attached to the PP surface at short time of reaction followed by the generation of a network by cross reaction between grafted growing chains, brushes entanglements and strong hydrogen bonds [24]. The improvement in barrier properties was attributed to the formation of such a rigid PAA layer onto the PP surface [24].

Despite it has been claimed that surface grafting theoretically occurs without detriment of the bulk mechanical properties of the polymer [25], undesirable changes in the mechanical performance of different polymeric films modified by photo-grafting techniques have been reported (see for example in [22, 26–28]). To a large extent, the tendency and level of concomitant changes in the material properties depend on whether crosslinking or degradation dominates during the irradiation of the polymer [29, 30]. UV irradiation may induce the formation of free radicals, which promotes crosslinking. This in turn minimizes the anisotropic character of the polymer leading to an increased degree of molecular disorder. If this occurs, bulk mechanical properties of a polymeric film would be impaired since they are highly dependent on molecular orientation.

The present paper is focused on determining the mechanical properties of a bi-oriented PP film before and after surface photo-grafting with PAA chains. To this aim the bulk mechanical behavior was characterized by evaluating uniaxial tensile deformation, quasi-static fracture and dart impact properties. In addition depth sensing indentation experiments [31–36] were carried out in order to gain a deeper insight into differences in surface mechanical characteristics of PAA-grafted and neat films.

2. Experimental section

2.1. Film grafting procedure

A commercial polypropylene film (PP) (Converflex S.A., Buenos Aires, Argentina), was surface modified by radical grafting polymerisation initiated by UV light. The appropriate reaction conditions were previously investigated [23]. The procedure was as follows: Acrylic acid was used as grafting co-monomer. The initiator benzophenone (Fluka AG, Buchs, Switzerland) was dissolved in the acrylic acid (BASF, New Jersey, USA) and distilled water was added. The solution in contact with the PP film was enclosed into a photo-reactor and irradiated with UV light (medium pressure UV lamp Engelhard-Hanovia, Slough, England) under nitrogen atmosphere at room temperature for 10 min. The grafted film was extensively washed with a NaOH solution (pH = 8) in order to remove traces of un-reacted monomer and formed homopolymer as well as to extract rests of the initiator.

Before characterization, surface modified films were left in a pH 8 solution for 24 h in order to disrupt the hydrogen bonds.

The thickness (t) of the neat PP film determined with a micrometer was $34 \pm 1 \mu\text{m}$. The difference between the thickness values of the neat and the PA-grafted films was determined with a Mitutoyo coordinate measuring machine. Measurements made on at least ten different locations for each sample yielded an averaged value of $4.5 \mu\text{m}$ for the PAA layer.

Hereafter, unmodified films and surface modified films are designated as PP and *sm*PP films, respectively.

2.2. Physical and chemical characterization

2.2.1. Chemical structure

Fourier transform infrared spectroscopy (FTIR) measurements of the surface modified films were obtained from a Nicolet 5 SXC FTIR spectrophotometer operating in the transmission mode in order to characterize the chemical modification. Each spectrum was collected by cumulating 32 scans at a resolution of 8 cm^{-1} .

Gravimetric measurements of films before and after grafting reactions were carried out to determine the grafting percentage by means of the Equation (1) [37, 38]:

$$\% \text{Grafting} = 100 \cdot \left[\frac{\text{weight of smPP sample} - \text{weight of PP sample}}{\text{weight of PP sample}} \right] \quad (1)$$

The weight of grafted layer was also estimated by volumetric titration of the COOH groups grafted onto the PP surface with a 0.01 M NaOH solution.

2.2.2. Surface feature, topography and roughness

Scanning electron microscopy (SEM) observations were made by using a Jeol JSM-6460LV scanning electron microscope operating at an accelerated voltage of 15 kV. Sample surfaces were coated with a thin layer of gold.

Scanning probe microscopy (SPM) analyses were made using the SPM module of the Triboindenter Hysitron. Sample surfaces were explored with an imaging type tip at a scan rate of 0.5 Hz and a set-point force of $1\ \mu\text{N}$. The arithmetic mean surface roughness (R_a) was calculated from the SPM images as the average of the absolute values of the surface height deviations measured from the mean plane within a box of $400\ \mu\text{m}^2$.

2.2.3. Wettability

Static contact angle measurements were performed by the sessile drop method at room temperature. The 'NIH' image software was used with a MV-50 camera and a magnification of $6\times$. The contact angles of water droplets on PP and surface modified PP surfaces were used to determine the change

in hydrophilicity of the film surface. Five measurements were recorded and an average contact angle was calculated for each material [39].

2.2.4. Transparency

Light transmittance measurements were carried out by using a Leica DMLB microscope incorporating a photo-detector in its optical path. The light transmittance signal (I_T) measured for PP and smPP samples were used to estimate the loss of film transparency according to the following definition (Equation (2)):

$$\text{Loss of transparency} = \frac{I_T(\text{smPP}) - I_T(\text{PP})}{I_T(\text{PP})} \cdot 100 \quad (2)$$

2.2.5. Microstructure and orientation

The main factors that determine the mechanical properties are the molecular orientation and the crystalline level.

The anisotropy developed during the planar deformation that films underwent during blowing was not identifiable from the simple naked eye inspection. The main film orientation directions were identified from the birefringence using polarizing microscopy. Machine (MD) and transverse (TD) directions of biaxially oriented films coincide with the two orthogonal axes defined by the four positions in which light extinguishes when the film is rotated under cross polarizers [40].

The crystalline fraction (X_c) was determined using thermal analysis. DSC measurements were performed in a Perkin Elmer Pyris 1 equipment at $10^\circ\text{C}/\text{min}$. For the sake of simplicity, samples were directly put in the DSC capsules. In X_c calculations, the enthalpy of fusion of 100% crystalline PP was taken as $209\ \text{J/g}$ [41].

2.3. Near Surface mechanical properties

Near surface mechanical properties of the films were investigated up to the micron scale using a Hysitron Triboindenter® testing system [<http://www.hysitron.com>]. While a diamond indenter drives into the film surface, the system is able to collect the applied force and displacement data. Samples were indented with a conospherical dia-

mond tip of nominal radius of curvature equal to 1 μm. Indentations were performed using trapezoidal loading curves in order to minimize the ‘nose effect’ caused by the viscoelastic nature of polymers [33]. Maximum applied loads were varied between 4000 and 9000 μN at a constant loading rate of 250 μN/s. The holding time between loading and unloading stages was 20 s. Indentations were load-controlled and repeated at least 20 times for every load on different locations of the films surfaces.

The Oliver-Pharr method [42], which proposes the estimation of the slope of the unloading curve by first fitting the entire unloading data, was employed to determine reduced elastic modulus (E_r) and the hardness (H) of the materials. The reduced elastic modulus is related to the elastic modulus of the sample (E) and the contact stiffness (S) by Equations (3) and (4):

$$E_r = \left[\frac{1-\nu^2}{E} + \frac{1-\nu_i^2}{E_i} \right]^{-1} \quad (3)$$

$$E_r = \frac{1}{2} \left(\frac{\pi}{A_{\max}} \right)^{\frac{1}{2}} S \quad (4)$$

where ν is the Poisson’s ratio and subscript i denotes the indenter material. A_{\max} is the surface contact area at the maximum displacement. The contact stiffness (S) is the slope of the unloading curve taken as the first derivative in the maximum depth of a fitted power law function of the unloading segment of the curve.

The material hardness (H) is defined as the maximum load, P_{\max} , divided by the projected area of the indentation under this load, see Equation (5):

$$H = \frac{P_{\max}}{A_{\max}} \quad (5)$$

The surface contact area versus contact depth function of the tip $A(h_c)$ was empirically determined by performing multiple indentations on a polycarbonate block of known E_r as suggested in [33]. The obtained calibrated area function was used in the computation of E_r and H values (Equations (3) and (4)).

2.4. Bulk mechanical properties

Both PP and surface modified PP films were tested along with (MD) and transversely to the machine direction (TD) at room temperature. Experiments were carried out in an Instron 4467 universal testing machine at a crosshead speed of 10 mm/min.

Uniaxial tensile tests were performed on dumbbell-shaped specimens, which were die-cut from the films. Longitudinal strain was measured with the aid of a video extensometer in which the deformation of the material is assessed from the current distortion of a close array of two ink dots printed onto the samples prior to deformation [43]. Yield stress (σ_y) was determined as the stress where two tangents to the initial and final parts of the load-elongation curve intersect [44]. Elastic modulus was calculated from the stress–strain curves. Properties were averaged from at least five tests.

Fracture experiments were performed using Deeply double edge-notched samples (DENT, Mode I) prepared by cutting the sheets into rectangular coupons of total length Z_i 80 mm (with a length between the grips of $Z = 60$ mm) and a width $W = 40$ mm. A special device was used to perform the two notches, allowing them to be perfectly aligned. Notches were then sharpened by pushing through the material a fresh razor blade into the tip to a depth of 1 mm. The length of each notch a was 10 mm.

Fracture toughness was determined by using the J -integral approach, as defined by Equation (6):

$$J_c = \frac{\eta U_{tot}}{B(W-a)} \quad (6)$$

with U_{tot} the overall fracture energy i.e. the total area under the load-deflection curve, B the thickness of tested specimens, and η a geometry factor expressed as Equation (7) [45]:

$$\eta = -0.06 + 5.99 \left(\frac{a}{W} \right) - 7.42 \left(\frac{a}{W} \right)^2 + 3.29 \left(\frac{a}{W} \right)^3 \quad (7)$$

In order to complete the bulk characterization, dart impact experiments were carried out since it has been shown that such tests are very sensitive to surface modifications in polymeric systems [46]. Dart impact experiments were conducted on a Fractovis Ceast falling weight type machine at room temperature at 3 m/s, using an instrumented high-speed

dart with hemispherical end onto disk specimens of 80 mm of diameter. The modified surface was placed opposite to the impact tip in order to induce tension loads on the modified surface. The thickness related energy (U/t) was determined by numerical integration of the experimental load-displacement data. Disc maximum strength (σ_d) was computed from the recorded traces through the following relationship (see Equation (8)) [47]:

$$\sigma_d = 2.5 \frac{P_{\max}}{t^2} \quad (8)$$

3. Results and discussion

3.1. Surface modification

FTIR spectra of the films are shown in Figure 1, in which an intense $-C=O$ absorption (1718 cm^{-1}) characteristic of polyacrylic acid is seen in the curve of the surface modified PP film.

The grafting percentage obtained by both techniques (gravimetric measurements and volumetric titration) was 12.9% (Equation (1)).

PP and surface modified PP films displayed melting endotherms of very similar shape: besides the main melting peak at 168°C a small peak appeared at about 160°C (Figure 2). During heating, the disorientation process that occurs in crystalline oriented polymers is often accompanied by dimensional shrinkage. For isotactic polypropylene, Sun and Magill [48] demonstrated that shrinkage and melting take place concomitantly producing multiple melting peaks. Since any slight difference in X_c values of PP and surface modified PP samples is within experimental error, PP crystalline fraction, X_c , is about 40%. Based on the DSC results, it

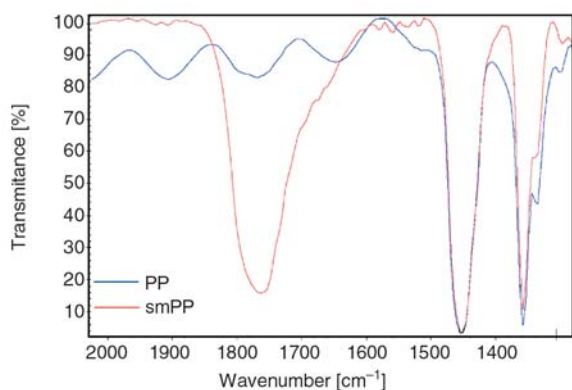


Figure 1. FTIR spectra of PP and surface modified PP films

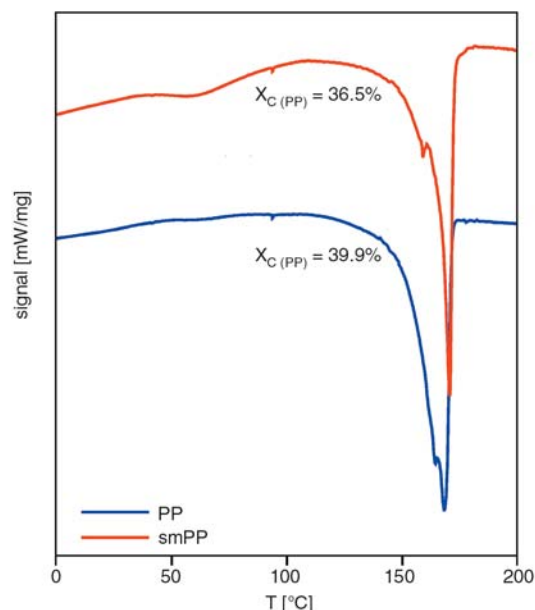


Figure 2. DSC thermograms showing the melting behavior of PP and surface modified PP films

appears that the grafting process did not affect supramolecular structure of the neat PP film.

SEM and SPM images of both films surfaces are shown in Figures 3 and 4, respectively. It is clear

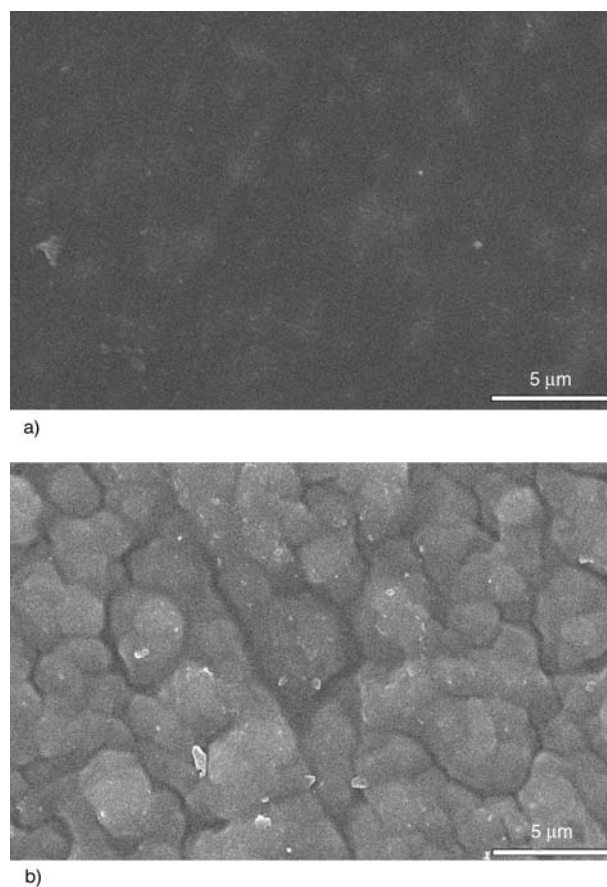


Figure 3. SEM micrographs showing the topography of PP (a) and surface modified PP (b) films

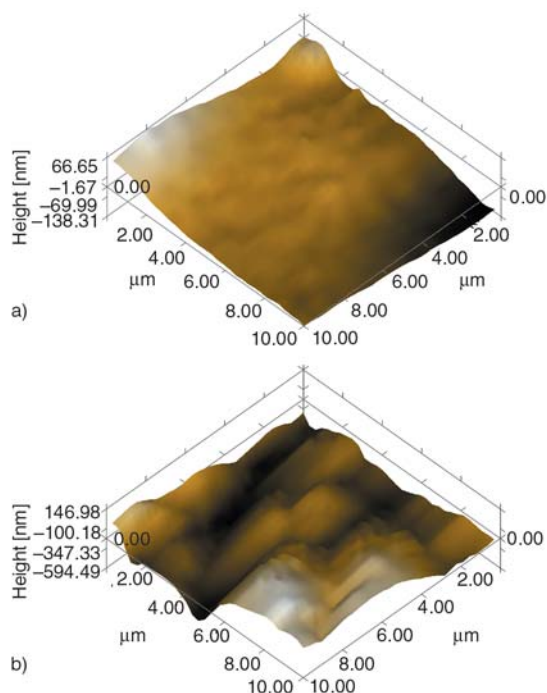


Figure 4. Typical SPM images of PP (a) and surface modified PP (b) film surfaces used in roughness measurements

that the surface topography of PP and grafted PP films is significantly different. The PP film exhibits a smooth surface pattern free of defects and a surface roughness, R_a , equal to 21 nm. On the contrary, the surface of modified film is rougher ($R_a = 357$ nm) showing a pin-hole free, textured dense pattern, composed of a number of clusters distributed along the substrate in a ‘patchy’ fashion. The patches join together to form a continuous structure.

The transmitted light intensity measured through the surface modified PP film was 16% lower than the one measured through the neat PP film. The additional scattering arises from the enlarged surface roughness displayed by grafted films since crystalline fraction was not altered.

Figure 5 shows images of a water droplet on the surface of PP and grafted PP films. The liquid contact angles on both films were markedly different: $79.7 \pm 1.1^\circ$ for the PP film surface and $18.6 \pm 3.5^\circ$ for the PAA grafted surface. The smaller contact angle of water droplet on the surface grafted film indicates a stronger hydrophilicity nature on the surface given for grafting modification. This increase in the hydrophilicity and wettability is due to the presence of a hydrophilic grafted chain of the PAA and it is markedly increased by the electrostatic repulsion

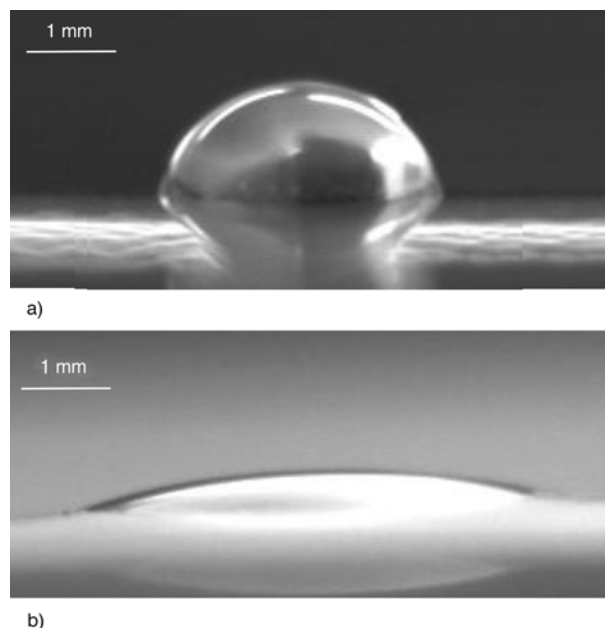


Figure 5. Pictures of typical sessile droplets found in contact angle experiments for PP (a) and surface modified PP (b) films

between the negatively charged carboxylic groups ($-\text{COO}^-$) present in the grafted chains.

3.2. Near surface mechanical properties

Depth sensing indentation experiments have been performed to characterize the mechanical properties of the near surface layer of the neat and grafted PP films. Typical curves are shown in Figure 6 while parameters obtained from indentation tests are shown in Figure 7 as a function of maximum applied load. The measured load-depth curves for the grafted films appeared widely scattered (Figure 6b) in contrast to the neat film traces. Reduced elastic modulus (Figure 7a) as well as hardness (Figure 7b) of PP and surface modified PP films are not dependent on penetration depth, which actually increased as the maximum load applied increased (Figure 7c).

The values of nanomechanical parameters of neat PP films are in coincidence with the ones reported in literature for other PP grades [49–51].

E_r and H values of the modified film correspond to the PAA grafted layer since the indentation depths achieved during the experiments were lower than the thickness of the grafted layer (Figures 7a to 7c). These values appeared widely scattered, but they were always larger than their homologues corresponding to neat films. The scattering arises from

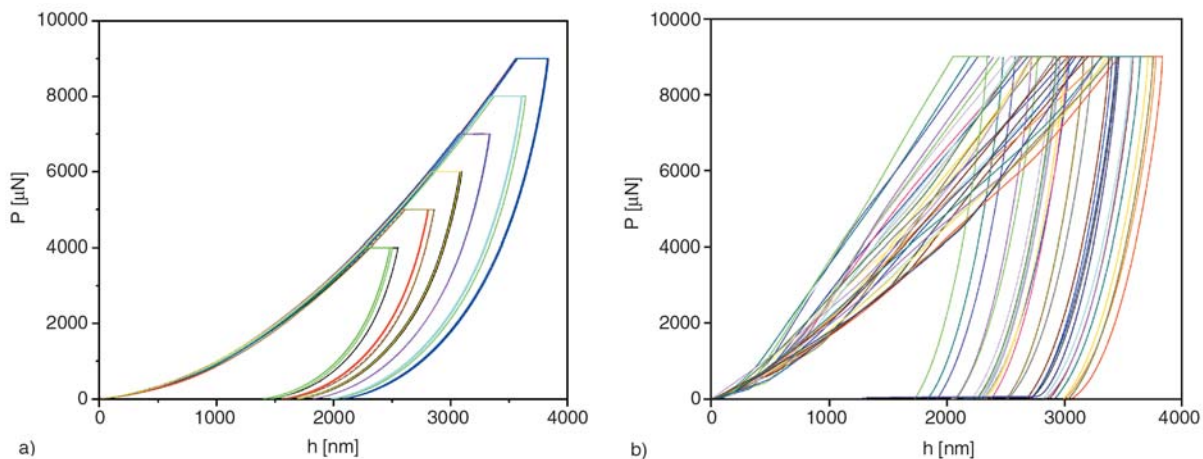


Figure 6. Typical load and depth curves obtained in indentation experiments for a) PP samples at different maximum applied loads and b) *smPP* samples at the same load

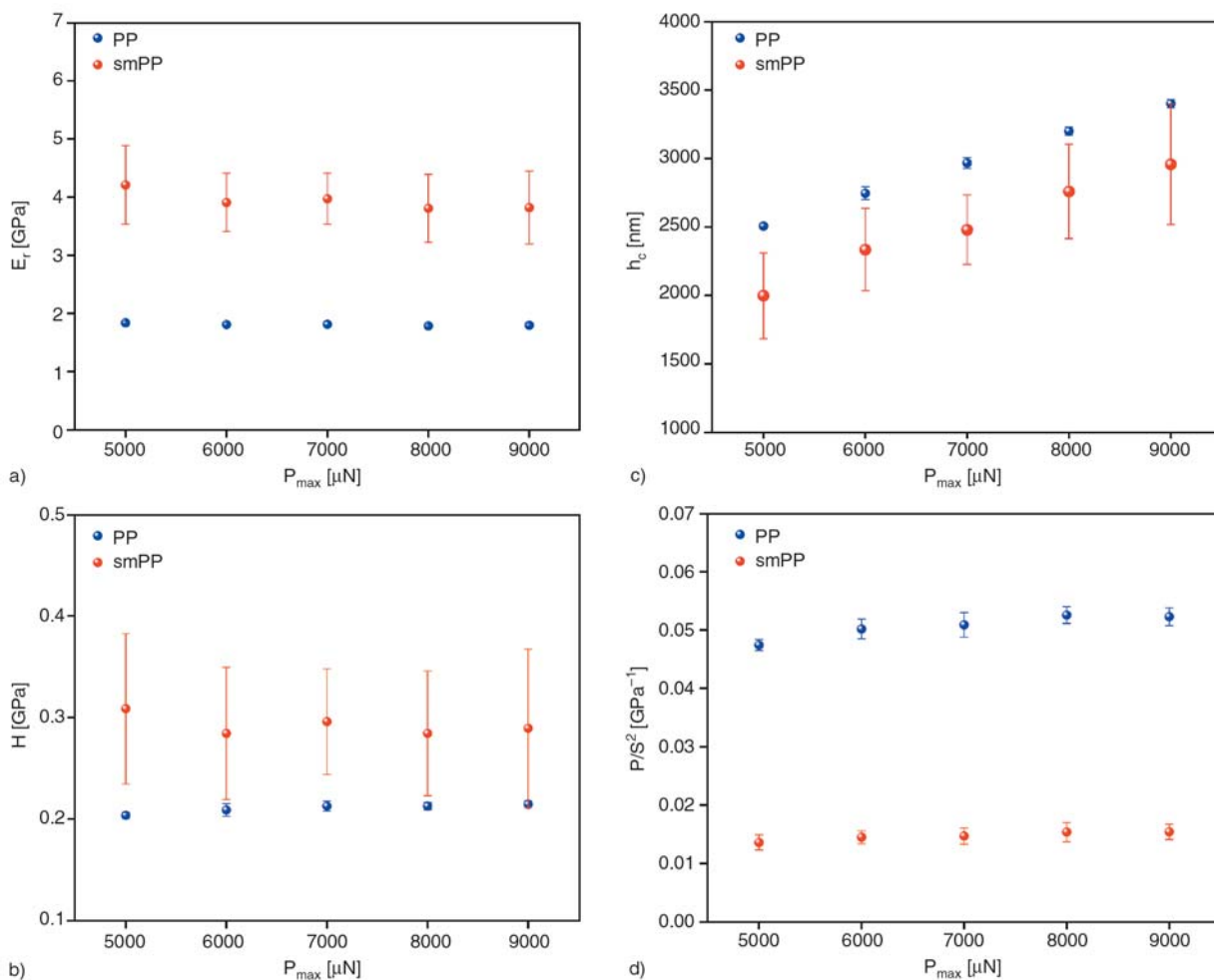


Figure 7. Reduced elastic modulus (a), universal hardness (b), contact depth (c) and P/S^2 (d) parameters arisen from nanoindentation experiments

the large surface roughness of the PAA layer, which was a consequence of the grafting process (see section 3.1.). It is well known that if the surface roughness is too large the actual penetration depth of the indenter may be smaller than the

sensed depth [52]. This yields large errors in the calculated contact area values (A_{max}), which generates a wide scattering in the parameters calculated through Equations (3) and (4) from multiple indents in a material. Note that as H is proportional

to $1/A_m$ and E_r is proportional to $1/A_{max}^{1/2}$, scattering in hardness values is wider than in elastic modulus values.

Joslin and Oliver [52] proposed an alternative method to analyze nanoindentation data for samples that are less than ideal surfaces. By combining Equations (4) and (5), it emerges that, according to Equation (9):

$$\frac{P_{max}}{S^2} \propto \frac{H}{E_r^2} \tag{9}$$

The ratio of the maximum load to the stiffness squared parameter, P_{max}/S^2 , is a mechanical property that describes material’s resistance to plastic deformation. When the indenter is forced a certain distance beyond the initial contact point, the interference between the indenter and the specimen is accommodated in two ways: elastic deformation and plastic (or permanent) deformation. For a given hardness, the lower the modulus, the greater the elastic accommodation and the smaller the permanent damage to the specimen when the indenter is removed. On the contrary, for a given modulus, if the hardness is increased, the plastic strain is reduced. The P_{max}/S^2 ratio is a directly measurable experimental parameter that is independent of the contact area provided the hardness and elastic modulus do not vary with depth.

Indentation data were re-analyzed following Equation (9) and plotted in Figure 7d. The scattering in the P_{max}/S^2 parameter is now negligible, confirming that the sole source of scattering is the large surface roughness of the surface modified PP film.

H/E_r^2 data determined for materials displaying different mechanical characteristics are plotted together versus the P_{max}/S^2 parameter in Figure 8. Note that the resistance to plastic deformation of the PAA layer falls close to the values displayed by amorphous glassy polymers, specially polymethylmethacrylate (PMMA). This result is consistent with the chemical similarity between PAA and PMMA and the extra stiffness usually shown by polymer brushes subjected to neighboring chains confinement [53].

From depth sensing indentation experiments it emerges that the graft amorphous PAA layer is stiffer, harder and more resistant to mechanical compression and indentation than the neat surface thanks to its glassy nature.

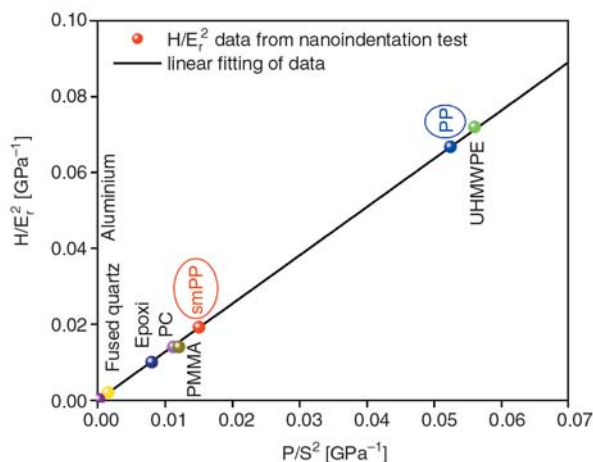


Figure 8. H/E_r^2 parameter for several materials tested by depth sensing indentation: Al (aluminum), Qz (fused Quartz), PC (polycarbonate), PMMA (polymethylmethacrylate), UHMWPE (ultra high molecular weight polyethylene)

3.3. Bulk mechanical properties and fracture behavior

Typical uniaxial tensile stress-strain curves are shown in Figure 9 while the derived uniaxial tensile parameters are listed in Table 1. PP and surface modified PP films showed the same behavior under uniaxial tensile deformation. In each curve the stress increases continuously with strain, showing only a change of slope near the yield point. As expected, films show themselves to be highly anisotropic displaying large differences in Young’s modulus and yield point between TD and MD directions. The recognition that molecular orientation produces important variations in the mechanical properties of polymers has long been established [54].

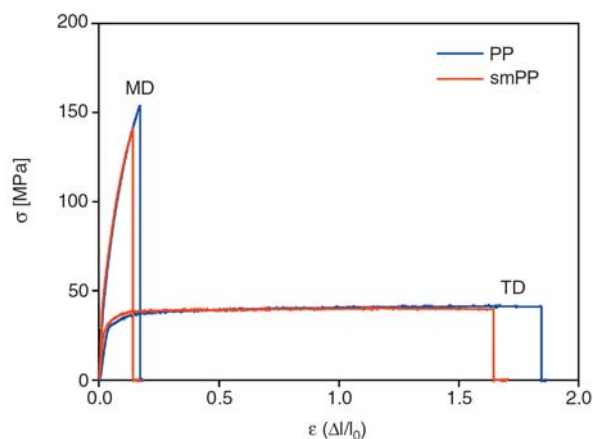
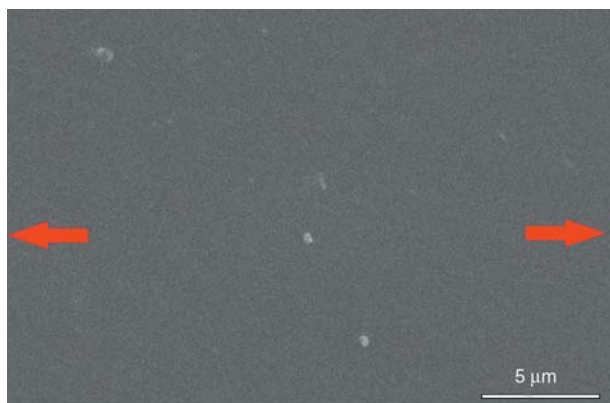


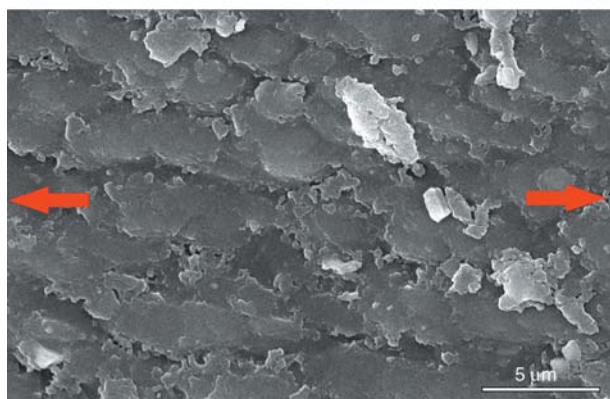
Figure 9. Typical stress-strain curves of PP and surface modified PP samples under uniaxial drawing

Table 1. Summary of bulk mechanical properties

Test		Uniaxial tensile		Fracture mechanics	Dart impact	
Parameter		E [GPa]	σ_y [MPa]	Jc [N/mm]	U/t [J/mm]	σ_d [GPa]
PP	MD	3.6 ± 0.8	35.6 ± 0.7	40.9 ± 1.1	32.1 ± 6.4	115.6 ± 17.9
	TD	1.1 ± 0.2	24.2 ± 0.7	20.3 ± 1.9		
smPP	MD	3.7 ± 0.2	34.3 ± 1.7	41.7 ± 2.8	30.6 ± 4.8	113.9 ± 23.9
	TD	1.2 ± 0.3	22.6 ± 2.6	22.6 ± 2.0		



a)



b)

Figure 10. SEM micrograph of uniaxial tensile deformed PP (a) and surface modified PP (b) samples. Red arrows indicate drawing direction.

SEM inspection of stretched surface modified PP samples (Figure 10) revealed that during deformation disruption of the clustered structure of the PAA-grafted layer occurred without transferring cracks to the substrate suggesting weak interactions between chains.

Typical load-displacement traces displayed by DENT samples are shown in Figure 11. Again, the feature of the curves depended on stretching direction but not on surface modification. All samples exhibited initially stable crack propagation followed by sudden unstable crack growth up to final fracture. The feature of the fracture surfaces in the stable propagation regime is illustrated in Figure 12. No striking differences are evidenced in

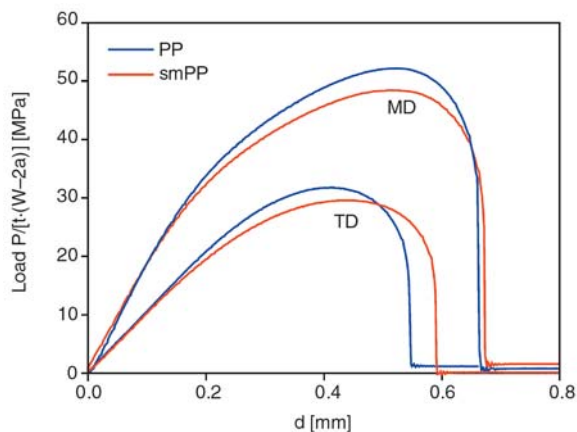
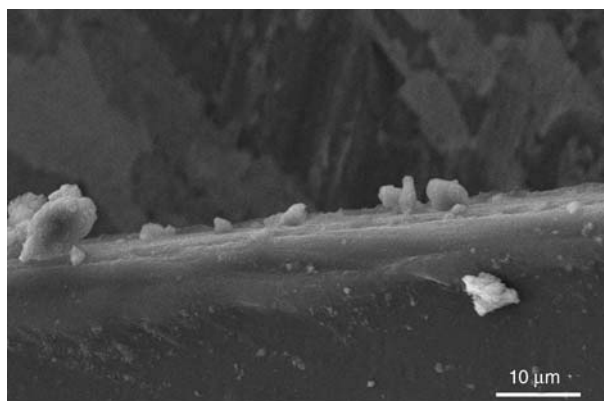
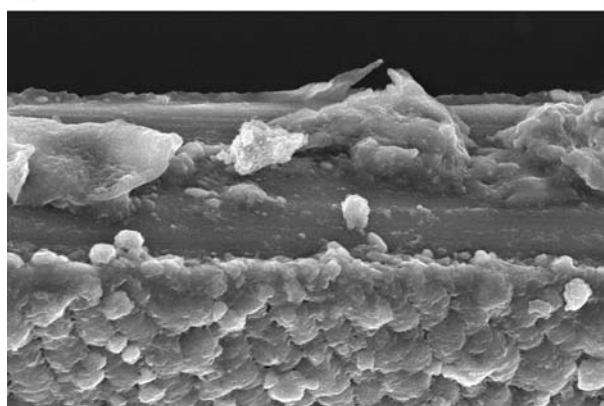


Figure 11. Typical normalized load vs. displacement curves of PP (a) and surface modified PP (b) DENT samples



a)



b)

Figure 12. SEM micrographs of fracture surfaces of PP (a) and surface modified PP (b) DENT samples tested in MD

both fracture surfaces. Fracture toughness parameters, J_c , reported in Table 1, show that the resistance to unstable propagation is twice when the crack propagates passing through the machine orientation direction (MD) than when it propagates along with it. The observed fracture behavior

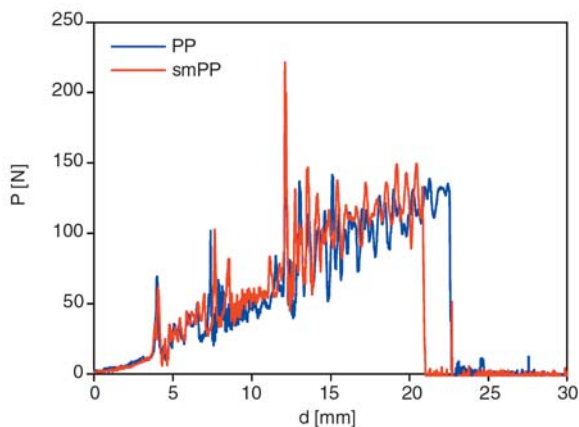


Figure 13. Typical load-displacement curves of PP (a) and surface modified PP (b) samples under biaxial impact deformation



a)



b)

Figure 14. Failure feature of PP (a) and surface modified PP (b) falling dart impacted specimens

reflects the imbalanced properties between the machine direction and the comparatively weak transverse direction.

Typical dart impact load-displacement curves are shown in Figure 13 while the derived dart impact properties are reported in Table 1. TOM images of the dart impacted region of PP and smPP specimens are shown in Figure 14. Both films behave in the same way exhibiting a semi-brittle fracture pattern as judged from the load deflection records characteristic (Figure 13) and the feature of the broken samples (Figure 14). Load-displacement curves dropped to zero instantaneously upon reaching the maximum load. A punch-like fractured surface with a punch-out-cap still attached to the specimen and two radial main cracks responsible for the final failure of the specimen are observed in the broken samples.

Both the fracture patterns and the derived parameters point out that the surface modification has not influenced the biaxial impact response of the neat PP film.

4. Conclusions

Through this paper a complete investigation of the mechanical response of surface modified polypropylene films by photo-grafting with acrylic acid was carried out. The principal findings are:

- the degree of grafting induced in the films was high enough to alter the topographical pattern and physico-chemical properties of the surface, such as roughness, wettability, hydrophilicity and transparency of PP films. Besides, the presence of specific functional groups offers the opportunity to use them as anchorage sites for further derivatization. They could be used to bond covalently specific organic molecules (dye, antimicrobial or antifungal drugs, etc.)
- the near surface indentation behaviour displayed by the grafted surface indicate that a glassy layer of PAA, which can be viewed as a sort of laminate was formed onto the PP surface.
- uniaxial deformation properties, fracture behavior and biaxial impact performance of the neat films were retained after chemical modification. It is evident that the mechanical response of surface modified film is governed only by PP resistance to deformation, thus, confirming the hypothesis that the PAA chains which were

strongly attached to the PP film, only interact among each other through the formation of physical entanglements and secondary bonds without constraining the PP surface.

- the beneficial original degree of molecular orientation of neat films was not altered after photo-grafting. This means that the UV-irradiation involved in the grafting procedure induces negligible cross-linking and degradation in the neat PP.

Acknowledgements

This work was financial supported by CONICET project number PIP 6253 and by ANPyCT Project number PICT 2004 N°25530.

References

- [1] Bhattacharya A., Misra B.: Grafting: A versatile means to modify polymers. Techniques, factors and applications. *Progress in Polymer Science*, **29**, 767–814 (2004).
- [2] Kwon O. H., Nho C. Y., Chen J.: Surface modification of polypropylene film by radiation-induced grafting and its blood compatibility. *Journal of Applied Polymer Science*, **88**, 1726–1736 (2003).
- [3] Chen H. J., Shi X. H., Zhu Y. F., Zhang Y., Xu J. R.: Polypropylene surface modification by entrapment of polypropylene-graft-poly(butyl methacrylate). *Applied Surface Science*, **254**, 2521–2527 (2008).
- [4] Xing, C-M., Deng J-P., Yang W-T.: Synthesis of antibacterial polypropylene film with surface immobilized polyvinylpyrrolidone-iodine complex. *Journal of Applied Polymer Science*, **97**, 2026–2031 (2005).
- [5] Xu Z-K., Dai Q-W., Wu J., Huang X-J., Yang Q.: Covalent attachment of phospholipid analogous polymers to modify a polymeric membrane surface: A novel approach. *Langmuir*, **20**, 1481–1488 (2004).
- [6] Yang J. M., Lin H. T., Wu T. H., Chen C. C.: Wettability and antibacterial assessment of chitosan containing radiation-induced graft nonwoven fabric of polypropylene-g-acrylic acid. *Journal of Applied Polymer Science*, **90**, 1331–1336 (2003).
- [7] Vartiainen J., Rättö M., Tapper U., Paulussen S., Hurme E.: Surface modification of atmospheric plasma activated BOPP by immobilizing chitosan. *Polymer Bulletin*, **54**, 343–352 (2005).
- [8] Lai J., Sunderland B., Xue J., Yan S., Zhao W., Folkard M., Michael B. D., Wang Y.: Study on hydrophilicity of polymer surfaces improved by plasma treatment. *Applied Surface Science*, **252**, 3375–3379 (2006).
- [9] Ciszewski A., Gancarz I., Kunicki J., Bryjak M.: Plasma-modified polypropylene membranes as separators in high-power alkaline batteries. *Surface and Coatings Technology*, **201**, 3676–3684 (2006).
- [10] Zhang P. Y., Rånby B.: Surface modification by continuous graft copolymerization. I. Photoinitiated graft copolymerization onto polyethylene tape film surface. *Journal of Applied Polymer Science*, **40**, 1647–1661 (1990).
- [11] Li Y., Desimone J. M., Poon C. D., Samulski E. T.: Photoinduced graft polymerization of styrene onto polypropylene substrates. *Journal of Applied Polymer Science*, **64**, 883–889 (1997).
- [12] Decker C., Zahouily K.: Surface modification of polyolefins by photografting of acrylic monomers. *Macromolecular Symposia*, **129**, 99–108 (1998).
- [13] Piletsky S. A., Matuschewski H., Schedler U., Wilpert A., Piletskaya E. V., Thiele T. A., Ulbricht M.: Surface functionalization of porous polypropylene membranes with molecularly imprinted polymers by photograft copolymerization in water. *Macromolecules*, **33**, 3092–3098 (2000).
- [14] Chun J., Cho S. M., Lee Y. M., Le H. K., Suh T. S., Shinn K. S.: Graft copolymerization of mixtures of acrylic acid and acrylamide onto polypropylene film. *Journal of Applied Polymer Science*, **72**, 251–256 (1999).
- [15] Ma H., Davis R. H., Bowman C. N.: A novel sequential photoinduced living graft polymerization. *Macromolecules*, **33**, 331–335 (2000).
- [16] Bamford C. H., Al-Lamee K. G.: Studies in polymer surface functionalization and grafting for biomedical and other applications. *Polymer*, **35**, 2844–2852 (1994).
- [17] Rieser T., Lunkwitz K., Meier-Haack J., Müller M., Cassel F., Dioszeghy Z., Simon F.: Surface modification of microporous polypropylene membranes by polyelectrolyte multilayers. *ACS Symposium Series*, **744**, 189–204 (2000).
- [18] Sciarratta V., Vohrer U., Hegemann D., Müller M., Oehr C.: Plasma functionalization of polypropylene with acrylic acid. *Surface and Coatings Technology*, **174–175**, 805–810 (2003).
- [19] Dogué L. J., Förch R., Mermilliod N.: Plasma-induced hydrogel grafting of vinyl monomers on polypropylene. *Journal of Adhesion Science and Technology*, **9**, 1531–1545 (1995).
- [20] Kato K., Uchida E., Kang E-T., Uyama Y., Ikada Y.: Polymer surface with graft chains. *Progress in Polymer Science*, **28**, 209–259 (2003).
- [21] Rånby B., Gao Z., Hult A., Zhang P.: Modification of polymer surfaces by photoinduced graft copolymerization. in ‘Chemical Reactions on Polymers’ (eds.: Benham J. L., Kinstle J. F.) *ACS Symposium Series*, Washington, vol 364. 168–186 (1988).
- [22] Naguib H. F., Aly R. O., Sabaa M. W., Mokhtar S. M.: Gamma radiation induced graft copolymerization of vinylimidazole-acrylic acid onto polypropylene films. *Polymer Testing*, **22**, 825–830 (2003).
- [23] Costamagna V., Wunderlin D., Larranaga M., Mondragón I., Strumia M.: Chemical modification of polyolefin films with acrylic acid as grafting agent. *Journal of Applied Polymer Science*, **102**, 2254–2263 (2006).

- [24] Costamagna V., Strumia M., López-González M., Riande E.: Gas transport in surface grafted polypropylene films with poly(acrylic acid) chains. *Journal of Polymer Science Part B: Polymer Physics*, **45**, 2421–2431 (2007).
- [25] Jagur-Grodzinski J.: *Heterogeneous modification of polymers: Matrix and surface reactions*. John Wiley and Sons, Chichester (1997).
- [26] Aliev R., Gracia P., Burillo G.: Graft polymerization of acrylic acid onto polycarbonate by the preirradiation method. *Radiation Physics and Chemistry*, **58**, 299–304 (2000).
- [27] Taher N. H., Dessouki A. M., Khalil F. H.: Radiation grafting of acrylic acid onto polypropylene films. *Radiation Physics and Chemistry*, **36**, 785–790 (1990).
- [28] Taher N., Hegazy E-S. A., Dessouki A. M., El-Arnaouty M. B.: Graft copolymers obtained by radiation grafting of methacrylic acid onto polypropylene films. *Radiation Physics and Chemistry*, **33**, 129–134 (1989).
- [29] Singh A., Silverman J.: *Radiation processing of polymers*. Hanser, Munich (1992).
- [30] Woods R. J., Pikaev A. K.: *Applied radiation chemistry: Radiation processing*. Wiley, New York (1994).
- [31] Briscoe B. J., Fiori L., Pelillo E.: Nano-indentation of polymeric surfaces. *Journal of Physics. D: Applied Physics*, **31**, 2395–2405 (1998).
- [32] Fischer-Cripps A. C.: A review of analysis methods for sub-micron indentation testing. *Vacuum*, **58**, 569–585 (2000).
- [33] Klapperich C., Pomvopoulos K., Pruitt L. A.: Nanomechanical properties of polymers determined from nanoindentation experiments. *Journal of Tribology*, **123**, 624–632 (2001).
- [34] Bull S. J.: Nanoindentation of coatings. *Journal of physics D: Applied Physics*, **38**, 393–413 (2005).
- [35] Ebenstein D. M., Pruitt L. A.: Nanoindentation of biological materials. *Nanotoday*, **1**, 26–33 (2006).
- [36] Frontini P. M.: Nanoindentation: An emerging technique for polymer surface mechanical characterization. *Express Polymer Letters*, **1**, 640 (2007).
- [37] Guthrie J. T., Huglin M. B., Phillips G. O.: Graft copolymerization to cellulose by mutual irradiation. *Journal of Polymer Science, Part C*, **37**, 205–219 (1972).
- [38] Kaith B. S., Kalia S.: Graft copolymerization of MMA onto flax under different reaction conditions: A comparative study. *Express Polymer Letters*, **2**, 93–100 (2008).
- [39] Battle R., Nerín C.: Application of single-drop microextraction to the determination of dialkyl phthalate esters in food simulants. *Journal of Chromatography A*, **1045**, 29–35 (2004).
- [40] Read J. C., Duncan B. E., Meyer D. E.: Birefringence techniques for the assessment of orientation. *Polymer Testing*, **4**, 143–164 (1984).
- [41] Bartczak Z., Martuscelli E.: Orientation and properties of sequentially drawn films of an isotactic polypropylene/hydrogenated oligocyclopentadiene blend. *Polymer*, **38**, 4139–4149 (1997).
- [42] Oliver W. C., Pharr G. M.: An improved technique for determining hardness and elastic modulus using load and displacement sensing indentation experiments. *Journal of Materials Research*, **7**, 1564–1583 (1992).
- [43] G'Sell C., Hiver J. M., Dahoun A., Souahi A.: Video-controlled tensile testing of polymers and metals beyond the necking point. *Journal of Materials Science*, **27**, 5031–5039 (1992).
- [44] Ward I. M., Hadley D. W.: Yielding and instability in polymers. in 'An introduction to the Mechanical Properties of Solid Polymers' (eds.: Ward I. M., Sweeney J.) John Wiley and Sons, Chichester, 241–272 (1993).
- [45] Grellmann W., Reincke K.: Quality improvement of elastomers – Application of instrumented notched tensile-impact testing for assessment of toughness. *Materialprüfung Jahrgang*, **46**, 168–175 (2004).
- [46] Bucknall C. B.: Characterizing toughness using empirical tests. in 'Polymer Blends' (eds.: Paul D. R, Bucknall C. B.) John Wiley and Sons, New York, vol 2. 59 (2001).
- [47] Jones D. P., Leach D. C., Moore D. R.: The application of instrumented falling weight impact techniques to the study of toughness in thermoplastics. *Plastics and Rubber Processing and Applications*, **6**, 67–75 (1986).
- [48] Sun D. C., Magill J. H.: Thermal interactions in oriented polymeric materials: Shrinkage, crystallization, and melting. *Polymer Engineering and Science*, **29**, 1503–1510 (1989).
- [49] Brun C., Delobelle P., Fromm M., Berger F., Chambaudet A., Jaffiol F.: Mechanical properties determined by nanoindentation tests of polypropylene modified by He+ particle implantation. *Materials Science and Engineering: A*, **315**, 63–69 (2001).
- [50] Lee S-H., Wang S., Pharr G. M., Xu H.: Evaluation of interphase properties in a cellulose fiber-reinforced polypropylene composite by nanoindentation and finite element analysis. *Composites Part A: Applied Science and Manufacturing*, **38**, 1517–1524 (2007).
- [51] Tranchida D., Piccarolo S.: Relating morphology to nanoscale mechanical properties: From crystalline to mesomorphic iPP. *Polymer*, **46**, 4032–4040 (2005).
- [52] Joslin D. L., Oliver W. C.: A new method for analyzing data from continuous depth-sensing microindentation tests. *Journal of Materials Research*, **5**, 123–126 (1990).
- [53] Huck W. T. S.: Effects of nanoconfinement on the morphology and reactivity of organic materials. *Chemical Communications*, 4143–4148 (2005).
- [54] Ward I. M., Hadley D. W.: *An introduction to the mechanical properties of solid polymers*. John Wiley and Sons, Chichester (1993).

Effect of extender oils on the stress relaxation behavior of thermoplastic vulcanizates

H. H. Le, Q. Zia, S. Ilisch, H. J. Radusch*

Martin Luther University Halle-Wittenberg, Center of Engineering Sciences, Chair Polymer Technology,
D-06099 Halle (Saale), Germany

Received 3 September 2008; accepted in revised form 23 September 2008

Abstract. The long term mechanical behavior of oil extended thermoplastic vulcanizates (TPV) based on polypropylene (PP) and acrylonitrile-butadiene rubber (NBR) has been characterized by means of stress relaxation experiments. The morphology of TPV and the phase specific oil distribution which depend on the content and type of oil as well as on the mixing regime have been characterized by means of Atomic Force Microscopy (AFM), Dynamic Mechanical Thermal Analysis (DMTA) and Differential Scanning Calorimetry (DSC). The discussion of the stress relaxation behavior was carried out using the two-component model, which allows splitting the initial stress into two components: a thermal activated stress component and an athermal one. A master curve was created by shifting the relaxation curves vertically and horizontally towards the reference curve. The vertical shift factor b_T is a function of the temperature dependence of the athermal stress components. It was found that the oil distribution strongly affects the athermal stress component which is related to the contribution of the structural changes, e.g. crystallinity of the PP phase and the average molecular weight between the cross-links of the NBR phase. From the temperature dependence of the horizontal shift factor a_T the main viscoelastic relaxation process was determined as the α -relaxation process of the crystalline PP phase. It is not dependent on the polarity and content of the oil as well as the mixing regime.

Keywords: polymer blends and alloys, thermoplastic vulcanizates, stress relaxation, extender oil

1. Introduction

Thermoplastic vulcanizates (TPV) are produced by melt mixing of an elastomer with a thermoplastic component and simultaneously but selective cross-linking of the elastomer phase during melt mixing. The resulting blend comprises a thermoplastic resin filled with a high concentration of dispersed rubber particles [1–3]. In order to improve the processability, reduce the material cost and enhance the performance of the end-use products, oil often has been added into thermoplastic vulcanizates. The addition of extender oil alters the viscoelastic properties of these heterogeneous thermoplastic vulcanizates significantly. Although the viscoelastic behavior of heterogeneous thermoplastic-rubber systems

was already investigated [4–7], the influence of the extender oil on the relaxation behavior of such systems was not sufficiently investigated so far.

In the present work the two-component model [8–10] was used to characterize the effect of extender oils on the stress relaxation behavior of TPV by correlating the structural features and the effect of oil content, polarity and distribution on it.

2. Experimental

2.1. Materials

NBR (Perbunan NT 3465, Bayer, Germany) with acrylonitrile content of 33% and iPP (Stamylan P14, Sabic, Germany) were used as elastomeric and

*Corresponding author, e-mail: hans-joachim.radusch@iw.uni-halle.de
© BME-PT and GTE

Table 1. Formulation of TPV-oil mixtures

Sample name	TPV content [wt%]	Oil content [wt%]	Oil type	Oil addition
TPV	100	0	–	–
A-N-10	90	10	Non-polar	Oil added after dynamic vulcanization process
A-N-20	80	20		
A-N-30	70	30		
A-P-10	90	10	Polar	Oil added after dynamic vulcanization process
A-P-20	80	20		
A-P-30	70	30		
B-P-10	90	10	Polar	Oil premixed into rubber phase before dynamic vulcanization process
B-P-20	80	20		
B-P-30	70	30		

thermoplastic components, respectively. The ratio of NBR to PP was kept 65 to 35. Phenolic resin (Vulkarensen PA 510, Vianova Resins, Germany) acted as cross-linking agent. Compatibilizer used was separately prepared by mixing 75 wt% maleic anhydride functionalized PP (Exxelor PO 1020, Exxon, Germany) and 25 wt% amine terminated NBR (Hycar ATNB 1300 X16, Goodrich, Germany). A polar oil (Enerdex 65, BP/Tudalen-65, H & R Group, Germany) having a freezing temperature of -37°C and polar bonds of 8 wt% and a non-polar oil (Enerpar 1927, BP/Tudalen-1927, H & R Group, Germany) having a freezing temperature of -63°C and polar bonds of 1.2 wt% were used, respectively. The formulations of polymer-oil mixtures are shown in Table 1.

2.2. Mixing regime and sample preparation

Thermoplastic vulcanizates were prepared using a double-rotor lab mixer (Plasticoder PL-2100, Brabender, Germany) with rotor speed of 65 rpm at a starting temperature of 180°C . The mixing regime is given in Table 2 and Table 3 for different mix-

Table 2. Mixing regime for A-N and A-P samples

Mixing time [min]	Ingredients
0	PP + Compatibilizer
2	NBR
4	Cross-linking agent
6	Non-polar oil (A-N samples) Polar oil (A-P samples)
12	Stop

Table 3. Mixing regime for B-P samples

Mixing time [min]	Ingredients
0	NBR
2	Polar oil
4	PP + Compatibilizer
7	Cross-linking agent
12	Stop

tures. After discharge from the mixer, all samples were compression molded at a temperature of 200°C and pressure of 70 bar to produce sheets of 0.3 mm thickness for stress relaxation experiments and 1 mm specimens for the other test methods.

2.3. Morphology characterization, thermal and mechanical testing

The phase morphology was investigated using an Atomic Force Microscope (Q-Scope 250, Quesant) under intermittent mode. The cantilever stiffness is 40 N/m and the resonance frequency nearly 170 kHz. Samples were cryo-cutted by means of a microtome (HM 360/CM 30, Microm) at -110°C with a diamond knife in order to get a smooth surface of the sample.

A heat flux calorimeter (DSC 820, Mettler Toledo) equipped with a liquid nitrogen cooling assembly was used to investigate the thermal behavior of the blends. Temperature range selected was from -80 to 180°C with a heating and cooling rate of 10 K/min.

Dynamic mechanical behavior was characterized using a dynamic mechanical analyzer (Qualimeter Eplexor 500 N, Gabo) in tensile mode at a frequency of 1 Hz at different temperatures ($-135^{\circ}\text{C} < T < 170^{\circ}\text{C}$) with a heating rate of 1 K/min.

Tensile tests of all the blends were carried out according to EN ISO 527 using a universal testing machine (Zwick 1425, Zwick/Roell) at room temperature. Dumbbell-shaped specimens were used with an initial length of 20 mm; the clamp distance was 50 mm. A crosshead speed of 50 mm/min was applied. Minimum five samples were tested.

For the determination of the residual strain after a hysteresis run, dumbbell-shaped specimens were used with the initial length of 20 mm. Samples

were strained with a crosshead speed of 50 mm/min to an elongation of 100%. For release, the same rate was used. The residual strain is a measure for the elastic behaviour.

Stress relaxation experiments were performed using a dynamic mechanical analyzer (DMTA Mark 3E, Rheometric Scientific) in tensile mode. The instrument was equipped with a temperature chamber enabling a long-term constancy of the temperature (deviation < 0.1 K). Relaxation curves for all the samples were recorded at a draw ratio of $\lambda = 1.5$ ($\epsilon = 50\%$) within the temperature range from 30 to 120°C over a period of 30 minutes to 15 hours depending on test temperature and oil content. The two-component model used in the

present study has been described in a previous work [4]. No steady state stress value was observed even after 15 hours. Therefore, an extrapolation method proposed by Li [11] was used to determine the athermal stress component σ_{∞} .

3. Results

3.1. Morphology characterization of oil extended TPV

The blend morphology and the phase specific oil distribution in TPV have been characterized using the AFM images and the DMTA results presented in Figure 1 and Figure 2. Figures 1a and 1b show the morphology of TPV filled with different oil

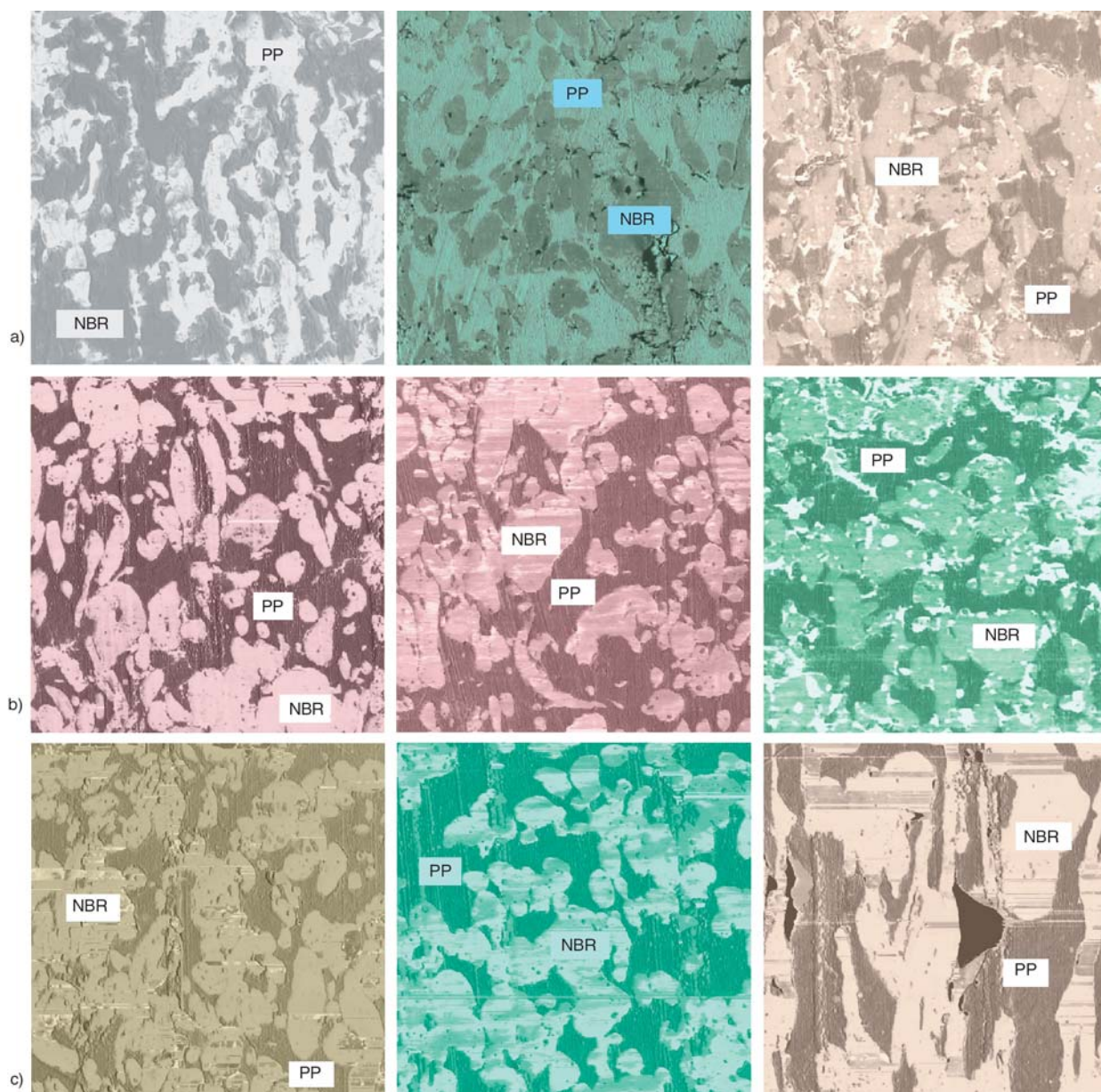


Figure 1. AFM images of different TPV: A-N-10, A-N-20 and A-N-30 (a), A-P-10, A-P-20 and A-P-30 (b), B-P-10, B-P-20 and B-P-30 (c), image size 20 $\mu\text{m} \times 20 \mu\text{m}$

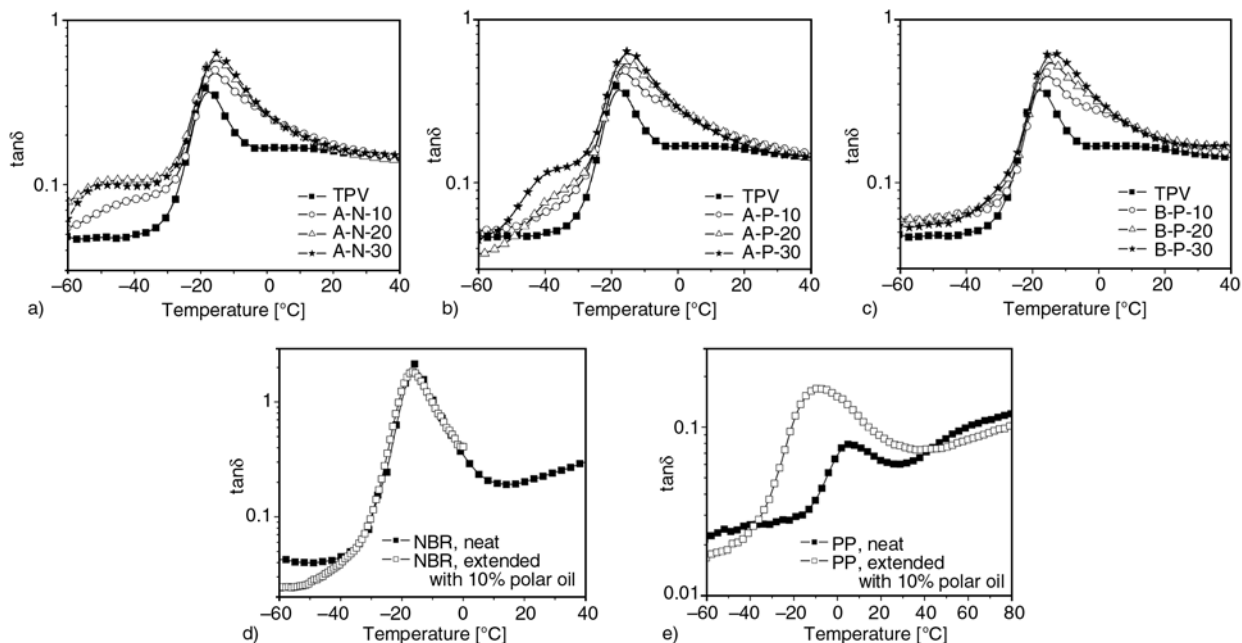


Figure 2. Temperature dependence of the loss factor $\tan\delta$ for A-N (a), A-P (b), B-P (c), NBR (d) and PP (e)

contents added after the dynamic vulcanization process. Both in series A-N and A-P the size of the rubber domains is enlarged with increasing oil content. The added oil first accumulates in the PP matrix and then migrates into the rubber domains during the mixing process. It is worth to note that the NBR phase was cross-linked before oil addition, thus the cross-linking density of the NBR phase is not influenced by the oil immigration. At higher oil content of 30 wt% a bright phase is observed in the AFM micrographs which is related to a neat oil phase. This can be proved by taking into account the DMTA results. The temperature dependence of the loss factor $\tan\delta$ of the series A-N and A-P is presented in Figures 2a and 2b. The neat TPV shows the characteristic NBR α -peak at -18°C and a shoulder for the β -relaxation of PP at about 8°C . Additionally, the oil extended TPVs show each a shoulder at lower temperatures of about -37 to -50°C . These shoulders are related to the oil phase. The magnitude of the loss factor in this region increases with rising oil content. It is observed, that the peak of the rubber phase slightly shifts to higher temperatures with enhanced oil content. That can be explained as follows: The oil present in the rubber domains actually does not influence the position of the rubber peak as shown in Figure 2d, but the oil present in the PP matrix shifts the β -peak of PP toward lower temperatures (Figure 2e). This peak overlaps the peak of the rub-

ber phase. As a result the rubber peak seems to shift towards higher temperatures.

When the oil is pre-mixed with rubber before the dynamic vulcanization process takes place, the rubber domains are comparatively large as seen in Figure 1c. The reason for this is the presence of oil in the rubber phase. The oil can hinder the vulcanization reaction and reduce the crosslink density [12] and thus the development of a fine dispersed rubber phase. At oil contents of 20 and 30 wt% a co-continuous phase morphology is observed, and no separate oil phase is visible in the AFM images (Figure 1c). Looking at the curve of the loss factor presented in Figure 2c, it is obvious that the peak of the oil is disappeared. Although the oil was pre-mixed only in the rubber phase, it is interesting to see that there is an effect caused by the oil-modified PP phase. The relaxation peak of rubber in the system B-P shifts to higher temperatures due to the overlapping with the β -PP peak. It can be concluded, that the oil pre-mixed in the rubber phase diffused partly into the amorphous PP phase during the compounding process.

As shown in our previous work [4], the stress relaxation behavior is strongly determined by the crystalline phase of TPV. Using DSC the crystallization temperature T_c , melting temperature T_m , and degree of crystallinity X_c of the PP phase in TPV were investigated and the results are summarized in Table 4. T_c and T_m of PP in TPV decrease with

Table 4. Degree of crystallinity and thermal parameters of TPV investigated

Sample name	X _c [%]	T _c [°C]	T _m [°C]
TPV	17.8	124	163
A-N-10	15.9	117	158
A-N-20	13.4	114	155
A-N-30	12.8	112	152
A-P-10	14.9	117	157
A-P-20	14.1	113	155
A-P-30	13.2	110	152
B-P-10	16.6	117	161
B-P-20	15.0	108	158
B-P-30	14.6	104	157

gradual incorporation of oil. Oil polarity, content and distribution in TPV affect the extent to which the *T_c* and *T_m* of PP drop down. Crystallinity is also diminished with the increasing amount of oil. The presence of oil and rubber domains affects the crystallinity of these vulcanizates by influencing the perfection of the growing iPP crystals. Similar findings were reported by other researchers [13].

3.2. Short term mechanical behavior

Figure 3a shows a comparison between the stress-strain behavior of TPV containing different types and contents of oil added after the dynamic vulcanization process. The presence of oil in the rubber and/or matrix phase significantly affects the mechanical properties [14]. The values of both stress and strain at break are reduced with increasing oil content as compared to neat TPV. Both A-N and A-P samples show a comparable behavior due to the presence of similar crystalline thermoplastic and cross-linked rubber phases.

For B-P samples in which oil was pre-mixed in the rubber phase the slope of the stress-strain curves in the range of larger deformations is strongly reduced. This feature is typical for the TPV with a low cross-linking density of the elastomer phase [15]. As discussed above, the decrease of the cross-linking density is caused by the presence of oil in the NBR phase (Figure 3b).

The residual strain as a measure for the elastic behavior of the TPVs investigated was characterized by hysteresis tests. As shown in Figure 4, a good strain recovery was observed for the A-N and A-P samples with increasing oil content due to the reduced crystallinity of the TPV. In contrast, the residual strain of B-P samples increases with rising oil content mainly due to the decreased crosslink density.

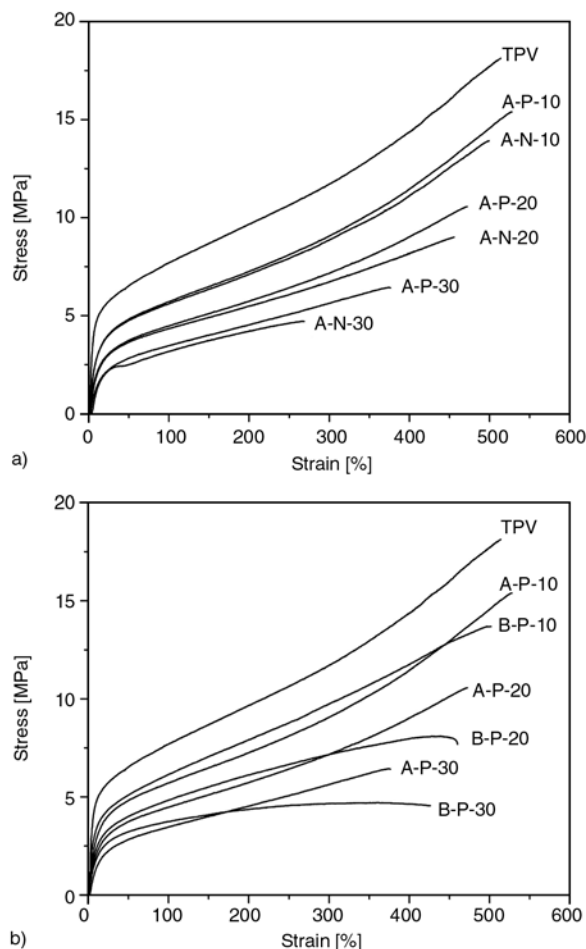


Figure 3. Stress-strain behavior of neat and oil extended TPV, A-P compared with A-N (a), A-P compared with B-P (b)

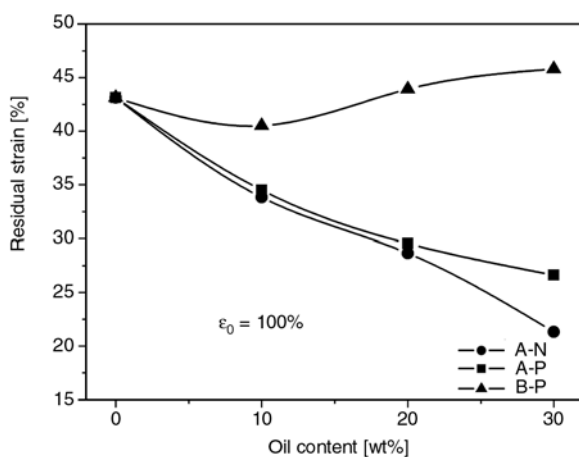


Figure 4. Residual strain measured from hysteresis experiments

3.3. Stress relaxation behavior

3.3.1. Stress relaxation behavior of neat TPV

In our previous work the stress relaxation behavior of neat TPV has already been studied using the

two-component model [4]. To evaluate the relaxation curve, the applied stress σ is separated into two components, a relaxing stress component $\Delta\sigma$ and a non-relaxing stress component σ_∞ according to Equation (1) [8–10]:

$$\sigma(t) = \Delta\sigma(t) + \sigma_\infty \quad (1)$$

According to Seeger [8] the relaxing stress component $\Delta\sigma(t)$ is called thermal stress component, because it acts on short-range obstacles, which can be overcome by stress aided thermal activation. It depends on the plastic deformation rate $\dot{\epsilon}$ and the temperature T according to Eyring’s rate theory [9]. In contrast to the relaxing stress component, the non-relaxing stress component σ_∞ is called athermal stress component. σ_∞ is originated from long-range stress fields, which cannot be overcome by thermal activation.

Figure 5a shows the stress relaxation behavior of neat TPV measured at different temperatures. With increasing temperature the relaxation curves shift horizontally to shorter times and vertically to lower

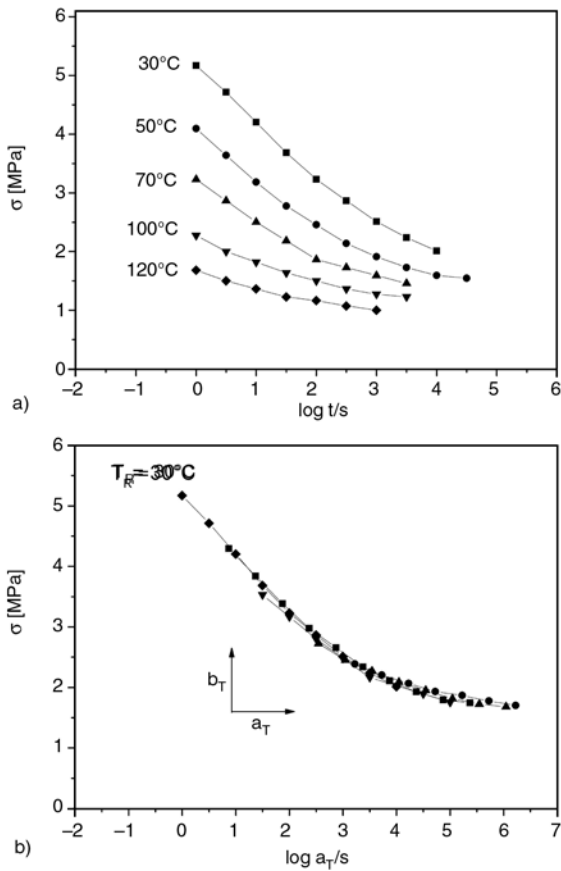


Figure 5. Stress relaxation curves of neat TPV measured at different temperatures (a) and master curve created by vertical and horizontal shift procedure (b)

stress. The horizontal shift is caused by a reduction of the thermal stress component $\Delta\sigma$ and the vertical shift of the relaxation curves originates from a linear decrease of the athermal stress component σ_∞ [16].

The procedure for creation of a master curve as described in our previous work [4] consists of a vertical and a horizontal shift of the curves to the reference curve measured at the reference temperature $T_R = 30^\circ\text{C}$. The vertical shift factor b_T is determined by the temperature dependence of the athermal stress component as shown in Equation (2):

$$b_T = \sigma_\infty(T_R) - \sigma_\infty(T) \quad (2)$$

The master curve for a reference temperature of 30°C determined from the experimental results is shown in Figure 5b. A very good fit is observed for the experimental data.

In Figure 6 the temperature dependence of the horizontal and vertical shift factor of the neat TPV is presented. The temperature dependence of the horizontal shift factors a_T follows the Arrhenius approach corresponding to Equation (3):

$$\log a_T = A + \frac{0.43E_A}{RT} \quad (3)$$

The Arrhenius diagram (Figure 6a) shows a straight line at temperatures between 30 and 120°C that means that only one relaxation process takes place in the investigated temperature range. From the slope of the line an activation energy of $E_A = 90 \text{ kJ/mol}$ was calculated. This activation energy is close to the activation energy of the α -relaxation process of the crystalline PP phase measured in this temperature range determined in our previous work ($E_A = 110 \text{ kJ/mol}$) [4, 16] and to the corresponding results in the literature (107–150 kJ/mol) [17].

In Figure 6b the temperature dependence of the vertical shift factor b_T determined by the athermal stress component is presented as a straight line. The larger the slope, the more strongly the relaxation curve shifts vertically to lower stresses at increasing temperature. It is obvious that the athermal stress component σ_∞ consists of two contributions, namely, σ_∞^{PP} and σ_∞^{NBR} . As discussed in [4, 16, 18, 19], the decrease of the athermal stress component σ_∞^{PP} of the PP phase with increasing temperature

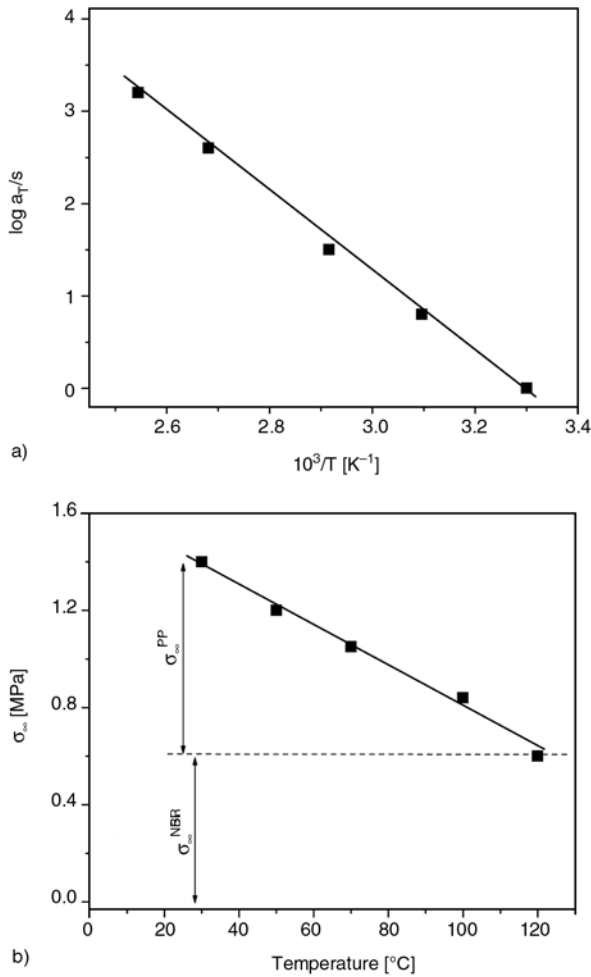


Figure 6. Temperature dependence of the horizontal shift factor a_T (a) and athermal stress component σ_∞ of neat TPV (NBR/PP = 65/35) (b)

relates to the temperature dependent structural changes of the crystalline network of the PP phase. The shape of network points created by the PP lamella changes due to the slippage process of the PP lamella which is accelerated at higher temperatures. The athermal stress contribution of the crystalline PP phase σ_∞^{PP} decreases linearly and becomes zero at 120°C. Thus, the value of the athermal stress component σ_∞ at this temperature is determined only by the contribution of the rubber phase. The athermal stress component σ_∞^{NBR} of the NBR phase is caused by the deformation of the chemical network made by the cross-link points. It increases with increasing temperature according to the entropy elasticity theory described in Equation (4) [20]:

$$\sigma_\infty^{NBR} = (\lambda - \lambda^{-2}) \cdot E_\infty^{NBR} = (\lambda - \lambda^{-2}) \cdot \frac{3\rho kT}{M_C^{NBR}} \quad (4)$$

In Equation (4) the rubber elastic modulus E_∞^{NBR} is calculated from the athermal stress component σ_∞^{NBR} and the draw ratio λ . It depends also on the density ρ , the Boltzmann constant k , the absolute temperature T and the average molecular weight between the crosslinks M_C^{NBR} . In comparison to the big change of σ_∞ the temperature dependent change of σ_∞^{NBR} can be considered as insignificant.

3.3.2. Stress relaxation behavior of oil extended TPV

The oil effect on the stress relaxation behavior of TPV can be discussed structurally by two quantities: the activation energy E_A and the athermal stress component σ_∞ . They characterize two different temperature-dependent processes, i.e. the viscoelastic processes and the temperature dependent structural changes.

The temperature dependence of the horizontal shift factor a_T of all oil extended TPV can be described only by one straight line as shown in Figure 7. From the slope of the straight line an activation energy of 87 kJ/mol was calculated, which displays the α -relaxation process of the crystalline PP phase as the main viscoelastic deformation process taking place during the relaxation experiment and it does not depend on the oil content, its polarity and distribution in TPV.

The effect of oil addition on the athermal stress component for all systems is presented in Figure 8 at two test temperatures 30 and 120°C. As discussed in our previous works [4, 16] at high temperatures, e.g. 120°C, σ_∞^{PP} becomes zero, thus, only

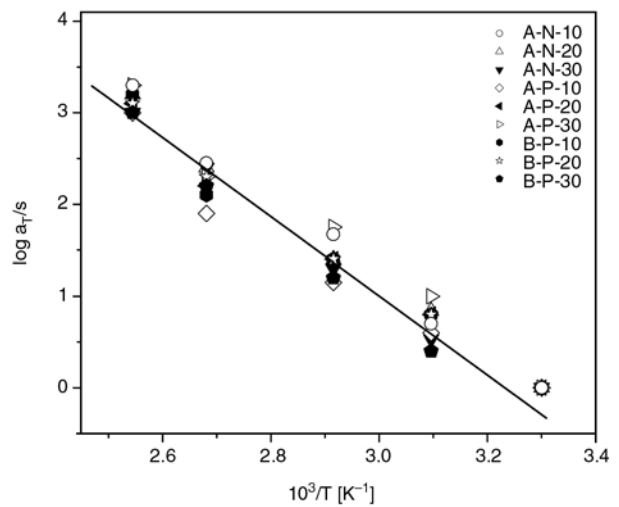


Figure 7. Temperature dependence of the horizontal shift factor a_T of oil extended TPV

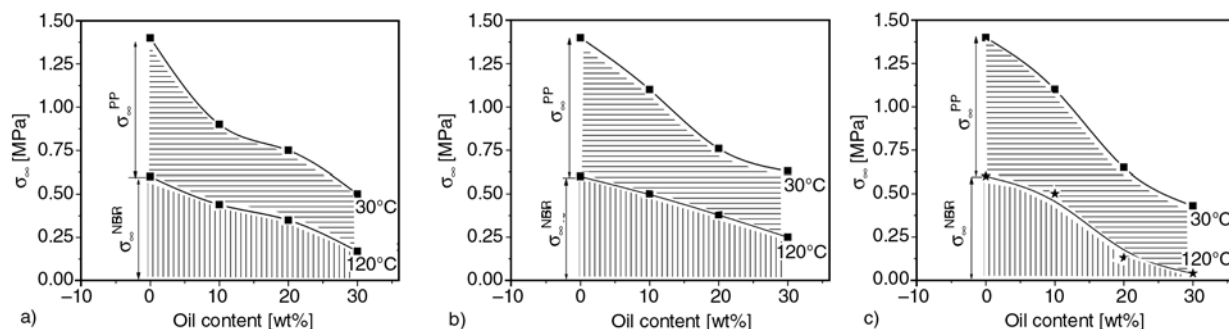


Figure 8. Effect of oil content on the athermal stress component σ_{∞} for A-N (a), A-P (b) and B-P (c) samples at different temperatures

the cross-linked rubber phase contributes to the athermal stress component. As a result, we can distinguish the contribution of the PP phase and NBR phase in dependence on the oil content as shown in Figures 8a, 8b and 8c for three systems. It is obvious that in all systems both athermal stress components σ_{∞}^{PP} and σ_{∞}^{NBR} decrease differently with the oil addition. Because the athermal stress component is directly determined by the cross-link state, an attempt has been done in order to determine the average molecular weight between two crosslinks M_C^{PP} and M_C^{NBR} for both phases according to Equation (4). The calculated M_C^{PP} and M_C^{NBR} in dependence on the oil content for three systems are presented in Figure 9.

For the PP phase, the average molecular weight between two crosslinks (lamellae) M_C^{PP} of the three systems increased with increasing oil content. Due to the oil immigration process in all systems oil was always present in the PP phase regardless of the different mixing regime. Oil existent in PP swells the PP phase to a larger volume on the one hand, and

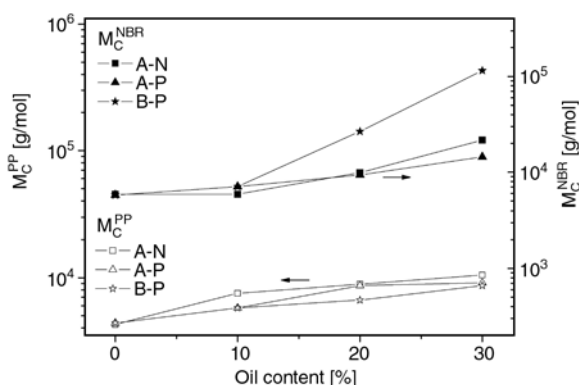


Figure 9. Average molecular weight between two crosslinks M_C^{PP} and M_C^{NBR} of the PP and NBR phase, respectively, in dependence on the oil content

on the other hand oil causes a slight decrease of the crystallinity X_C (Table 4). The decrease of X_C leads to a reduction of crystalline cross-links (lamellae) in the PP phase that also contributes to the increase of M_C^{PP} . Only a minor difference between M_C^{PP} of the three systems is observed. That means the quantity of oil in the PP phase seems to be the same.

In the systems A-N and A-P the oil addition does not affect the dynamic vulcanization process and thus the average molecular weight between two chemical cross-links M_C^{NBR} of the NBR phase. However, the calculated M_C^{NBR} of the three systems increases with increasing oil content in different manner (Figure 9). Thus is worth to note that the calculated M_C^{NBR} is not a true value but only an apparent one. That is related to the fact that the oil is homogeneously and finely dispersed in the rubber domains and thus the oil extended rubber domains are considered as a uniform phase having a larger volume compared to the non-extended rubber phase. For an oil extended rubber compound a true M_C can be determined by use of the extraction experiment when oil is extracted from the compound [21]. Using Equation (4) only an apparent M_C is calculated and it often differs from the true value [22]. In Figure 9 the similar increase of M_C^{NBR} in these systems is related to the swelling effect of the oil present in the NBR phase. A strong increase of M_C^{NBR} in the system B-P was observed at an oil content of more than 10%. Beside the swelling effect of the added oil the ineffective cross-link reaction of the NBR phase in presence of the oil is the main reason for the high value of M_C^{NBR} . That leads accordingly to the diminishment of the athermal stress component σ_{∞}^{NBR} in the system B-P (Figure 8c).

4. Conclusions

In the present work the stress relaxation behavior of the oil extended thermoplastic vulcanizates (TPV) has been characterized by means of the two-component model which allows splitting the initial stress into two components: a thermal activated stress component and an athermal one. It was found that the oil distribution strongly affects the athermal stress component which is related to the contribution of the structural changes, e.g. crystallinity of the PP phase and the average molecular weight between two cross-links of the NBR phase. A master curve was created by shifting the relaxation curves vertically and horizontally towards the reference curve. The vertical shift factor b_T is determined from the temperature dependence of the athermal stress component. From the temperature dependence of the horizontal shift factor a_T the main viscoelastic relaxation process was determined as the α -relaxation process of the crystalline PP phase, which is not dependent on the polarity and content of the oil as well as the mixing regime.

Acknowledgements

The authors gratefully acknowledge the financial support by Deutsche Forschungsgemeinschaft (DFG).

References

- [1] Coran A. Y., Patel R. P.: Rubber-thermoplastic compositions. Part I. EPDM-polypropylene thermoplastic vulcanizates. *Rubber Chemistry and Technology*, **5**, 141–150 (1980).
- [2] Xiao H. W., Huang S. Q., Jiang T.: Morphology, rheology, and mechanical properties of dynamically cured EPDM/PP blend: Effect of curing agent dose variation. *Journal of applied Polymer Science*, **92**, 357–362 (2004).
- [3] Babu R. R., Singha N. K., Naskar K.: Studies on the influence of structurally different peroxides in polypropylene/ethylene alpha olefin thermoplastic vulcanizates (TPVs). *Express Polymer Letters*, **2**, 226–236 (2008).
- [4] Le H. H., Lüpke T., Pham T., Radusch H-J.: Time dependent deformation behavior of thermoplastic elastomers. *Polymer*, **40**, 4589–4597 (2003).
- [5] Long D., Sotta P.: Stress relaxation of large amplitudes and long timescales in soft thermoplastic and filled elastomers. *Rheologica Acta*, **46**, 1029–1044 (2007).
- [6] Baeurle S. A., Hotta A., Gusev A. A.: A new semi-phenomenological approach to predict the stress relaxation behavior of thermoplastic elastomers. *Polymer*, **46**, 4344–4354 (2005).
- [7] Asaletha R., Bindu P., Aravind I., Meera A. P., Val-saraj S. V., Yang W., Thomas S.: Stress-relaxation behavior of natural rubber/polystyrene and natural rubber/polystyrene/natural rubber-graft-polystyrene blends. *Journal of Applied Polymer Science*, **198**, 904–913 (2008).
- [8] Seeger A.: *Handbuch der Physik*. Springer, Berlin (1958).
- [9] Krausz A. S., Eyring H.: *Deformation kinetics*. Wiley, New York (1975).
- [10] Ferry J. D.: *Viscoelastic Properties of polymers*. Wiley, New York (1980).
- [11] Li J. C. M.: Dislocation dynamics in deformation and recovery. *Canadian Journal of Physics*, **45**, 493–509 (1967).
- [12] Le H. H., Prodanova I., Ilisch S., Radusch H-J.: Online electrical conductivity as a measure to characterize the carbon black dispersion in oil containing rubber compounds with a different polarity of rubber. *Rubber Chemistry and Technology*, **77**, 815–829 (2004).
- [13] Yang Y., Chiba T., Saito H., Inoue T.: Physical characterization of a polyolefinic thermoplastic elastomer. *Polymer*, **39**, 3365–3372 (1998).
- [14] Baranov A. O., Erina N. A., Medintseva T. I., Kuptsov S. A., Prut E. V.: The influence of the interphase layer on the properties of isotactic polypropylene/ethylene-propylene rubber blends. *Polymer Science, Series A*, **43**, 1177–1183 (2001).
- [15] Huy T. A.: *Rheo-optische Charakterisierung des Deformationsverhaltens dynamischer Vulkanisate*. PhD Thesis, Martin Luther University Halle-Wittenberg, Germany (1999).
- [16] Le H. H.: *Spannungsrelaxationsuntersuchungen zur Charakterisierung des zeitabhängigen Deformationsverhaltens thermoplastischer Elastomere*. PhD Thesis, Martin Luther University Halle-Wittenberg, Germany (2002).
- [17] Brandrup J., Immergut E. H.: *Polymer handbook*. Wiley, New York (1989).
- [18] Shapery R. A.: On the characterization of nonlinear viscoelastic materials. *Polymer Engineering and Science*, **9**, 295–310 (1969).
- [19] Boyd R.: Relaxation processes in crystalline polymers: Experimental behaviour -A review. *Polymer*, **26**, 323–347 (1985).
- [20] Treloar L. R. G.: *The physics of rubber elasticity*. Clarendon Press, Oxford (1975).
- [21] Flory P. J.: *Principles of polymer chemistry*. Cornell University Press, Ithaca, New York (1953).
- [22] Ilisch S., Menge H., Radusch H-J.: Vernetzungsausbau an konventionellen und dynamischen Vulkanisaten. *Kautschuk und Gummi Kunststoffe*, **53**, 206–212 (2000).

Low frequency dielectric relaxation processes and ionic conductivity of montmorillonite clay nanoparticles colloidal suspension in poly(vinyl pyrrolidone)-ethylene glycol blends

R. J. Sengwa*, S. Choudhary, S. Sankhla

Dielectric Research Laboratory, Department of Physics, J N V University, Jodhpur – 342005, India

Received 22 August 2008; accepted in revised form 26 September 2008

Abstract. The dielectric dispersion behaviour of montmorillonite (MMT) clay nanoparticles colloidal suspension in poly(vinyl pyrrolidone)-ethylene glycol (PVP-EG) blends were investigated over the frequency range 20 Hz to 1 MHz at 30°C. The 0, 1, 2, 3, 5 and 10 wt% MMT clay concentration of the weight of total solute (MMT+PVP) were prepared in PVP-EG blends using EG as solvent. The complex relative dielectric function, alternating current (ac) electrical conductivity, electric modulus and impedance spectra of these materials show the relaxation processes corresponding to the micro-Brownian motion of PVP chain, ion conduction and electrode polarization phenomena. The real part of ac conductivity spectra of these materials obeys Jonscher power law $\sigma'(\omega) = \sigma_{dc} + A\omega^n$ in upper frequency end of the measurement, whereas dispersion in lower frequency end confirms the presence of electrode polarization effect. It was observed that the increase of clay concentration in the PVP-EG blends significantly increases the ac conductivity values, and simultaneously reduces the ionic conductivity relaxation time and electric double layer relaxation time, which suggests that PVP segmental dynamics and ionic motion are strongly coupled. The intercalation of EG structures in clay galleries and exfoliation of clay sheets by adsorption of PVP-EG structures on clay surfaces are discussed by considering the hydrogen bonding interactions between the hydroxyl group (–OH) of EG molecules, carbonyl group (C=O) of PVP monomer units, and the hydroxylated aluminate surfaces of the MMT clay particles. Results suggest that the colloidal suspension of MMT clay nano particles in the PVP-EG blends provide a convenient way to obtain an electrolyte solution with tailored electrical conduction properties.

Keywords: nanocomposites, PVP-EG blend, MMT clay colloidal suspension, dielectric spectroscopy, electrical conductivity

1. Introduction

Miscibility of PVP with EG solvent is related to the formation of hydrogen bonds (H-bond) between carbonyl groups (C=O) of the repeating units of the PVP chain and hydroxyl groups (–OH) of the EG molecules. The PVP-EG complexation results the breaking of some of the H-bonded self-associated EG structures. It was confirmed that no more than 27 EG molecules bearing 54 hydroxyl groups involve themselves in complex formation per 100 monomer units of PVP molecules [1], which shows the presence of uncomplexed H-bonded pure EG

structures in the PVP-EG blends. The pressure-sensitive adhesive properties of PVP-EG blends find its extensive use as a reservoir vehicle controlling the rate of drug delivery [2, 3]. Besides the other parameters, in general, the rate of drug release in polymeric blend matrix depends on the polymer chain dynamics [3] and ionic conduction process [4]. The loading of MMT clay in hydrophilic polymer matrix enhances its potential application in medicine and pharmacy [5] and also in electrolytes [6–9].

*Corresponding author, e-mail: rjsengwa@rediffmail.com
© BME-PT and GTE

The polymeric grade MMT clay is 2:1 phyllosilicate, which is also called inorganic polymer, and chemically it is a metal silicate [10]. The dispersion of small amount of MMT clay in a suitable polymeric solvent has swelling properties. Swelling of the clay is mainly due to solvent intercalation (absorption) in the clay galleries, and also because of the adsorption of solvent molecules on the hydroxylated aluminate clay surfaces through H-bond interactions, which results the clay exfoliation. The intercalated and exfoliated clay sheets in polymeric solvent results the organic-inorganic nanocomposites of highly complicated structures, which is responsible for the improved thermal, mechanical, gas barrier and electrical properties of the polymer-clay nanocomposites (PCNs) [6–18]. The investigation of broadband dielectric spectroscopy (BDS) of the materials covers nowadays the extraordinary spectral range from 10^{-6} to 10^{12} Hz [19]. The BDS frequency ranges from 10^{-1} to 10^{-3} Hz and 10^{-4} to 10^{-6} Hz are denoted by very low and ultra low (quasi-dc) spectrums respectively, whereas $\sim 10^0$ – 10^4 Hz, $\sim 10^5$ – 10^7 Hz and $\sim 10^8$ – 10^{12} Hz are known as low frequency, middle frequency and high frequency spectrums, respectively. The BDS characterization of the dielectric materials provide the confirmative information on the intra- and intermolecular dynamics, the degree of intermolecular H-bond interactions, cooperativity between guest and host molecules, and ionic and electrode polarization processes related to the molecular structures [19, 20]. The BDS study of PVP-EG blends over the frequency range 20 Hz to 20 GHz are described by the sum of three relaxation processes with the contribution of dc conductivity [21]. The low frequency process (l-process) for PVP-EG blends is caused by electrode polarization and ionic conduction phenomena [21–24]. The middle frequency process (m-process) is observed corresponding to the micro-Brownian motion (local chain motion) of the PVP chain, whose time is of the order of about 10^{-6} s [21, 22]. The repeat unit of PVP has a bulky pyrrolidone ring as side group that the local chain motion need a large free volume and has large hindrance to its motion. The high frequency process (h-process) of the PVP-EG blends in the microwave frequency region occurs due to reorientation of EG molecules, which takes the duration of approximately 10^{-9} s [21, 25–27].

In this paper, we study the dielectric spectroscopy over the frequency range 20 Hz to 1 MHz of montmorillonite (MMT) clay colloidal suspension in the PVP-EG blend. The objective of present paper is to confirm the effect of clay concentration on the PVP micro-Brownian motion, and ionic conductivity and electrode polarization relaxation processes in the MMT clay loaded PVP-EG blends. All the intensive quantities, namely, complex relative dielectric function $\epsilon^*(\omega)$, electrical modulus $M^*(\omega)$ and electrical conductivity $\sigma^*(\omega)$, and extensive quantity i.e., complex impedance $Z^*(\omega)$, which is inverse of complex admittance $Y^*(\omega)$ were used to explore the low frequency processes contributed in the electrical/dielectric properties of the coexisting phases of colloidal suspension of the MMT clay (inorganic polymer) in the PVP-EG blend (organic polymer solvent).

2. Experimental

2.1. Materials

Laboratory grade poly(vinyl pyrrolidone) (PVP) of weight average molecular weight (M_w) 24000 g/mol was obtained from S.D. Fine-Chem, India. Ethylene glycol (EG) of laboratory grade was obtained from E. Merck, India. Polymer grade hydrophilic montmorillonite (MMT) clay (Nanoclay, PGV), a product of Nanocor®, was purchased from Sigma-Aldrich, USA. The Na⁺-MMT clay is white in colour, and have 145 meq/100 g cation exchange capacity (CEC), ~ 1 nm thickness sheets (platelets), 150–200 aspect ratio (length/width), 2.6 g/cc specific gravity, and 9–10 pH value on 5% dispersion.

2.2. Preparation of MMT clay colloidal suspension in PVP-EG blends

For preparation of the MMT clay nanoparticles colloidal suspension, 10 wt% (weight fraction) of total solute (MMT clay + PVP) (1.5 g) was added in the EG solvent (13.5 g) in two steps procedure. Firstly, the PVP-EG blends of varying concentration were prepared by dissolving the required amounts of the PVP solute (1.5, 1.485, 1.47, 1.455, 1.425, and 1.35 g) in EG solvent. Afterwards, the respective amounts of 0, 1, 2, 3, 5 and 10 wt% MMT clay concentration (0.00, 0.015, 0.03, 0.045, 0.075 and 0.15 g) of the total weight of the solute (1.5 g) were added in the respective prepared PVP-EG blends

for the preparation of varying clay concentration colloidal suspension in PVP-EG blends. The presence of hydrated Na⁺ cations makes the hydrophilic behaviour of MMT clay galleries so that polar hydrophilic PVP-EG blends can mix without the need of organic modification of the clay sheets. The MMT clay nanoparticles (also called nanoplatelets) colloidal dispersion (intercalation, exfoliation and tactoids) at room temperature were achieved by vigorous magnetic stirring of the samples for 2 hrs at 50°C, and immediately after this process, the colloidal samples were used for their dielectric characterization.

2.3. Dielectric measurements

Agilent 4284A precision LCR meter and Agilent 16452A liquid dielectric test fixture with a four terminals nickel-plated cobalt (an alloy of 17% cobalt + 29% nickel + 54% iron) electrodes of diameter 40 mm and spacing 0.5 mm, were used for the capacitance and resistance measurement in the frequency range 20 Hz to 1 MHz. The capacitances C_0 and C_P without and with sample, respectively and equivalent parallel resistance R_p with sample, were measured for the determination of all the dielectric/electrical function of the prepared materials. The short circuit compensation of the cell and its correction coefficient were considered to eliminate the effect of stray capacitance during the evaluation of the frequency dependent values of complex dielectric function. All measurements were made at 30°C and the temperature was controlled by Thermo-Haake DC10 controller.

The complex dielectric function $\epsilon^*(\omega)$ of the materials is determined from the Equation (1) [28]:

$$\epsilon^*(\omega) = \epsilon' - j\epsilon'' = \alpha \left(\frac{C_P - j}{C_0 \omega C_0 R_P} \right) \quad (1)$$

where $\omega = 2\pi f$ is the angular frequency and α is the correction coefficient of the cell.

Figure 1 shows the frequency dependent spectra of the real part of the relative dielectric function ϵ' , dielectric loss ϵ'' , and loss tangent $\tan\delta = \epsilon''/\epsilon'$ with varying MMT clay concentration colloidal suspension in the PVP-EG blend, at 30°C. The $\tan\delta$ spectra has the peak value corresponding to the electrode polarization (EP) relaxation frequency f_{EP} , which is used to evaluate the EP relaxation time

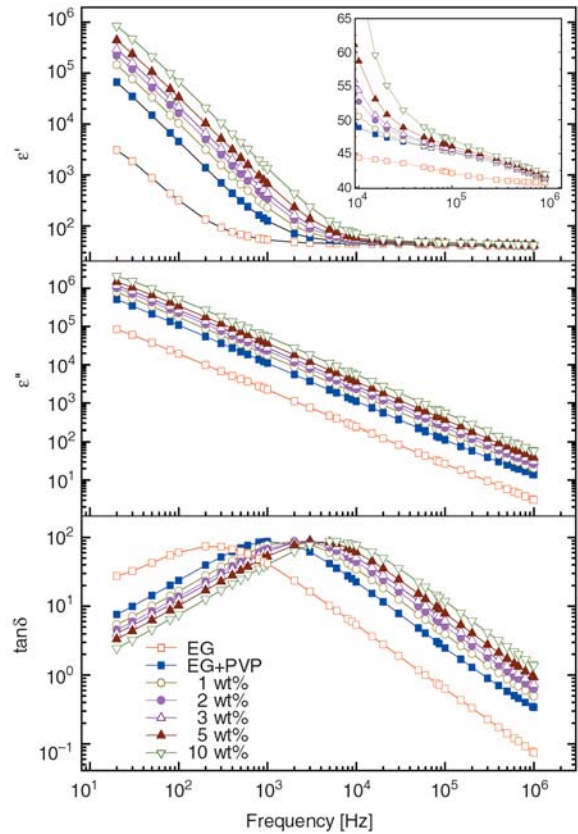


Figure 1. Frequency dependence of real part of dielectric function ϵ' and loss ϵ'' , and loss tangent $\tan\delta$ of MMT clay nanoparticles colloidal suspension in PVP-EG blends at varying clay concentration. Inset shows that the gradual shift in ϵ' dispersion of the m-process corresponds to the local chain motion of PVP towards higher frequencies with increase of the clay concentration in the PVP-EG blends.

$\tau_{EP} = (2\pi f_{EP})^{-1}$ [22–24, 29–33]. The correct value of f_{EP} of these materials were determined by $\tan\delta(f)$ data fit using the Origin® non-linear curve fitting tool.

The frequency dependent real part σ' and the imaginary part σ'' of the alternating current (ac) complex conductivity $\sigma^*(\omega)$ of the samples were obtained from the Equation (2) [20, 34]:

$$\sigma^*(\omega) = \sigma' + j\sigma'' = j\omega\epsilon_0\epsilon^*(\omega) = \omega\epsilon_0\epsilon'' + j\omega\epsilon_0\epsilon' \quad (2)$$

where ϵ_0 ($8.854 \cdot 10^{-12}$ F·m⁻¹) is free space dielectric constant. Figure 2 shows the σ' spectra of the investigated MMT clay colloidal suspension in the PVP-EG blends.

Considering the charges as the independent variable, conductivity relaxation effects can be suitably

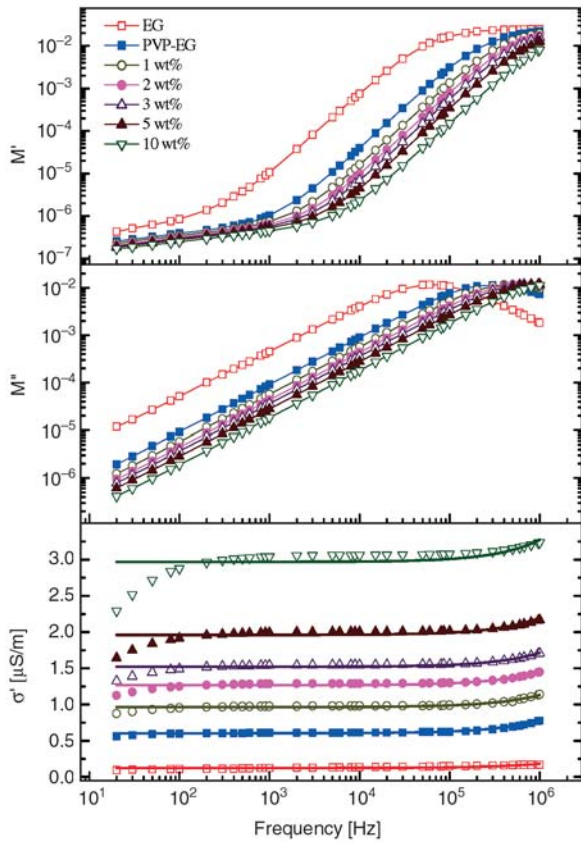


Figure 2. Frequency dependence of real part of electric modulus M' and loss M'' , and real part of ac conductivity σ_{ac} of MMT clay nanoparticles colloidal suspension in PVP-EG blends at varying clay concentration. The continuous solid line in σ' spectra represents the fit of experimental data to the power law $\sigma'(\omega) = \sigma_{dc} + A\omega^n$.

analyzed within the modulus formalism in terms of a dimensionless quantity, called electric modulus $M^*(\omega)$. The frequency dependent values of $M^*(\omega)$ is obtained from the Equation (3) [8, 29, 30, 35]:

$$M^*(\omega) = \frac{1}{\epsilon^*(\omega)} = M' + jM'' = \frac{\epsilon'}{\epsilon'^2 + \epsilon''^2} + j \frac{\epsilon''}{\epsilon'^2 + \epsilon''^2} \quad (3)$$

The main advantage of this formulation is that, the space charge effects often do not mask the features of the spectra, owing to suppression of high capacitance phenomena in $M''(f)$ plots. The spectra of the evaluated values of the real part M' and the imaginary part M'' of the electric modulus of varying MMT clay concentration colloidal suspension in the PVP-EG blend is also shown in Figure 2, along with the conductivity spectra. The $M''(f)$ spectra of these materials have peaks, and the frequency f_σ

corresponding to these peaks is related to the most probable ionic conductivity relaxation time τ_σ [29]. The exact values of f_σ were determined from the fit of $M''(f)$ data to the Origin® non-linear curve fitting tool. The τ_σ values were obtained directly from the values of f_σ by the relation $\tau_\sigma = (2\pi f_\sigma)^{-1}$ [29].

The complex impedance plane plots (Z'' vs. Z') are commonly used to separate the bulk material and the electrode surface polarization phenomena [7, 8, 22–24, 30, 31, 36]. A common feature of dielectrics with dc conductivity is a discontinuity at electrode/dielectric interface, which has different polarization properties with the bulk dielectric material. The frequency dependent values of the real part Z' and reactive part Z'' of the complex impedance $Z^*(\omega)$ of the materials were evaluated by the Equation (4) [30, 31]:

$$Z^*(\omega) = \frac{1}{Y^*(\omega)} = Z' - jZ'' = \frac{R_p}{1 + (\omega C_p R_p)^2} - j \frac{\omega C_p R_p^2}{1 + (\omega C_p R_p)^2} \quad (4)$$

Figure 3 shows the Z'' vs. Z' plots of the varying MMT clay concentration colloidal suspension in PVP-EG blends. Figure 4 shows the ‘master curves representation’ [22, 23, 29, 32, 33] of the real and imaginary parts of all the intensive quantities along with $\tan\delta$ values of 1 wt% MMT clay concentration of the solute in PVP-EG blend. It is noticed that the intersection of all the real and imaginary parts of intensive quantities occurs at the same frequency f_σ , and below it direct current (dc) conduction dominates.

3. Results and discussion

3.1. Complex dielectric function spectra

The increase of clay concentration in the PVP-EG blend gradually increases the ϵ' and ϵ'' values over the entire frequency spectra (Figure 1). The loading of hydrophilic MMT clay in the PVP-EG blend results the intercalation and exfoliation of the clay sheets. As compared to the intercalation of PVP-EG complex structures, there is larger probability of the intercalation of uncomplexed EG structures in the hydrophilic clay galleries, because EG molecules have smaller size as compared to the PVP monomer units which has a bulky pyrrolidone ring as side

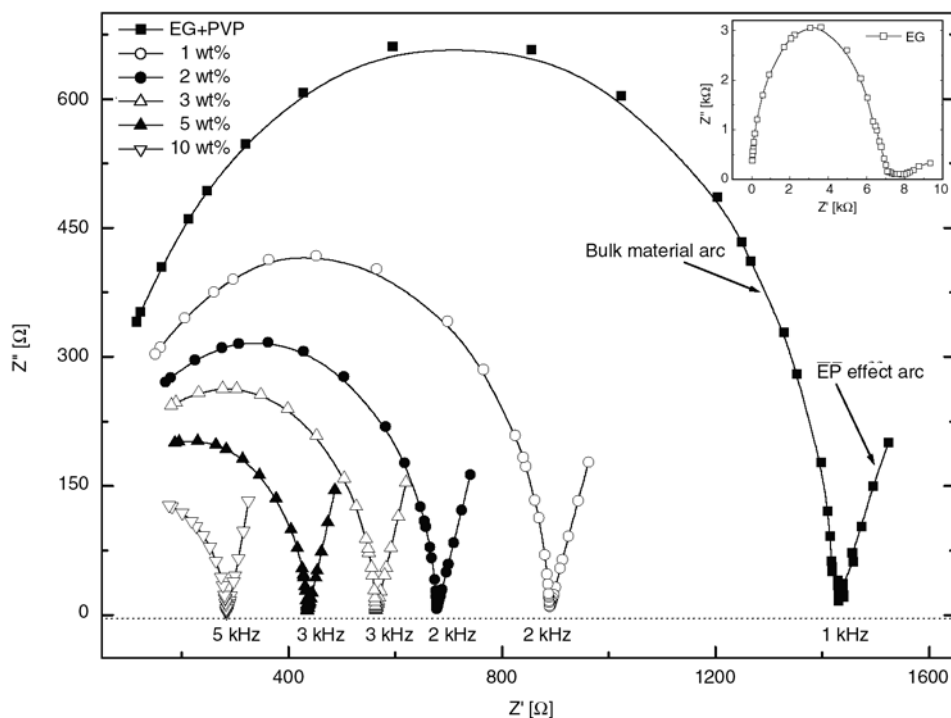


Figure 3. Complex plane plots (Z'' vs. Z') of MMT clay nanoparticles colloidal suspension in PVP-EG blends at varying clay concentration. Inset shows the complex plane plot of pure EG.

group. The adsorption of the PVP-EG complex structures on the clay sheets through H-bond interactions between the hydroxylated aluminate surfaces of the MMT clay and the C=O and –OH groups of PVP-EG blends results the clay exfoliation. The intercalation and exfoliation of MMT clay result both dipolar and free charge in the nanocomposite material, and hence there is increase in the complex dielectric function values [8, 9]. Further, the significant increase in ϵ' and ϵ'' values of these materials with increase of clay concentration may also be related to the formation of a percolation structure of the nanoparticles, which is confirmed by dielectric investigation on nanocomposites [37]. Pure EG, PVP-EG blends and MMT clay loaded PVP-EG blends have a large increase in the ϵ' values in the lower frequency side of the spectra (Figure 1), which is mainly due to the contribution of the electrode polarization (EP) [8, 21–24] and Maxwell-Wanger (MW) interfacial polarization [38, 39]. Further, the ϵ' values of the MMT clay loaded PVP-EG blends monotonously increases with the increase of clay concentration, which suggests the enhancement in number of free Na^+ cations and their mobility in the increased spacing of intercalated clay galleries.

The EP phenomena occurs due to formation of electric double layer (EDL) capacitances by the free charges build up at the interface between the electrolyte and the electrode surfaces in plane geometry [32, 40]. Whereas in case of MW phenomena, the free charges build up at the interfacing boundaries of various components of different dielectric constant in the composite dielectric material, which results the nanocapacitors of spherical geometry [38–41]. In EP region, the logarithmic slope of frequency dependent ϵ' values of the dielectric materials closer to -1 indicate leakiness of the EDL capacitances (blocking layers) to moving charges, whereas value close to 0 suggest a complete block of charge movement through the layers [20, 30, 42, 43]. The slope of the $\epsilon'(f)$ spectra (Figure 1) of the investigated materials closer to -1 suggest the leakiness behaviour of the EDL capacitances formed in the EP region. In general the peak in $\tan\delta$ spectra (Figure 1), which corresponds to electrode polarization (EP) relaxation frequency (f_{EP}) is used to separate the bulk material and EP phenomenas [29–32]. In the measurements, lower frequency range up to f_{EP} , EP polarization dominates the MW polarization.

The τ_{EP} involves charging and discharging time of EDL capacitance, which is associated with the

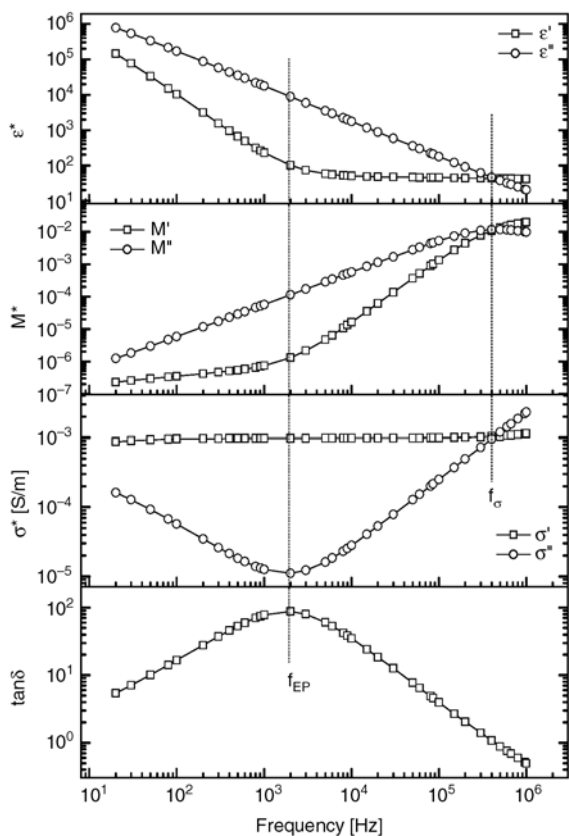


Figure 4. Simultaneous superpositions of the real and imaginary parts of the complex relative dielectric function ϵ^* , the electric modulus M^* , the complex conductivity σ^* , and loss tangent $\tan\delta$ for MMT clay nanoparticles colloidal suspension in PVP-EG blends with 1 wt% clay concentration

overall dynamics of the adsorbed ions on the electrode surfaces in the alternating electric field [29–33, 42]. The calculated τ_{EP} values of the clay loaded PVP-EG blend is plotted against MMT clay concentration [wt%] in Figure 5. In case of PVP-EG blend, the addition of 10 wt% PVP in EG solvent largely reduces the τ_{EP} value, which further decreases on loading of MMT clay in PVP-EG blends. The decrease of τ_{EP} values with increasing clay concentration suggests the faster dynamics of the EDL ions with the variation in the applied alternating electric field.

Inset of Figure 1 shows the ϵ' dispersion in the upper frequency region of the measurements of the clay loaded PVP-EG blends, which is corresponding to m-process of the PVP chain [21]. The comparative shapes of the m-process in the inset shows that the colloidal suspension of MMT clay nanoparticles in PVP-EG blends significantly influences the PVP local chain motion. Due to limita-

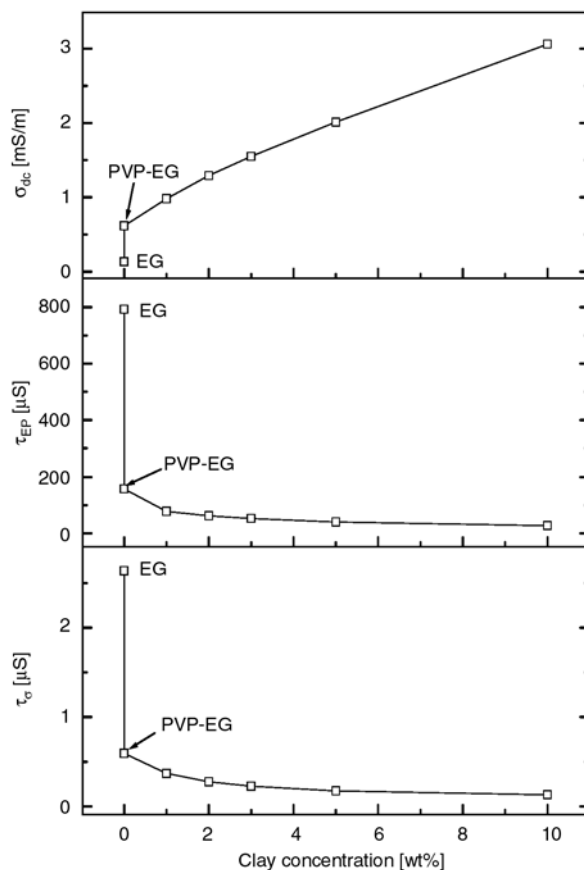


Figure 5. MMT clay concentration dependence of the dc conductivity σ_{dc} , the electrode polarization relaxation time τ_{EP} and ionic conduction relaxation time τ_c of MMT clay nanoparticles colloidal suspension in PVP-EG blends

tions of experimental upper frequency range, the relaxation time of m-process could not be evaluated because the inset spectra cover only the starting shoulder of the m-process dispersion.

3.2. AC conductivity spectra

The σ' spectra of the MMT clay loaded PVP-EG blends have frequency independent plateau (Figure 2), which corresponds to ionic or dc electrical conductivity σ_{dc} and exhibits dispersion at higher frequencies. This behaviour obeys Jonscher [34] power law $\sigma'(\omega) = \sigma_{dc} + A\omega^n$, where A is the pre-exponential factor and n is the fractional exponent ranging between 0 and 1 for the electrolyte. The solid line in the σ' spectra denotes the fit of experimental data to the power law expression and the fit values of σ_{dc} , A and n obtained by Origin® non-linear curve fitting software are recorded in Table 1. The evaluated σ_{dc} values of these materials are also

Table 1. Parameters obtained from fit to the experimental data to $\sigma'(\omega) = \sigma_{dc} + A\omega^n$ of various clay concentration MMT clay-(PVP-EG) blends

MMT clay [wt%]	$\sigma_{dc} \cdot 10^3$ [S/m]	$A \cdot 10^7$	n
EG	0.12	3.77	0.77
0	0.60	3.40	0.84
1	0.97	3.43	0.84
2	1.27	3.27	0.85
3	1.52	3.35	0.85
5	1.96	3.14	0.86
10	2.97	3.59	0.87

plotted against clay concentration [wt%] in Figure 5. The small deviation from σ_{dc} (plateau region) value in lower frequency side of the conductivity spectra is evidence of EP effect for these materials, whereas the small dispersion in higher frequency end of the σ' spectra is owing to the contribution of PVP segmental motion. The n values of these materials are found in the range 0.77 to 0.87 (Table 1). For electrolyte n value can be between 1 and 0.5 indicating the ideal long-range pathways and diffusion limited hopping (tortuous pathway), respectively [44].

It is known that in an electrolyte the electrical conductivity σ is given by the relation $\sigma = \sum n_i \mu_i q_i$, where n_i , μ_i and q_i refer to charge carrier density, ionic mobility, and ionic charge of i^{th} ion respectively [40]. The increase of ionic conductivity of a complex system is due to the increment of the number of mobile charge carriers introduced/produced in the material with the change in concentration of the constituent. In the polymer-clay nanocomposite materials, there is existence of three H-bond phases, namely organic polymer phase, inorganic polymer phase (some tactoids of agglomerated clay nanocomposites) and organic and inorganic components phase [45]. The structural properties and dynamical behaviour of these phases governs the electrical conductivity of the organic-inorganic nanocomposite [45].

The PEO-clay and PEG-clay nanocomposites are extensively attempted to make potential electrolyte material for rechargeable batteries [8, 9, 46–52]. Different spectroscopy investigation on poly(ethylene oxide) PEO-clay nanocomposites [46] confirmed that the intercalated PEO molecules between silicate galleries impede the polymer crystallization, which results in higher electrolyte conductivity compared to the system without clay. In regard to the structural behaviour of the PEO-MMT clay

nanocomposites, it was postulated that the PEO chains exist in helical structure in the intercalated state, forming some kind of tunnel that increases the mobility of the cations, and hence also the electrical conductivity [47]. The XRD study of these materials confirmed that the intercalated oxyethylene units are arranged in flattened monolayer arrangements with 4 Å interlayer expansions [5]. It is supported by trans conformation to at least a portion of (O–CH₂–CH₂–O) groups of the PEG chain [48]. Furthermore, the main driving force for the intercalation reaction results from orientation of the polymer chains such that they form hydrogen bond with the hydroxylated aluminate surfaces of the clay. For the maximum hydrogen bonding interaction, the PEG polymer adopts a conformation such that its oxygen matches up with the surface hydroxyl groups of the clay. For this the distances between oxygens in the polymer chain is roughly comparable to the distances between hydroxyl groups in clay sheets.

For clay, interhydroxyl distance is ~ 2.8 Å, and the oxyethylene group repeat every 2.8 Å all facing towards the surface of clay would be particularly favourable [48]. In case of MMT clay colloidal suspension in PVP-EG blends, the intercalated EG structures can be assumed like the intercalated PEG and PEO structures, because the EG molecules have repeat units of PEG and PEO molecules. The investigation on PVP-MMT clay confirmed that the H-bonding interaction between C=O groups of PVP chain and –OH on the silicate surfaces result the large clay exfoliation in PVP-clay nanocomposites, which enhances the nanocomposite thermal property [53]. Considering all the above said facts, in the present investigation, the large enhance in σ_{dc} values of the MMT clay loaded PVP-EG blends confirms that besides the increase of charge carriers density, there is significant enhance of structural symmetry which results the easy ionic conduction path. Such path in complex system facilitates the ions mobility and hence their large increase in σ_{dc} values of these materials with the increase of clay concentration (Figure 5).

3.3. Electric modulus spectra

The M' spectra of the clay loaded PVP-EG blend, which are free from space charge effect shows a large dispersion in the ionic conduction region

(above f_{EP}) (Figure 2), whereas M'' spectra shows the relaxation peaks for the conductivity relaxation processes. This suggests that ionic motion and PVP segmental motion are strongly coupled manifesting peak in the M'' spectra with no corresponding feature in dielectric spectra (Figure 1). Figure 4 shows the ‘master-curves representation’ of the intensive quantities of 1 wt% clay colloidal suspension in PVP-EG blend as one of the representative plot. Such plots are frequently used to find out the common intersection frequency f_{σ} of the real and imaginary parts of all intensive quantities in the ion conduction region [22–24, 29], which is corresponding to Maxwell-Wagner or ionic conductivity relaxation processes. In the conductivity spectra, f_{σ} value separates the change in ions from dc to ac transport. Figure 5 shows the τ_{σ} values [$\tau_{\sigma} = (2\pi f_{\sigma})^{-1}$] of these materials which decrease with increase of clay concentration.

Bur *et al.* [54] applied the f_{σ} (also known as f_{MW}) values for real-time measuring the extent of clay exfoliation during the polymer-clay nanocomposites process. They observed that f_{σ} value has the dependence upon the amount of the clay aggregate, intercalated or exfoliated state or any combination thereof. As exfoliation proceeds, nanosize silicate flakes present an ever expanding polymer/clay interface area that increases the internal capacitance of the composite where conducting ions can accumulate. Silicate flakes act as nanocapacitors in the melt polymer. In general, the MW relaxation time τ_{σ} (τ_{MW}) can be viewed as an electrical RC time constant where R is the resistance of the polymer matrix and C is the capacitance of the silicate particle. The decrease of τ_{σ} value with increase of clay concentration in PVP-EG blends suggest that the dynamics of the colloid suspension charges increases, which may be due to the extent of clay exfoliation in dynamic equilibrium. The H-bond interfacial bridging of exfoliated clay platelets with C=O groups and –OH groups of PVP-EG blend results the faster dynamics.

3.4. Complex impedance spectra

The frequency value of the experimental points increases on going from right to left side on the arcs of the complex impedance plane plot (Z'' vs. Z') of the MMT clay colloidal suspension in PVP-EG blend (Figure 3). All these plots have two separate

arcs, which are corresponding to the bulk material effect (the upper frequency arc) and the electrode surface polarization (the lower frequency arc) [7, 8, 22–24, 36, 55]. Pure EG also have similar type of arcs with comparatively large values of Z'' and Z' , and it is shown in the inset of Figure 3. The frequency values correspond to Z'' minimum value in the plots separates the bulk material and electrode polarization phenomena. These values are also marked in the same Figure. These values are exactly equal to the $\tan\delta$ peak frequency f_{EP} . In complex impedance plane plots the extrapolated intercept on the real axis Z' of the common part of two arcs gives the value of dc bulk resistance R_{dc} , of the dielectric material [7, 8, 55]. It is observed that the R_{dc} value of these materials decreases with the increase of MMT clay concentration, and hence the σ_{dc} values increases.

4. Conclusions

The dielectric dispersion behaviour and relaxation processes of MMT clay nanoparticles colloidal suspension in PVP-EG blends were investigated in the 20 Hz to 1 MHz frequency range. Two relaxation processes corresponding to ionic conduction and electrode polarization phenomena and the starting shoulder of PVP segmental motion were observed. The comparative analysis of the various dielectric/electrical quantities spectra confirms that the behaviour of ionic conduction and EDL dynamics is governed by the MMT clay concentration in these colloidal materials. The type of H-bonding interactions between the MMT clay and the PVP-EG blends and clay intercalation and exfoliation were recognized by comparative study of the intensive dielectric quantities. The dc conductivity of these materials can be tailored in the predicted manner with the change in MMT clay concentration, for their potential use as electrolyte material and other technological applications.

Acknowledgements

Authors are grateful to the Department of Science and Technology, New Delhi for providing the experimental facilities through project No. SR/S2/CMP-09/2002. One of the authors SC is thankful to the University Grants Commission, New Delhi for the award of RFSMS fellowship.

References

- [1] Feldstein M. M.: Peculiarities of glass transition temperature relation to the composition of poly(*N*-vinyl pyrrolidone) blends with short chain poly(ethylene glycol). *Polymer*, **42**, 7719–7726 (2001).
- [2] Li Y., Zhang R., Chen H., Zhang J., Suzuki R., Ohdaira T., Feldstein M. M., Jean Y. C.: Depth profile of free volume in a mixture and copolymers of poly(*N*-vinyl-pyrrolidone) and poly(ethylene glycol) studied by positron annihilation spectroscopy. *Biomacromolecules*, **4**, 1856–1864 (2003).
- [3] Feldstein M. M.: Adhesive hydrogels: Structure, properties, and application (A Review). *Polymer Science, Series A*, **46**, 1165–1191 (2004).
- [4] Craig D. Q. M.: Dielectric analysis of pharmaceutical systems. Taylor and Francis, London (1995).
- [5] Kokabi M., Sirousazar M., Hassan Z. M.: PVA-clay nanocomposite hydrogels for wound dressing. *European Polymer Journal*, **43**, 773–781 (2007).
- [6] Ray S. S., Bousmina M.: Biodegradable polymers and their layered silicate nanocomposites: In greening the 21st century material world. *Progress in Materials Science*, **50**, 962–1079 (2005).
- [7] Kim S., Hwang E.-J., Jung Y., Han M., Park S.-J.: Ionic conductivity of polymeric nanocomposite electrolyte based on poly(ethylene oxide) and organo-clay materials. *Colloids and Surfaces A*, **313–314**, 216–219 (2008).
- [8] Pradhan D. K., Choudhary R. N. P., Samantaray B. K.: Studies of structural, thermal and electrical behaviour of polymer nanocomposite electrolytes. *Express Polymer Letters*, **2**, 630–638 (2008).
- [9] Pradhan D. K., Choudhary R. N. P., Samantaray B. K.: Studies of dielectric relaxation and ac conductivity behaviour of plasticized polymer nanocomposite electrolytes. *International Journal of Electrochemical Science*, **3**, 597–608 (2008).
- [10] Bergaya F., Theng B. K. G., Lagaly G.: Handbook of clay science. Elsevier, Amsterdam (2006).
- [11] Burmistr M. V., Sukhyy K. M., Shilov V. V., Pissis P., Spanoudaki A., Sukha I. V., Tomilo V. I., Gomza Y. P.: Synthesis, structure, thermal and mechanical properties of nanocomposites based on linear polymers and layered silicates modified by polymeric quaternary ammonium salts (ionenes). *Polymer*, **46**, 12226–12232 (2005).
- [12] Auad M. L., Nutt S. R., Pettarin V., Frontini P. M.: Synthesis and properties of epoxy-phenolic clay nanocomposites. *Express Polymer Letters*, **1**, 629–639 (2007).
- [13] Pannirselvam M., Genovese A., Jollands M. C., Bhat-tacharya S. N., Shanks R. A.: Oxygen barrier property of polypropylene-polyether treated clay nanocomposite. *Express Polymer Letters*, **2**, 429–439 (2008).
- [14] Fritzsche J., Das A., Jurk R., Stöckelhuber K. W., Heinrich G., Klüppel M.: Relaxation dynamics of carboxylated nitrile rubber filled with organomodified nanoclay. *Express Polymer Letters*, **2**, 373–381 (2008).
- [15] Das A., Jurk R., Stöckelhuber K. W., Heinrich G.: Rubber curing chemistry governing the orientation of layered silicate. *Express Polymer Letters*, **1**, 717–723 (2007).
- [16] Chow W. S., Yap Y. P.: Optimization of process variable on flexural properties of epoxy/organo-montmorillonite nanocomposite by response surface methodology. *Express Polymer Letters*, **2**, 2–11 (2008).
- [17] Mishra S. B., Luyt A. S.: Effect of organic peroxide on the morphological, thermal and tensile properties of EVA-organoclay nanocomposites. *Express Polymer Letters*, **2**, 256–264 (2008).
- [18] Manoratne C. H., Rajapakse R. M. G., Dissanayake M. A. K. L.: Ionic conductivity of poly(ethylene oxide) (PEO)-montmorillonite (MMT) nanocomposites prepared by intercalation from aqueous medium. *International Journal of Electrochemical Science*, **1**, 32–46 (2006).
- [19] Kremer F.: Dielectric spectroscopy-yesterday, today and tomorrow. *Journal of Non-Crystalline Solids*, **305**, 1–9 (2002).
- [20] Kremer F., Schönhals A.: Broadband dielectric spectroscopy. Springer, Berlin (2002).
- [21] Shinyashiki N., Sengwa R. J., Tsubotani S., Nakamura H., Sudo S., Yagihara S.: Broadband dielectric study of dynamics of poly(vinyl pyrrolidone)-ethylene glycol oligomer blends. *The Journal of Physical Chemistry A*, **110**, 4953–4957 (2006).
- [22] Sengwa R. J., Sankhla S.: Solvent effects on the dielectric dispersion of poly(vinyl pyrrolidone)-poly(ethylene glycol) blends. *Colloid and Polymer Science*, **285**, 1237–1246 (2007).
- [23] Sengwa R. J., Sankhla S.: Dielectric dispersion study of poly(vinyl pyrrolidone)-polar solvent solutions in the frequency range 20 Hz–1 MHz. *Journal of Macromolecular Science Part B: Physics*, **46**, 717–747 (2007).
- [24] Sengwa R. J., Sankhla S.: Low-frequency dielectric response and chain dynamics study of poly(vinyl pyrrolidone)-poly(ethylene glycol) coexisting two-phase polymeric blends. *Indian Journal of Engineering and Materials Sciences*, **14**, 317–323 (2007).
- [25] Sengwa R. J., Abhilasha, Mehrotra S. C., Sharma B. R.: A comparative dielectric study of poly(vinyl pyrrolidone) in unlike hydroxyl group number containing polar solvents. *Indian Journal of Physics*, **78**, 1341–1348 (2004).
- [26] Sengwa R. J., Sankhla S., Abhilasha: Interaction effect on molecular dynamics of some polar solvents in poly(vinyl pyrrolidone) matrix studied by microwave dielectric relaxation measurements in dilute solutions. *Indian Journal of Physics*, **79**, 879–886 (2005).
- [27] Sengwa R. J., Kaur K., Chaudhary R.: Dielectric properties of low molecular weight poly(ethylene glycol)s. *Polymer International*, **49**, 599–608 (2000).
- [28] Agilent 16452A: Liquid test fixture – Operation and service manual. Agilent Technologies Ltd., Japan (2000).

- [29] Zhang S., Dou S., Colby R. H., Runt J.: Glass transition and ionic conduction in plasticized and doped ionomers. *Journal of Non-Crystalline Solids*, **351**, 2825–2830 (2005).
- [30] Pissis P., Kyritsis A.: Electrical conductivity studies in hydrogels. *Solid State Ionics*, **97**, 105–113 (1997).
- [31] Sengwa R. J., Sankhla S.: Dielectric dispersion study of coexisting phases of aqueous polymeric solution: Poly(vinyl alcohol) + poly(vinyl pyrrolidone) two-phase systems. *Polymer*, **48**, 2737–2744 (2007).
- [32] Klein R. J., Zhang S., Dou S., Jones B. H., Colby R. H., Runt J.: Modeling electrode polarization in dielectric spectroscopy: Ion mobility and mobile ion concentration of single-ion polymer electrolytes. *The Journal of Chemical Physics*, **124**, 144903 (pp 8) (2006).
- [33] Sengwa R. J., Sankhla S.: Characterization of ionic conduction and electrode polarization relaxation processes in ethylene glycol oligomers. *Polymer Bulletin*, **60**, 689–700 (2008).
- [34] Jonscher A. K.: *Dielectric relaxation in solids*. Chelsea Dielectric Press, London (1983).
- [35] Chanmal C. V., Jog J. P.: Dielectric relaxations in PVDF/BaTiO₃ nanocomposites. *Express Polymer Letters*, **2**, 294–301 (2008).
- [36] Thakur A. K., Pradhan D. K., Samantaray B. K., Choudhary R. N. P.: Studies on an ionically conducting polymer nanocomposite. *Journal of Power Sources*, **159**, 272–276 (2006).
- [37] Kosmidou Th. V., Vatalis A. S., Delides C. G., Logakis E., Pissis P., Papanicolaou G. C.: Structural, mechanical and electrical characterization of epoxy-amine/carbon black nanocomposites. *Express Polymer Letters*, **2**, 364–372 (2008).
- [38] Kyritsis A., Pissis P.: Dielectric relaxation spectroscopy in poly(ethylene oxide)/water systems. *Macromolecular Symposia*, **119**, 15–24 (1997).
- [39] Noda N., Lee Y-H., Bur A. J., Prabhu V. M., Snyder C. R., Roth S. C., McBrearty M.: Dielectric properties of nylon 6/clay nanocomposites from on-line process monitoring and off-line measurements. *Polymer*, **46**, 7201–7217 (2005).
- [40] MacCallum J. R., Vincent C. A.: *Polymer electrolyte reviews*, vol 1. Elsevier, London (1987).
- [41] Garrouch A. A., Lababidi H. M. S., Gharbi R. B.: Dielectric dispersion of dilute suspension of colloid particles: Practical applications. *The Journal of Physical Chemistry*, **100**, 16996–17003 (1996).
- [42] Craig D. Q. M., Newton J. M., Hill R. M.: An investigation into the low-frequency dielectric response of polyethylene glycols. *Journal of Material Science*, **28**, 405–410 (1993).
- [43] Craig D. Q. M., Barker S. A., Banning D., Booth S. W.: An investigation into the mechanisms of self-emulsification using particle size analysis and low frequency dielectric spectroscopy. *International Journal of Pharmaceutics*, **114**, 103–110 (1995).
- [44] Mauritz K. A.: Dielectric relaxation studies on ion motion in electrolyte-containing perfluorosulfonate ionomers. 4. Long range ion transport. *Macromolecules*, **22**, 4483–4488 (1989).
- [45] Mamunya Y., Kanapitsas A., Pissis P., Boiteux G., Lebedev E.: Water sorption and electrical/dielectric properties of organic-inorganic polymer blends. *Macromolecular Symposia*, **198**, 449–459 (2003).
- [46] Aranda P., Ruiz-Hitzky E.: Poly(ethylene oxide)/NH₄⁺-smectite nanocomposites. *Applied Clay Science*, **15**, 119–135 (1999).
- [47] Reinholdt M. X., Kirkpatrick R. J., Pinnavaia T. J.: Montmorillonite-poly(ethylene oxide) nanocomposites: Interlayer alkali metal behaviour. *The Journal of Physical Chemistry B*, **109**, 16296–16303 (2005).
- [48] Tunney J. J., Detellier C.: Aluminosilicate nanocomposite materials. Poly(ethylene glycol)-kaolinite intercalates. *Chemical Materials*, **8**, 927–935 (1996).
- [49] Chen W., Xu Q., Yuan R. Z.: The influence of polymer state on the electrical properties of polymer/layered-silicate nanocomposites. *Composites Science and Technology*, **61**, 935–939 (2001).
- [50] Liao B., Song M., Liang H., Pang Y.: Polymer-layered silicate nanocomposites. 1. A study of poly(ethylene oxide)/Na⁺-montmorillonite nanocomposites as polyelectrolytes and polyethylene-block-poly(ethylene glycol) copolymer/Na⁺-montmorillonite nanocomposites as fillers for reinforcement of polyethylene. *Polymer*, **42**, 10007–10011 (2001).
- [51] Chaiko D. J.: New poly(ethylene oxide)-clay composites. *Chemical Materials*, **15**, 1105–1110 (2003).
- [52] Lin-Gibson S., Kim H., Schmidt G., Han C. C., Hobbie E. K.: Shear-induced structure in polymer-clay nanocomposite solutions. *Journal of Colloid and Interface Science*, **274**, 515–525 (2004).
- [53] Koo C. M., Ham H. T., Choi M. H., Kim S. O., Chung I. J.: Characteristics of polyvinylpyrrolidone-layered silicate nanocomposites prepared by attrition ball milling. *Polymer*, **44**, 681–689 (2003).
- [54] Bur A. J., Lee Y-H., Roth S. C., Start P. R.: Measuring the extent of exfoliation in polymer/clay nanocomposites using real-time process monitoring methods. *Polymer*, **46**, 10908–10918 (2005).
- [55] Wang M., Dong S.: Enhanced electrochemical properties of nanocomposite polymer electrolyte based on copolymer with exfoliated clays. *Journal of Power Sources*, **170**, 425–432 (2007).

Mechanical properties and fire retardancy of bidirectional reinforced composite based on biodegradable starch resin and basalt fibres

*T. Wittek**, *T. Tanimoto*

Shonan Institute of Technology, Tsujido-Nishikaigan 1-1-25, Fujisawa, Kanagawa 251-8511, Japan

Received 1 August 2008; accepted in revised form 3 October 2008

Abstract. Environmental problems caused by extensive use of polymeric materials arise mainly due to lack of landfill space and depletion of finite natural resources of fossil raw materials, such as petroleum or natural gas. The substitution of synthetic petroleum-based resins with natural biodegradable resins appears to be one appropriate measure to remedy the above-mentioned situation. This study presents the development of a composite that uses environmentally degradable starch-based resin as matrix and basalt fibre plain fabric as reinforcement. Prepreg sheets were manufactured by means of a modified doctor blade system and a hot power press. The sheets were used to manufacture bidirectional-reinforced specimens with fibre volume contents ranging from 33 to 61%. Specimens were tested for tensile and flexural strength, and exhibited values of up to 373 and 122 MPa, respectively. Through application of silane coupling agents to the reinforcement fibres, the flexural composite properties were subsequently improved by as much as 38%. Finally, in order to enhance the fire retardancy and hence the applicability of the composite, fire retardants were applied to the resin, and their effectiveness was tested by means of flame rating (according to UL 94) and thermogravimetric analysis (TGA), respectively.

Keywords: *biodegradable polymers, starch resin, basalt fibres, silane coupling agents, fire retardants*

1. Introduction

The primary field of application for fibre reinforced polymer composites is the aerospace industry. For several years, however, composite materials have been increasingly used for various other technical tasks, where it is beneficial to apply lightweight construction materials which have high strength and stiffness characteristics. The favourable specific properties of fibre reinforced polymer composites are based on the low density of the matrix resins used, and the high strength of the embedded fibres.

Regarding utilisation after service life, conventional fibre reinforced composites are problematic. The combination of miscellaneous, often highly durable components complicates the recycling

process considerably, and landfill disposal or incineration are becoming increasingly difficult due to environmental concerns and legal requirements. An additional problem resulting from the use of polymer resins as matrix material, is the depletion of finite natural petrochemical resources increasingly accompanied by a rise in costs.

A possible solution to these issues may result from the use of natural fibre reinforced polymers based on renewable resources, or ‘green’ composites. By embedding natural fibres into matrices based on biopolymers, fibre reinforced polymers are obtained which integrate more readily into the natural biodegradation cycles, for example by CO₂-neutral incineration, which includes recovery of energy, or by composting. Advantages of biodegradable com-

*Corresponding author, e-mail: wittek@mate.shonan-it.ac.jp
© BME-PT and GTE

posites include: biological degradation, reduction in the volume of waste, preservation of fossil-based raw materials, and protection of climate through reduction of carbon dioxide emission.

Although research into 'green' composites has been conducted worldwide since at least the mid-1990s, practical application of these composites is still in the early stages. Most fibres that are currently used for manufacturing of 'green' composites are cellulose-based plant fibres. Although cellulose-based fibres possess several advantages, including low cost, low density, high specific mechanical properties and biodegradability, they exhibit some severe drawbacks. These include moisture absorption leading to fibre swelling, low thermal resistance, anisotropic fibre properties, low compressive and transverse strength, local or seasonal variations in quality and poor compatibility between the hydrophilic fibres and hydrophobic polymer matrices [1, 2].

The main aims of our research are twofold: to contribute to the enhancement of the application possibilities of 'green' composites by exploring natural mineral basalt fibres as reinforcement in biodegradable polymeric resins, and to develop a composite material that has mechanical properties similar to those of conventional glass fibre reinforced polymeric composites based on petrochemical resources, while exhibiting a lower degree of environmental impact.

Due to processability considerations and in order to achieve high fibre content, it was decided to use a resin emulsion based on thermoplastic starch and polycaprolactone (PCL) in combination with the basalt fibres. PCL is applied because it provides good mechanical properties, such as favourable tensile strength and elongation, and shows good compatibility with many types of polymers. On the other hand, starch helps to lower the cost of the final product and to improve several physical properties. In order to obtain thermoplastic properties, but also to overcome the poor miscibility between starch and PCL, denaturation of starch is one possible method. Other methods to overcome this miscibility issue, which have been reported recently, include acylation of starch in anhydride solutions [3], grafting of PCL by acrylic acid [4], addition of a compatibiliser constituted by modified PCL or the addition of a silane coupling agent [5].

The only ingredient used in the manufacture of basalt fibres is solidified volcanic lava in which SiO_2 accounts for the main part, followed by Al_2O_3 , then Fe_2O_3 , FeO , CaO and MgO [6–8]. Basalt rocks are classified according to the SiO_2 content as alkaline (up to 42% SiO_2), mildly acidic (43 to 46% SiO_2) and acidic basalts (over 46% SiO_2). Only acidic type basalts satisfy the conditions for fibre preparation [9]. Basalt fibres are extruded from basalt rock through a melting process without the application of additives. The fibres are cost-effective and possess several excellent properties, such as outstanding sound and thermal insulation, non-flammability and good mechanical strength [7, 10, 11]. The mechanical properties of basalt fibre are similar or superior to those of plant fibre and glass fibre. Also, basalt fibre is environmentally and ecologically harmless, and free of carcinogens and other health hazards [12].

Noteworthy recent research on basalt fibre composites includes the development of a new method for the production of short basalt fibres and related extensive results on the properties of basalt fibre reinforced hybrid thermoplastic and thermoset composites [11, 13–16].

Recent reports on polymer resin matrices reinforced with continuous basalt fibres include unidirectional basalt fibres and cross-ply in epoxy and phenolic resin [17], basalt twill weave reinforced epoxy and vinyl resin for applications in transportation [18, 19], and unidirectional basalt yarn as reinforcement in wheat gluten [20].

The initial steps of our research, as previously reported in [21], were to select an appropriate manufacturing method and to identify the processing parameters by manufacturing unidirectional basalt fibre reinforced 'green' composites and testing their mechanical properties, such as tensile strength, flexural strength and interlaminar shear strength. In this paper, we are focusing on the manufacturing and characterization of bidirectional basalt fibre reinforced composites, with the intent of increasing the applicability of these materials and turning them into functioning engineering composites. We also analysed the effectiveness of several additives with the aim of improving the composites mechanical properties and fire retardancy. The research on flame retardancy of biodegradable composites in particular is a subject which was hardly studied

until recently. The work of Matkó *et al.*, where the use of ammonium polyphosphate in different bio-composites was reported [22], is worth mentioning as the pioneering study in this field.

2. Experimental

2.1. Materials

2.1.1. Polymer matrix

The resin used during this study, termed Landy CP-300 and provided by Miyoshi Yushi Inc., is an emulsion with approximately 40% solid content, where particles with an average diameter of 4.2 μm are dispersed in water. CP-300 is a blend of Cornpol and polycaprolactone. Cornpol is a starch based biodegradable plastic, produced by Nihon Starch Ltd., Japan, by denaturing cornstarch with natural fats into an aliphatic ester [23]. The properties of CP-300 are summarized in Table 1.

2.1.2. Reinforcement fibres

We have chosen basalt plain weave fabric (BT-8) purchased from Sudaglass Fiber Technology Inc., Russia, as the reinforcement material for our research. BT-8 has an area density of 210 g/m^2 , a thickness of 0.18 mm, and warp and weft densities of 10 and 8 yarns/cm, respectively. The properties of the single fibres are shown in Table 1.

Table 1. Properties of base materials

	CP-300 resin	Basalt fibres
Density [g/cm^3]	1.17	2.7
Diameter [μm]	–	13.1
Tensile strength [MPa]	8.3	1540
Elastic modulus [GPa]	0.3	86
Elongation at break [%]	16.8	2.6
Flexural strength [MPa]	10.2	–
Flexural modulus [GPa]	0.5	–

Table 2. Chemical structures and descriptions of silane coupling agents

Chemical structure and name	Manufacturer	Product number	Designation	Molecular weight
$\begin{array}{c} \text{OCH}_2\text{CH}_3 \\ \\ \text{H}_2\text{N}-(\text{CH}_2)_3-\text{Si}-\text{OCH}_2\text{CH}_3 \\ \\ \text{OCH}_2\text{CH}_3 \end{array}$ 3-aminopropyl triethoxysilane	Shin-Etsu Chemical Co., Ltd.	LS-3150	APTS	221.4
$\begin{array}{c} \text{OCH}_2\text{CH}_3 \\ \\ \text{O}=\text{C}=\text{N}-(\text{CH}_2)_3-\text{Si}-\text{OCH}_2\text{CH}_3 \\ \\ \text{OCH}_2\text{CH}_3 \end{array}$ 3-(triethoxysilyl)propyl isocyanate	Tokyo Chemical Industry Co., Ltd.	I0556	TSPI	247.4

Burn-off tests indicated that the basalt woven cloth used in this study was furnished with about 1.4 wt% of proprietary sizing applied by the manufacturer. Although no information could be obtained about the nature of this sizing, initial tests were carried out with the fibre material in the state it was received.

2.1.3. Coupling agents

As initial tests suggested that the proprietary sizing applied by the manufacturer was not compatible with thermoplastic resins, two types of silane surface treating agents were selected for further use in this study. The coupling agents used were 3-aminopropyl triethoxysilane (APTS), produced by Shin-Etsu Chemical Co., Ltd., Japan, and 3-(triethoxysilyl)propyl isocyanate (TSPI), produced by Tokyo Chemical Industry Co., Ltd, Japan. The chemical structures and descriptions of these agents are listed in Table 2.

Both silane coupling agents were selected due to their known compatibility with thermoplastic resins and solubility in water. APTS is a well-studied monomeric silane which has been successfully applied with basalt fibres in several resin systems [24–26] and has shown its compatibility to different thermoplastic matrices, such as polycarbonate/silicon carbide [27] and PCL/starch/pine leaf [5].

2.1.4. Fire retardants

In order to preserve the environmentally friendly character of the ‘green’ composites when using fire retardants, it was decided to use a phosphorus-based system (Novared 120, provided by Rinkagaku Kogyo Ltd., Japan) and a metallic hydroxide system based on magnesium hydroxide (Magnifin H-7, provided by Albemarle Corporation, USA),

Table 3. Chemical structures and descriptions of fire retardants

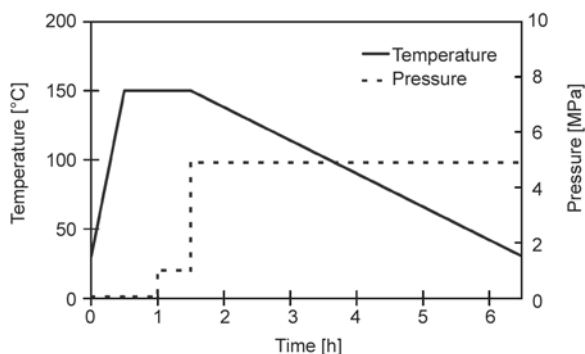
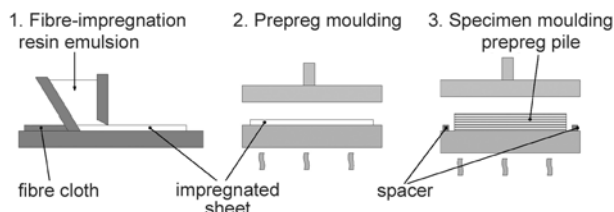
Chemical structure and name	Manufacturer	Product name	Designation	Specific weight	Consistency
P _n Red phosphor	Rinkagaku Kogyo Co.,Ltd.	Novared 120	RP	2.34	Phosphor: 86% Coating: 14%
Mg(OH) ₂ Magnesium hydroxide	Albemarle Corporation	Magnifin H-7	MH	2.40	Mg(OH) ₂ : 99.8%

instead of widely used, but rather toxic fire retardant additives such as halogens. Novared 120 is a red powder with a sublimation temperature of 416°C, while Magnifin H-7 is a white powder with a median particle size of 0.8–1.1 µm. Other properties and descriptions are displayed in Table 3.

2.2. Methods

2.2.1. Sample preparation

Samples were manufactured using the doctor blade-assisted prepreg sheet method, developed in accordance to [28]. Initially, pre-form sheets were manufactured by impregnating as-received basalt fibre plain weave using the doctor blade system (DP-150, Tsugawa Seiki Seisakusho Ltd., Japan), then drying the sheets overnight and cutting them to size. The pre-form sheets were then subjected to an initial pressure and heat application process using a hot power press (WF-37, Shinto Co., Japan), which converted them into prepreg sheets (prepreg moulding). After putting the sheets onto the lower plunger of the hot press, the heating device was engaged and the sheets heated until they reached a processing temperature of 150°C. Marginal pressure was then applied for 30 minutes to enable trapped air to escape and facilitate the impregnation of the matrix between the fibres. The pressure was subsequently increased to 4.9 MPa, while the heating device was switched off, allowing the sample to cool to room temperature at a rate of

**Figure 1.** Process chart for prepreg and sample moulding**Figure 2.** Composite manufacturing process

approximately 0.5°C/min, as detailed in the process chart (Figure 1). Afterwards, several layers of prepreg sheets were stacked and subjected again to a pressure and heat application process (sample moulding), applying the same equipment and parameters as in the previous manufacturing stage. Spacers were used during sample moulding to achieve a predefined sample thickness. The manufacturing process is depicted in Figure 2.

In order to determine the influence of the volume fibre fraction on the mechanical properties, textile composite samples were produced with varying numbers of prepreg-sheets. The number of prepreg-sheet layers used to manufacture tensile test specimens ranged from 4 to 7, while 6 to 12 layers of prepreg-sheets were used to manufacture flexural test specimens. The number of layers corresponded to fibre volume ranges of 32 to 61 vol% and 24 to 51 vol%, respectively.

2.2.2. Application of coupling agents

Before application of the silane coupling agent, the proprietary sizing with which the basalt fibres were coated by the manufacturer was burned off in a furnace at 350°C for 30 minutes. The coupling agents were then applied by first dissolving them in distilled water to form an aqueous solution. An important prerequisite in the preparation of the aqueous silane solution, and thus in the selection of the coupling agents, was the desire to keep the solution as plain as possible without the addition of chemical products other than the silanes. This was done with the intention of keeping the preparation process

itself as simple as possible and to avoid further components with potential negative environmental impact. Hence two water-soluble silane coupling agents, as described in 2.1.3, were chosen for application.

Although there are other parameters, such as treatment time, temperature and solvent composition, one of the principal experimental parameters for the optimised silane treatment on the fibre surface is concentration of the aqueous solution. As was previously shown in [29], the effectiveness of the silane treatment is more dependent on the silane concentration than on the dipping time. Therefore, aqueous solutions with 1, 2 and 3 wt% were prepared to evaluate the optimum concentration, while the dipping time was kept constant at 2 hours.

After applying the aqueous silane solution to the fibres, the fibres were removed and allowed to air dry for approximately 20 hours. A small sample of the dry, treated basalt fibre cloth was weighed and placed in a furnace at 350°C for 2 hours to remove any chemicals from the surface. After removal from the furnace, the samples were again weighed to determine the amount of silane coupling agent that had been burned off in the furnace. The results of this burn off indicated that the silane treated basalt fibre cloth had about 0.5 wt% silane coupling agent on the surface, which complies with the practical experience that only a very small proportion of silane at the interface is sufficient to provide marked improvement in composite properties [30]. Subsequently, the basalt fibres in combination with CP-300 resin were subject to the manufacturing procedure described in chapter 2.2.1.

To evaluate the effect of the silane coupling agent, laminate samples with 8 layers of basalt woven cloth, a fibre volume content of approximately 34 vol%, untreated and treated in APTS and TSPI solutions with different concentrations were tested for flexural strength.

2.2.3. Application of fire retardants

Composite samples with fire retardants were tested for flammability using horizontal and vertical burning tests, as well as being tested for flexural strength. Samples were prepared utilizing the doctor blade assisted prepreg sheet method as described in 2.2.1. The basalt fibres were burned at 350°C for 30 minutes to remove the sizing applied

by the manufacturer and treated in 1%-APTS solution. The fire retardant additives were mixed by hand directly into the liquid resin before impregnation of the fibre. The uniform distribution of the retardants in the resin was visible by the uniform change of the resin colour.

When handling red phosphorus it is important to notice that by prolonged contact with water, or contact with water under elevated temperature, slow decomposition occurs. This decomposition can cause traces of hydrogen phosphide, a toxic and flammable gas, to be formed in time. As shown by the results of the retardancy test, described in 3.3, the contact with the water content of the liquid resin was not prolonged enough to decrease the functionality of the red phosphorus noticeably.

Laminate flexural samples with a thickness of 2 mm and 8 layers of basalt woven cloth, and combustion performance samples with a thickness of 1 mm and 4 layers of woven cloth, corresponding to a volume fibre fraction of approximately 34% and a weight fraction of approximately 55% were manufactured. Fire retarded composite samples were prepared with fire retardant additive amounts of 9 and 4.5 wt%.

2.3. Tests

2.3.1. Tensile strength

An Instron universal material-testing machine, model 4200, was used for the tension tests. The tests were carried out according to [31] with a displacement rate of 1.0 mm/min. All samples had a length of 200 mm, a width of 10 mm and a thickness of 1 mm. End tabs with chamfered edges and manufactured of cross-plyed glass fibre reinforced epoxy resin were attached to the specimens using an appropriate adhesive to avoid untimely failure at the load transmission points. During the tests the initiated load was recorded by an attached computer system, while the tensile strain was quantified by means of strain gauges.

2.3.2. Flexural strength

A Shimadzu AGS-1000B universal material-testing machine was used for the flexural tests. The tests were carried out according to [32] as 3-point-bending tests, with a displacement rate of 1.0 mm/min. Samples had a length of 60 mm, a width of 15 mm

and a thickness of 2 mm. During the tests the initiated load was recorded by an attached computer system; the flexural strain was quantified by means of strain gauges.

2.3.3. Combustion performance

Flammability was characterised by UL 94 tests, according to [33]. The UL 94 method classifies the materials with horizontal and vertical burning tests. In the horizontal burning test, specimens with a length of 127 mm, width of 12.7 mm and thickness of 1 mm are held horizontally and tilted at a 45° angle. A flame fuelled by natural gas is applied to the freestanding end of the specimens for 30 seconds. The time for the flame to reach from the first reference mark at 25.4 mm from the ignited end to the second reference mark at 101.6 mm is measured. Three specimens are tested for each sample. When the burning rate is lower than 76.2 mm/min or the specimens stop burning before the second mark, they are rated with the lowest fire retardancy rating, HB. The most flammable polymers, which cannot be classified according to this method, are marked with a code NR (no rating).

For vertical testing, a specimen with the same dimensions as those used in the horizontal case, is supported in a vertical position and the flame applied to the bottom of the specimen. The flame is applied for ten seconds and then removed until flaming stops at which time the flame is reapplied for another ten seconds and then removed. Two sets of five specimens, which were prepared under different conditions, are tested per sample. One set of

specimens was kept under room temperature for 2 days; the other set was kept for 7 days in a hot air kiln at 60°C and afterwards for 4 hours in a desiccator. If the specimens do not burn with flaming or glowing combustion up to the specimen holding clamp, they receive a vertical flame rating. V0 represents an exceptionally flame retardant material, while V2 and V1 indicate flame retardancy levels between V0 and HB.

2.3.4. Thermal analysis

Thermogravimetric analysis (TGA) measurements were performed with a TG1180 thermal analyzer, produced by Rigaku Corporation, Japan, using 20 mg samples at a heating rate of 10°C/min up to 500°C in air.

2.3.5. Morphology observation

The surfaces of the specimens obtained after the UL94 burning tests, as well as the tensile and flexural samples, were observed with a DSC-T70 digital camera, produced by Sony Corp., Japan.

3. Results and discussion

3.1. Mechanical properties as a function of fibre volume fraction

Using as-received basalt fibre plain weave in combination with CP-300, 'green' composites with a tensile strength of more than 370 MPa and a flexural strength of about 120 MPa have been manufac-

Table 4. Effect of fibre volume content on tensile properties; CP: CP-300 resin; BaF: basalt fibres; AR: as received

Sample designation	Fibre volume fraction [%]	Tensile strength [MPa]	Elastic modulus [GPa]	Fracture strain [%]
CP	0	8.3 ± 0.7	0.3 ± 0.1	16.75 ± 5.75
CP/BaF(AR)32	32	280.9 ± 15.2	11.8 ± 0.2	3.30 ± 0.12
CP/BaF(AR)37	37	301.4 ± 43.8	13.4 ± 1.7	3.01 ± 0.11
CP/BaF(AR)50	50	365.8 ± 31.8	17.3 ± 0.5	3.13 ± 0.25
CP/BaF(AR)61	61	373.3 ± 14.7	15.8 ± 0.4	3.74 ± 0.12

Table 5. Effect of fibre volume content on flexural properties; CP: CP-300 resin, BaF: basalt fibres, AR: as received

Sample designation	Fibre volume fraction [%]	Flexural strength [MPa]	Flexural modulus [GPa]
CP	0	10.2 ± 0.3	0.5 ± 0.1
CP/BaF(AR)24	24	72.8 ± 3.0	9.7 ± 0.8
CP/BaF(AR)34	34	99.0 ± 10.0	15.2 ± 2.5
CP/BaF(AR)37	37	100.6 ± 13.9	15.2 ± 3.4
CP/BaF(AR)42	42	114.2 ± 5.5	17.4 ± 0.3
CP/BaF(AR)51	51	122.3 ± 13.4	19.7 ± 0.9

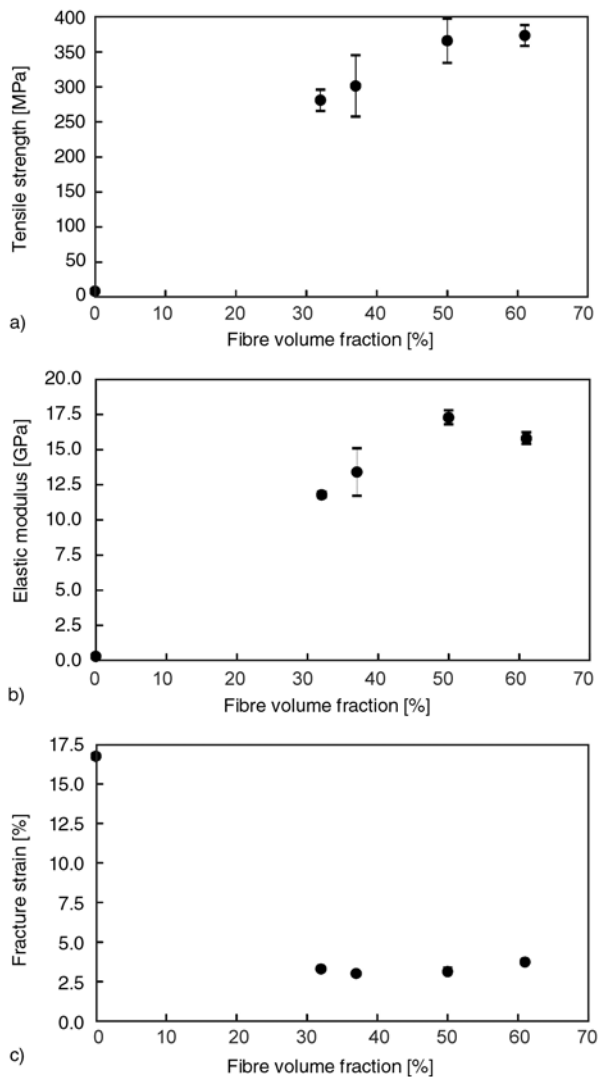


Figure 3. Effect of fibre volume fraction on tensile strength (a), elastic modulus (b) and fracture strain (c)

tured. The composites' tensile and flexural property values are shown in Tables 4 and 5, respectively. Figure 3 presents the tensile strength and the elastic modulus of the plain weave reinforced composite against the fibre volume content. The tensile strength of the composite achieves a value of 281 MPa with a volume fibre content of 32%. An increase in the fibre volume fraction of up to 50% leads to an increase in tensile strength to 366 MPa, but once the fibre volume content exceeds 50% and continues through to a fibre volume content of 61% the tensile strength value remains almost constant at 373 MPa.

These tensile properties of samples with high fibre loading can be explained by non-sufficient fibre wetting, which increases at higher volume fractions. Comparing the fracture behaviour of a 33%-

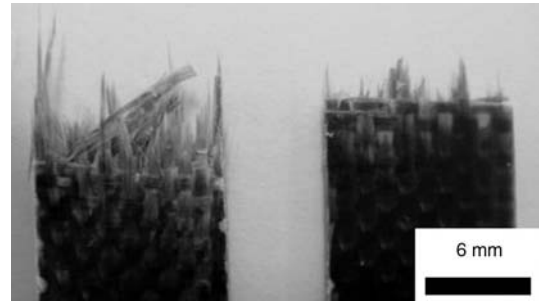


Figure 4. Fracture behaviour of composite specimens; left: $V_f = 50\%$, right: $V_f = 33\%$

sample and a 50%-sample, it is evident that the former shows an almost linear fracture surface, while the latter exhibits a rather brush-like appearance, which suggests an increased fibre pull-out (Figure 4).

The behaviour of the elastic modulus in tension against the change of the fibre volume content is similar to the behaviour of the tensile strength. The elastic modulus value of 11.8 GPa, which was achieved with a fibre volume fraction of 32%, initially went up as expected with the increase in the fibre volume fraction to 17.3 GPa at 50%. The modulus value, however, dropped to 15.8 GPa with an increase in the fibre volume fraction to 61%. The slightly increasing, and subsequently even decreasing values of the elastic modulus may be assigned to the higher void content and low interfacial shear strength, which resulted in less efficiency of load transfer with the increase in fibre content.

Figure 3 also presents the fracture strains of the composites as a function of the fibre volume content. It indicates that the strain values of the fibre reinforced samples are largely independent of the fibre content. This demonstrates that the fibres are the main load-bearing component in the tested fibre volume range.

Figure 5 shows the flexural strength and flexural modulus against the fibre volume fraction. The flexural strength and the flexural modulus show a steady linear rise with the increase in fibre content. The flexural strength rises from 73 MPa at $V_f = 24\%$ to 122 MPa at $V_f = 51\%$, and the flexural modulus increases within the same range of fibre content from 9.7 to 19.7 GPa.

During the three point-bending test, the lower layers are under tension and the upper layers are subject to compression. Flexural samples exhibit compressive fracture caused by fibre buckling failure. Buckling of fibres is mainly restricted by the sur-

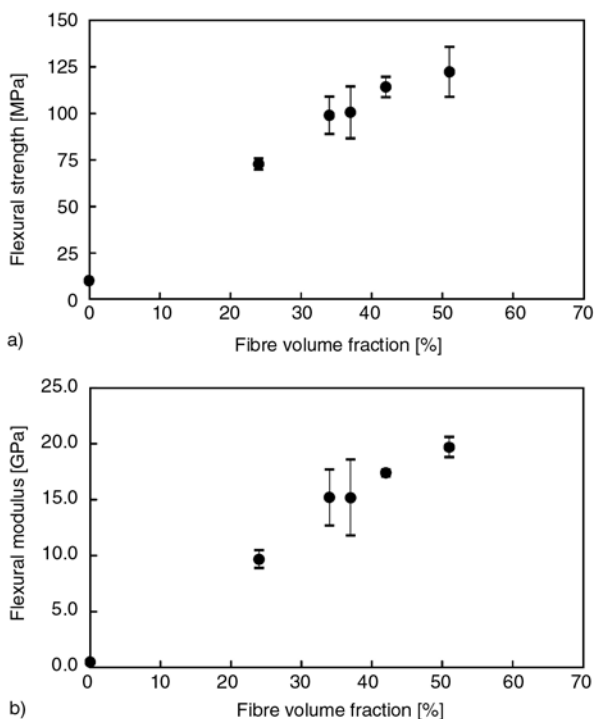


Figure 5. Effect of fibre volume fraction on flexural strength (a) and flexural modulus (b)

rounding matrix and, therefore, dependent on resin properties and the quality of fibre-matrix bond.

3.2. Effect of silane coupling agent

The results of the flexural tests on composites manufactured using desized and silane treated basalt woven cloth are summarised in Table 6. Although no positive effect resulting from the APTS treatment was observed for flexural modu-

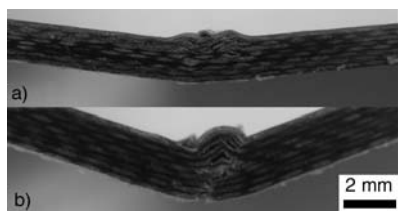


Figure 6. Flexural fracture behaviour of samples with untreated basalt fibres (a) and with fibres treated with APTS (1%) (b)

lus, treatment of the basalt fibres with 1 wt% aqueous APTS solution increased the composites' flexural strength by 38%, from 99 to 136.6 MPa. Figure 6 shows the difference in the flexural fracture behaviour of 1 wt% APTS-treated samples and untreated samples. Both cases display fibre buckling in the upper compression layers. The fibre buckling of the APTS-treated sample, however, is limited to a smaller range of the sample length, indicating that higher compressive powers are needed to cause the buckling of the fibres. While in the untreated case fibre buckling is the main cause for compressive failure, the failure mode of the treated sample is a combination of compressive failure and tension failure by fibre failure in the lower layers, indicating a stronger fibre-matrix bond. With the increase in the concentration of the aqueous solution to 2 wt%, the flexural strength remained virtually unchanged. A further increase up to 3 wt% led to a decrease in the flexural strength to 116.2 MPa.

As further shown in Table 6, composite samples with basalt fibres treated in 1%-TSPI solution exhibited lower tensile strength values than samples with APTS-treated fibres, but still had a 17% higher value than samples using as-received fibres. Although several mechanisms have been proposed to explain the interfacial reinforcement by silane coupling agents, chemical bonding is the most widely accepted [30]. Both coupling agents used in this study are ethoxy derivatives. Their chemical structure may be summarised as $RSi(OEt)_3$, where OEt is the hydrolysable ethoxy group, and R the functional organic group. The ethoxy groups hydrolyse in the presence of water to form the silanol groups, the active agent in the reaction with the mineral surfaces.

The hydroxyl groups of the silanols then react with the hydroxyl groups of the basalt fibre surface through siloxane or hydrogen bonding (Figure 7). In addition to those reactions of silanols with

Table 6. Effect of silane coupling agent application on flexural properties; CP: CP-300 resin; BaF: basalt fibres; SA: APTS; SB: TSPI

Sample designation	Silane treatment		Flexural strength [MPa]	Flexural modulus [GPa]
	Type	Solution content		
CP/BaF34/SA	APTS	1%	136.3 ± 11.3	15.2 ± 1.0
CP/BaF34/SA2	APTS	2%	135.6 ± 5.7	13.1 ± 1.0
CP/BaF34/SA3	APTS	3%	129.1 ± 11.3	14.5 ± 0.9
CP/BaF34/SB	TSPI	1%	116.2 ± 9.3	12.8 ± 1.1

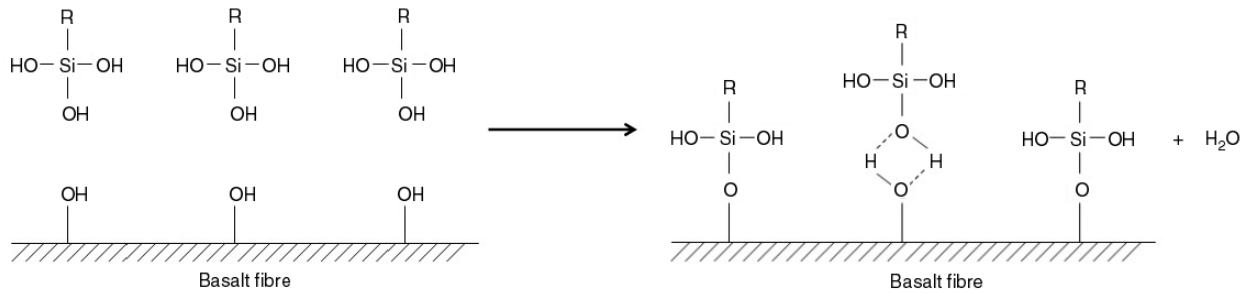


Figure 7. The bonding process of the silanol groups to the basalt fibre surface

hydroxyls on the fibre surface, the formation of polysiloxane structures also can take place [34].

In case of thermoplastic resins it is widely accepted that an interphase layer is generated. This layer may have partial solution compatibility with the matrix resin and forms an interpenetrating network (IPN) as the siloxanols and matrix resin cure separately with a limited amount of cross-linking [35]. The results of our study show that APTS has a higher compatibility with the thermoplastic constituents, PLC and starch, than TSPI and the proprietary sizing applied by the manufacturer.

An explanation for the decrease of the flexural strength with a concentration of 3 wt% may be connected with the thickness of the silane interphase. In general, more than one layer is necessary to form chemical bonds, an interpenetrating network and the proper orientation of functional groups. As the thickness of the deposited silanes increases, the non-bonded oligomeric interphase between the two main substrates of the composites has the opposite effect on the interfacial properties. This interphase has low mechanical strength and low resistance to environmental attack as the oligomeric interphases can be hydrolysed easily. An indicator of the existence of non-hydrolysed interphases might be the appearance of the woven cloth just after impregnation with the resin emulsion, as shown in Figure 8.

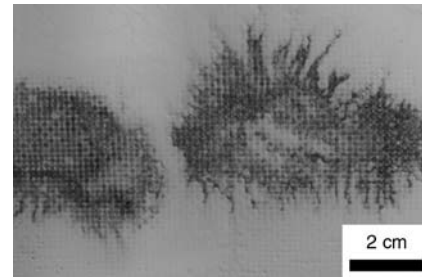


Figure 8. Appearance of freshly impregnated fibres, treated with 3 wt% APTS solution

As such flaws were only observed with plain weave treated with a concentration of 3 wt% APTS, it is conceivable that the reaction of non-hydrolysed ethoxy groups with the water from the emulsion was the cause of this phenomenon.

3.3. Fire retardancy

Table 7 shows combustion and flexural properties of non-reinforced CP resin and basalt fibre reinforced ‘green’ composites with and without application of fire retardant additives. The UL 94 horizontal test results for the non-reinforced CP resin display a very high burning rate, showing that the resin is highly flammable. Incorporation of approximately 34 vol% of non-flammable natural basalt fibres into the resin results in a substantial decrease in the burning speed from 199 to 38 mm/min, lead-

Table 7. Composition of samples tested for combustion performance and effect of fire retardants on combustion performance and flexural properties; x: specimens stopped burning; CP: CP-300 resin; BaF: basalt fibres, SA: APTS; RA: APTS and RP; RB: APTS and MH; RAB: APTS, RP and MH

Sample designation	Ingredients [wt%]				Burning rate [mm/min]				Flexural strength [MPa]	Flexural modulus [GPa]
	CP resin	Basalt fibres	RP	MH	UL 94 H	UL 94 V	UL 94 V7	Rating		
CP	100	–	–	–	199 ± 95	–	–	NR	10.2 ± 0.3	0.5 ± 0.1
CP/BaF34/SA	45	55	–	–	38 ± 4	–	–	HB	136.3 ± 11.3	15.2 ± 1.0
CP/BaF34/RA9	36	55	9	–	×	146 ± 17	155 ± 18	HB	99.6 ± 6.1	13.8 ± 0.7
CP/BaF34/RA	40.5	55	4.5	–	×	162 ± 30	176 ± 17	HB	107.4 ± 4.8	11.6 ± 1.1
CP/BaF34/RB	40.5	55	–	4.5	×	127 ± 6	133 ± 4	HB	103.8 ± 3.7	11.3 ± 0.4
CP/BaF34/RAB	40.5	55	2.25	2.25	×	146 ± 5	154 ± 12	HB	108.9 ± 6.1	13.1 ± 1.0

ing to a HB rating for the composite even without the use of fire retardant additives. Applications of RP and MH, respectively, result in further enhancement of burning behaviour by extinguishing the flaming of the horizontal samples after only a few seconds. This indicates that both additives can be effectively used as fire retardants for starch based basalt fibre reinforced composites at relatively low loadings.

In order to further investigate and to compare the effect of the fire retardant additives, vertical burning tests were conducted as well. The effect of the fire retardants on the burning rates of the vertical combustion samples can be seen in Figure 9. Composite samples with 4.5 wt% RP displayed burning rates of 162 and 176 mm/min, respectively. While an increase in the RP loading to 9 wt% shows a 10% improvement in the flame retardancy, the replacement of 4.5 wt% RP with the same amount of MH improves the composites flame retardancy by more than 20%. The combination of RP with MH in a ratio of 1:1, with an overall fire retardant content of 4.5 wt%, displayed about the same values as samples with 9 wt% RP, but showed lower values than samples with MH only.

Metallic hydroxides such as MH provide flame retarding effects by various mechanisms. Those mechanisms include [36]:

- reduction of the temperature increase of the burning polymer and delay of ignition and flame propagation due to water releasing decomposition,
- reduction of combustible gas concentrations due to water moisture vapour,
- blocking of available oxygen caused by the generation of combustion barriers and delay of flame propagation by adiabatic effect,
- reduction of the amount of burnable material, and
- smoke reduction due to acceleration of the oxidative reaction of fine particle carbon (soot) caused by emerging MgO.

RP is an amorphous polymeric modification of phosphorus. The fire retardancy effectiveness of RP depends slightly on the polymer used, because of different mechanisms which depend on the surrounding environment of RP particles. The retardancy of RP is based on its ability to turn into polyphosphoric acid derivatives while burning, facilitating the formation of char layers. This effect is efficient in the case of oxygen-bearing resins, but the efficiency decreases if the generation of char layers depends solely on oxygen found on the burning surface of the polymer [37].

Both fire retardants effectively reduce the flammability of the composite at low content. Although the oxygen content inherent in both starch and PCL was sufficient for RP to bring its fire retarding mechanism into effect, forming char layers as seen in Figure 10, MH displays higher retarding effectiveness with the same weight content. As further seen by the appearance of both specimens in Figure 10, the dominant fire retarding mechanism by application of MH was similar to the fire retardant mechanism of RP. For this reason, no synergistic

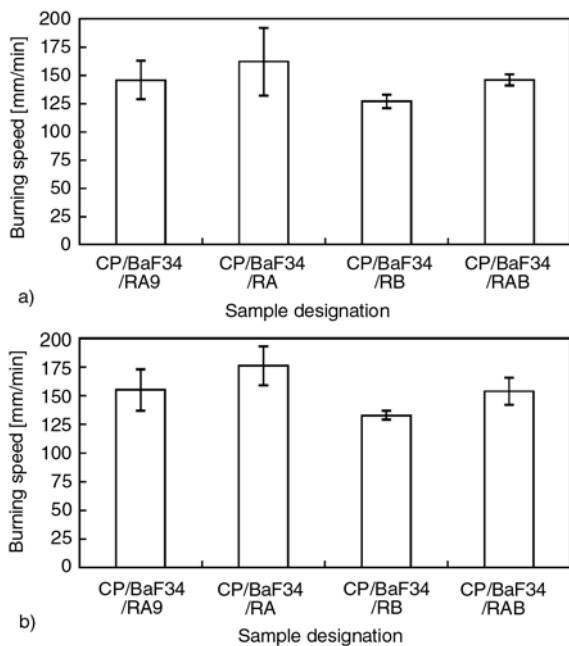


Figure 9. Effect of the fire retardant additives on UL 94 horizontal burning rate of samples stored for 2 days at RT (a) and 7 days at 60°C (b) before testing

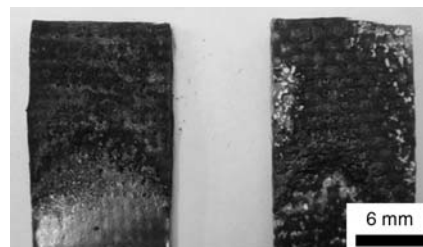


Figure 10. Photographs of specimens after UL 94 horizontal burning test of formulations with 4.5 wt% red phosphorus (CP/BaF34/RA, left) and 4.5 wt% magnesium hydroxide (CP/BaF34/RB, right)

effect was observed by using the fire retardants simultaneously.

Figure 11 shows the TGA curves of the flame retarded resins used in the sample designations CP/BaF34/RA and CP/BaF34/RB containing 10 wt%

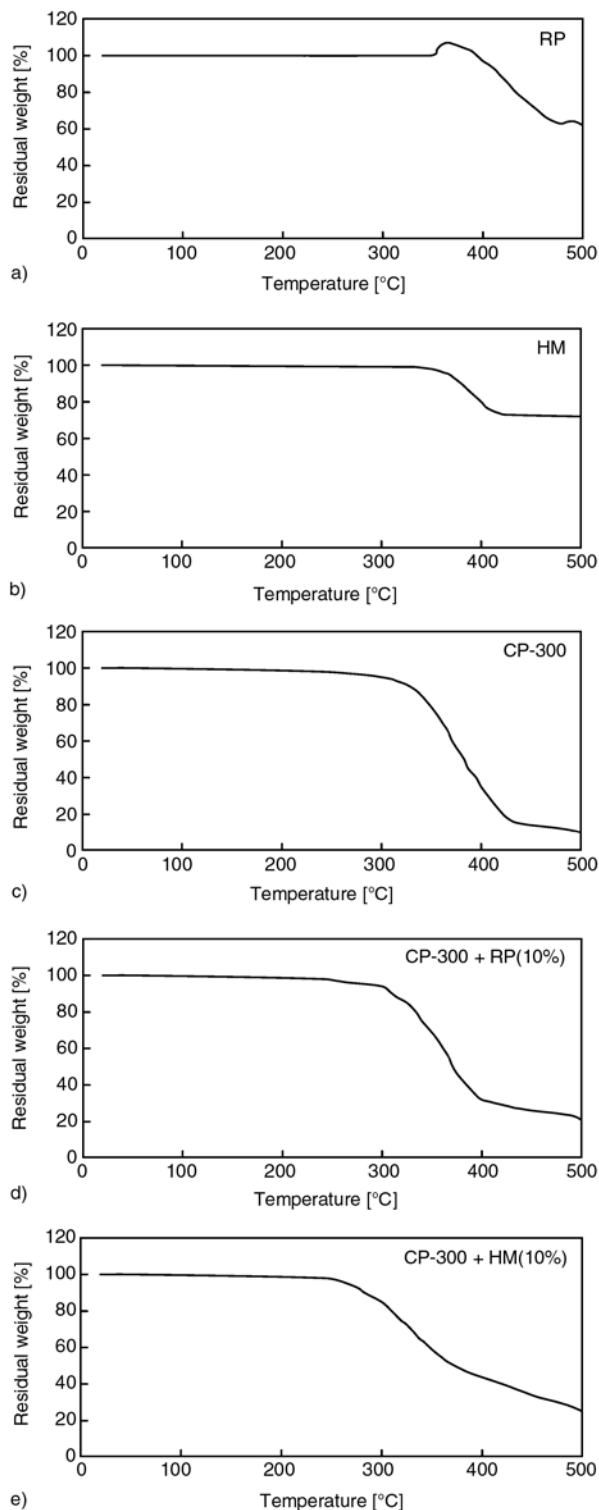


Figure 11. TGA curves of red phosphor (RP) (a), magnesium hydroxide (MH) (b), CP-300 base resin (c) and mixtures of the base resin with 10% RP (d) and MH (e), respectively

RP and MH, respectively, together with the TGA curves of each flame retardant and the base resin CP-300. The decomposition of CP-300 starts at 250°C, continues quickly and reaches a residual weight of 16% at 430°C, with a remaining residue of 10% at 500°C. Both flame retardants start to decompose at 350°C. MH decomposes steadily until 410°C reaching a residual weight of 75% with a remaining residue of 72% at 500°C. RP displays a slight mass increase at 350°C due to its highly oxidative character and then starts to decompose leaving a char residue of 62% at 500°C. The effect of the flame retardants on the base resin can be clearly seen by looking at the residues at 500°C. The amount of residue of CP-300 with 10% RP is, with 21%, twice as high as the amount in the case of the base resin. The value of CP-300 with 10% MH is, with 25%, even higher. This indicates that the resulting char-like residue observed during the UL 94 tests and shown in Figure 10 is formed from the present flame retardants starting with the decomposition process of the base resin at around 250 to 300°C.

Table 7 also displays the flexural properties of the flame retardant composite mixtures. Despite the application of the silane coupling agent, the addition of flame retardant additives shows a negative influence on the flexural properties of the composites, and the properties of the composites with 4.5% flame retardants display a reduction in flexural strength of 20 to 24 %. At the same loading values samples with RP only exhibited slightly better properties than samples with HM or with both retardants, which might be indicative of non-uniform distribution of HM inside the resin.

4. Conclusions

High strength bi-directional ‘green’ composites with woven basalt cloth as reinforcement and starch based resin as base material have been successfully manufactured through the utilization of a hot press machine and a doctor blade system. Furthermore, this study showed that by application of silane coupling agents compatible with the resin system, flexural properties of the composite could be improved significantly. The flammability behaviour of the base resin and of the composites with and without flame retardants, as well as the effect of flame retardant additives on the flexural proper-

ties of basalt fibre reinforced starch based composite was studied. It was shown that basalt fibres are a natural reinforcement material which significantly improves the flammability behaviour of the thermoplastic matrix. It was further shown that magnesium hydroxide and red phosphor can effectively reduce the flammability of the composite with contents as low as 4.5 wt%. The flexural properties of the retardant-filled composite exhibited a slight decrease compared to the composite without flame retardants, but at the same time showed better properties compared to the composites without treatment with silane coupling agent compatible to the polymer system.

Further tests, especially on durability and resistance against environmental conditions, have to be performed in order to evaluate the application possibilities of the developed material and to assess if basalt fibre reinforced CP-300 is adaptive for parts which are exposed to environmental influences, as for example automotive under body panels.

Acknowledgements

The authors gratefully acknowledge financial support by the Itoyama International Foundation and the Rotary Yoneyama Memorial Foundation. Furthermore, the authors would like to thank Miyoshi Yushi Inc. for supplying the base resin, and Rinkagaku Kogyo Ltd. and Albemarle Overseas Development Corporation, Japan, for supplying the fire retardant additives.

References

- [1] Stamboulis A., Baille C., Peijs T.: Effects of environmental conditions on mechanical and physical properties of flax fibers. *Composites Part A: Applied Science and Manufacturing*, **32**, 1105–1115 (2001).
- [2] Bismarck A., Mishra S., Lampke T.: Plant fibres as reinforcement in green composites. in 'Natural Fibers, Biopolymers and Biocomposites' (eds.: Mohanty A. K., Misra M., Drzal L. T.) Taylor and Francis, Boca Raton, 37–108 (2005).
- [3] Wootthikanokkhan J., Santikunakorn S.: Effects of propionyl content on the morphology, mechanical properties, and biodegradability of esterified cassava starch/polycaprolactone blends. *Journal of Applied Polymer Science*, **96**, 2154–2162 (2004).
- [4] Wu C-S.: Performance of an acrylic acid grafted polycaprolactone/starch composite: Characterization and mechanical properties. *Journal of Applied Polymer Science*, **89**, 2888–2895 (2003).
- [5] Kim E. G., Kim B. S., Kim D. S.: Physical properties and morphology of polycaprolactone/starch/pine-leaf composites. *Journal of Applied Polymer Science*, **103**, 928–934 (2007).
- [6] Dzhigiris D. Z., Makhova M. F., Gorobinskaya V. D., Bombyr L. N.: Continuous basalt fiber. *Glass and Ceramics*, **40**, 467–470 (1983).
- [7] Morozov N. N., Bakunov V. S., Morozov E. N., Aslanova L. G., Granovskii P. A., Prokshin V. V., Zemlyanitsyn A. A.: Materials based on basalts from the european north of russia. *Glass and Ceramics*, **58**, 100–104 (2001).
- [8] Sokolinskaya M. A., Zabava L. K., Tsybulya T. M., Medvedev A. A.: Strength properties of basalt fibers. *Glass and Ceramics*, **48**, 435–437 (1991).
- [9] Militky J., Kovacic V.: Ultimate mechanical properties of basalt filaments. *Textile Research Journal*, **66**, 225–229 (1996).
- [10] Gur'ev V. V., Neproshin E. I., Mostovoi G. E.: The effect of basalt fiber production technology on mechanical properties of fiber. *Glass and Ceramics*, **58**, 62–65 (2001).
- [11] Czigány T.: Basalt fiber reinforced hybrid polymer composites. *Materials Science Forum*, **473-474**, 59–66 (2005).
- [12] Kogan F. M., Nikitina O. V.: Solubility of chrysotile asbestos and basalt fibers in relation to their fibrogenic and carcinogenic action. *Environmental Health Perspectives*, **102**, 205–206 (1994).
- [13] Czigány T., Vad J., Pölöskei K.: Basalt fiber as a reinforcement of polymer composites. *Periodica Polytechnica, Mechanical Engineering*, **49**, 3–14 (2005).
- [14] Szabó J. S., Czigány T.: Material properties: Static fracture and failure behavior of aligned discontinuous mineral fiber reinforced polypropylene composites. *Polymer Testing*, **22**, 711–719 (2003).
- [15] Vas L. M., Pölöskei K., Felhős D., Deák T., Czigány T.: Theoretical and experimental study of the effect of fiber heads on the mechanical properties of non-continuous basalt fiber reinforced composites. *Express Polymer Letters*, **1**, 109–121 (2007).
- [16] Matkó S., Anna P., Marosi G., Szép A., Keszei S., Czigány T., Pölöskei K.: Use of reactive surfactants in basalt fibre reinforced polypropylene composites. *Macromolecular Symposia*, **202**, 255–267 (2003).
- [17] Ozawa Y., Kikuchi T., Isohata M.: Mechanical behavior of basalt fiber reinforced polymer composites in temperature condition. in 'Proceedings of 3rd International Workshop on Green Composites (IWGC-3). Kyoto, Japan' 124–127 (2005).
- [18] Liu Q., Shaw M. T., Parnas R. S., McDonell A. M.: Investigation of basalt fiber composite mechanical properties for applications in transportation. *Polymer Composites*, **27**, 41–48 (2006).
- [19] Liu Q., Shaw M. T., Parnas R. S., McDonell A-M.: Investigation of basalt fiber composite aging behavior for applications in transportation. *Polymer Composites*, **27**, 475–483 (2006).

- [20] Ye P., Reitz L., Horan C., Parnas R.: Manufacture and biodegradation of wheat gluten/basalt composite material. *Journal of Polymers and the Environment*, **14**, 1–7 (2006)
- [21] Wittek T., Tanimoto T.: Biodegradable starch-based resin reinforced with continuous mineral fibres – Processing, characterisation and mechanical properties. *Advanced Composite Materials*, in press (2008).
- [22] Matkó S., Toldy A., Keszei S., Anna P., Bertalan G., Marosi G.: Flame retardancy of biodegradable polymers and biocomposites. *Polymer Degradation and Stability*, **88**, 138–145 (2005).
- [23] Tanaka H.: Starch emulsion (in Japanese). *Engineering Materials*, **51**, 58–62 (2003).
- [24] Park J. M., Subramanian R. V.: Interfacial shear strength and durability improvement by monomeric and polymeric silanes in basalt fiber/epoxy single-filament composite specimens. *Journal of Adhesion Science and Technology*, **5**, 459–477 (1991).
- [25] Park J. M., Subramanian R. V., Bayoumi A. E.: Interfacial shear strength and durability improvement by silanes in single-filament composite specimens of basalt fiber in brittle phenolic and isocyanate resin. *Journal of Adhesion Science and Technology*, **8**, 133–150 (1994).
- [26] Park J-M., Shin W-G., Yoon D-J.: A study of interfacial aspects of epoxy-based composites reinforced with dual basalt and SiC fibres by means of the fragmentation and acoustic emission techniques. *Composites Science and Technology*, **59**, 355–370 (1999).
- [27] Park J-M., Chong E-M., Yoon D-J., Lee J-H.: Interfacial properties of two SiC fiber-reinforced polycarbonate composites using the fragmentation test and acoustic emission. *Polymer Composites*, **19**, 747–758 (1998).
- [28] Tanimoto T.: Continuous-fibre CMC fabrication by using pre-impregnated sheets. *Composites Part A: Applied Science and Manufacturing*, **30**, 583–586 (1989).
- [29] Kobayashi T., Takahashi S., Fujii N.: Silane coupling agent having dithiocarbamate group for photografting of sodium styrene sulfonate on glass surface. *Journal of Applied Polymer Science*, **49**, 417–423 (1993).
- [30] Plueddemann E. P.: *Silane coupling agents*. Plenum Press, New York (1982).
- [31] JIS K 7113: Testing method for tensile properties of plastics (1995).
- [32] JIS K 7017: Fibre-reinforced plastics composites – Determination of flexural properties (1999).
- [33] JIS K 6911: Testing methods for thermosetting plastics (1995).
- [34] Arkles B., Steinmetz J. R., Zazyczny J., Mehta P.: Factors contributing to the stability of alkoxy silanes in aqueous solutions. *Journal of Adhesion Science and Technology*, **6**, 193–206 (1992).
- [35] Plueddemann E. P.: Reminiscing on silane coupling agents. *Journal of Adhesion Science and Technology*, **5**, 261–277 (1991).
- [36] Hornsby P. R., Watson C. L.: Mechanism of smoke suppression and fire retardancy in polymers containing magnesium-hydroxide filler. *Plastics and Rubber Processing and Applications*, **11**, 45–51 (1989).
- [37] Troitzsch J.: *Plastics flammability handbook: Principles, regulations, testing and approval*. Hanser Publishers, Munich (2004).

Preparation and third-order nonlinear optical property of poly(urethane-imide) containing dispersed red chromophore

F. X. Qiu^{1,2*}, D. Y. Yang¹, P. P. Li², X. Wang¹

¹School of Chemistry and Chemical Engineering, Jiangsu University, Zhenjiang, 212013, China

²Jiangsu Provincial Key Laboratory of Modern Agricultural Equipment and Technology, Zhenjiang 212013, China

Received 10 August 2008; accepted in revised form 13 October 2008

Abstract. A novel poly(urethane-imide) (PUI) containing dispersed red chromophore was synthesized. The PUI was characterized by FT-IR, UV-Vis, DSC and TGA. The results of DSC and TGA indicated that the PUI exhibited high thermal stability up to its glass-transition temperature (T_g) of 196°C and 5% heat weight loss temperature of 229°C. According to UV-Vis spectrum and working curve, the maximum molar absorption coefficient and absorption wavelength were measured. They were used to calculate the third-order nonlinear optical coefficient $\chi^{(3)}$. At the same time, the chromophore density of PUI, nonlinear refractive index coefficient and molecular hyperpolarizability of PUI were obtained. The fluorescence spectra of PUI and model compound DR-19 were determined at excitation wavelength 300 nm. The electron donor and acceptor in polymer formed the exciplex through the transfer of the electric charges. The results show that the poly(urethane-imide) is a promising candidate for application in optical devices.

Keywords: polymer synthesis, third-order nonlinear optics, molecular hyperpolarizability, nonlinear refractive index coefficient

1. Introduction

It is well known that nonlinear optical (NLO) materials can be used for a number of photonic applications, for example, optical signal processing, optical communication, optical computing, electro-optic modulation, optical limiting effect, etc. Polymer is attractive medium for application in optical electronic devices [1–3]. Recently, there has been growing interest in the third-order nonlinearity of azo-dye doped polymer materials for their large $\chi^{(3)}$ value, which are interesting for application in optical-limiting and optical switching application. Photoisomerization of azo-molecules makes it easy to modify linear and nonlinear polarizabilities of molecular as well as optical nonlinear refraction. The optical properties of azo-polymer can be controlled optically, which aroused considerably the interest of people [4, 5].

Polyurethane (PU) is a versatile polymer and can be easily prepared by a simple polyaddition reaction of polyol, isocyanate and a chain extender. Unfortunately, the conventional PU is known to exhibit poor thermal stability which limits its applications. Research focused on improving the thermal stability of PU has attempted to achieve this goal in various ways. The most accepted approach for the improvement of thermal stability of PU is a chemical modification in the structure by introducing thermally stable heterocyclic polymers like polyimides [6–8]. Polyimides (PI) are the most important members of heterocyclic polymers with remarkable heat resistance and excellent mechanical, electrical, chemical and durability properties. So the incorporation of polyimide or oligoimide unit into PU has been attempted, resulting in an imide-modified PU (i.e. poly(urethane-imide),

*Corresponding author, e-mail: fxquichem@163.com
© BME-PT and GTE

PUI), which is a type of organic polymer characterized by its outstanding thermal stability, good solubility and film formation ability.

In this paper, the isocyanate groups ($-NCO$) terminated polyurethane containing a diazo non-linear optical chromophore in the side-chain was synthesized based on toluene diisocyanate (TDI) with two active isocyanate groups and dispersed red 19 (DR-19) with two isolated hydroxyl groups, and then the polyurethane terminated with $-NCO$ groups was used to synthesize the poly (urethane-imide) (PUI) with 4,4'-(Hexafluoroisopropylidene) diphthalic Anhydride (6FDA). The structure, the thermal property, third-order nonlinear coefficient and nonlinear refractive index coefficient and molecular hyperpolarizability of the PUI were characterized and obtained. The experimental results showed that the PUI obtained possessed excellent heat-resistance and high third-order nonlinear property.

2. Experimental

2.1. Materials

Dispersed red 19 was obtained from the ACROS ORGANICS. The 4,4'-(Hexafluoro-isopropylidene) diphthalic Anhydride (6FDA) was obtained from TCI Co. and used without further purification. N,N-dimethylformamide (DMF, A. R.) was provided by Shanghai Gaoqiao petrochemical company. Toluene-2,4-diisocyanate (TDI, industry product) was supplied by Huls Co. and was purified before use.

2.2. Characterization

FT-IR spectra of the prepared thin films were obtained on a KBr pellet using Nicolet AVATAR 360 spectrometer. Thermogravimetric analysis (TGA) and differential scanning calorimetry (DSC) were performed on NETZSCH STA449C. The programmed heating range was from room temperature to 700°C, at a heating rate of 10°C/min under nitrogen atmosphere. The measurement was taken using 6–10 mg samples. The UV-Vis spectrum of the PUI solution was measured by Shimadzu UV-240 spectrophotometer. The photoluminescence measurement was performed on a VARIAN Cary Eclipse spectrofluorophotometer.

2.3. Preparation of PUI

The Toluene-2,4-diisocyanate (TDI) 1.25 g (7.2 mmol) and 15 ml DMF were added into a 250 ml flask equipped with mechanical stirrer, nitrogen inlet, condenser and thermometer to react at room temperature, and then the DR-19 1.12 g (3.4 mmol) dissolved in 15 ml DMF was dropped slowly into the system. The reaction was carried out at 40, 75 and 90°C for 2 h, respectively. After cooling to the room temperature, the 4,4'-(Hexafluoroisopropylidene) diphthalic Anhydride (6FDA) 1.51 g (3.4 mmol) was dissolved in 30 ml DMAC and dropped into the system and reacted with the $-NCO$ groups at 40 and 90°C for 2 h, respectively. The product was deposited in the solution of methanol and water (V:V = 1:1). The red poly(urethane-imide) (PUI) was obtained after filtration and

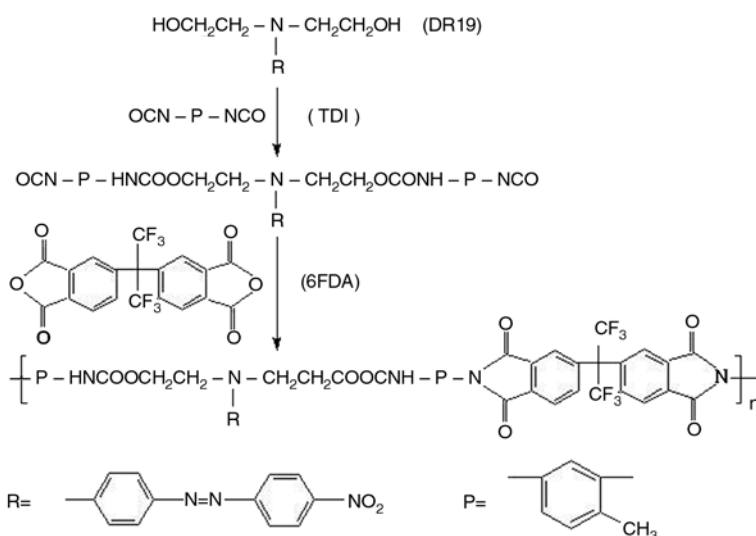


Figure 1. Synthesis of poly (urethane-imide) (PUI)

drying in vacuum at 60°C. The synthetic route for PUI is shown in Figure 1.

3. Results and discussion

3.1. Structure characterization and thermal property of PUI

The UV-Vis spectra of the prepared poly(urethane-imide) material and DR-19 were shown in Figure 2. The content of PUI or DR-19 was $3.0 \cdot 10^{-5} \text{ mol} \cdot \text{l}^{-1}$. From Figure 2, the absorption peak of DR-19 in DMF was 500 nm, while the absorption peak of PUI in DMF was 454 nm. The result indicated that the absorption peak had blue shift after polymerization. The two hydroxyl groups in DR-19 formed urethane bond after polycondensation. The electron cloud in azobenzene groups of DR-19 shifted to the ester bond because of the electron acceptor character of C=O, which decreased the electron cloud density in azobenzene groups, so absorption band of azobenzene groups would shift to the UV region with the high energy demand of the electron transfer. Because the absorption of PUI was from the azobenzene groups in its side-chain, the UV-Vis data verified the graft reaction of azobenzene monomer with polymer.

Figure 3 illustrates the FT-IR spectrum of the prepared poly(urethane-imide). It shows that the band at 3410 cm^{-1} is fairly broad and corresponds to the stretching vibration of free and hydrogen-bonded NH groups. Meanwhile, the characteristic absorption bands are observed at 1784, 1719 and 1501 cm^{-1} corresponding to the stretch vibration of C–N bond, symmetry coupling vibration of the carbonyl in imide ring, anti-symmetric coupling vibration of

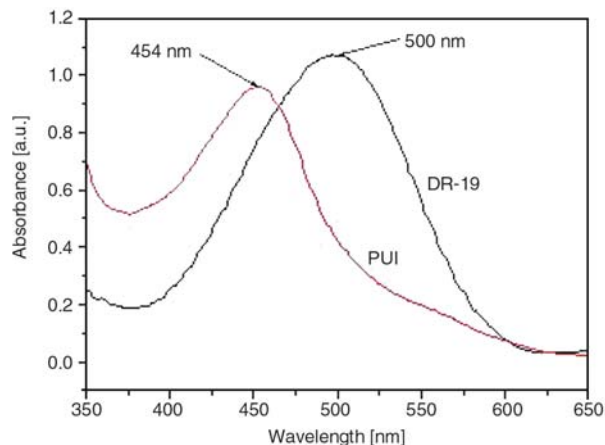


Figure 2. UV-Vis spectra of PUI and DR-19

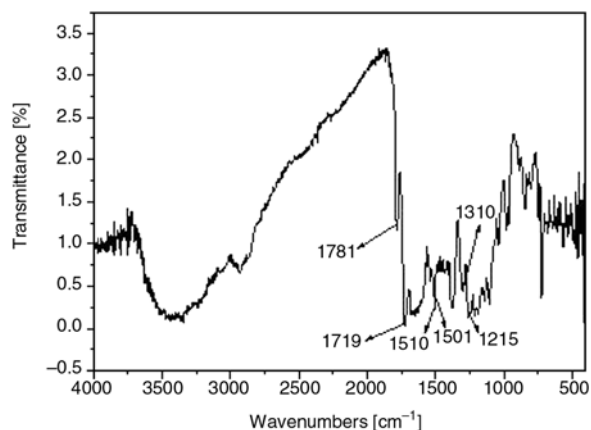


Figure 3. FT-IR spectrum of PUI

the carbonyl in imide ring and the anti-symmetric stretch vibration of $-\text{N}=\text{N}-$ bond, respectively [9]. And the absorption bands at 1510 and 1310 cm^{-1} are assigned to the symmetric and anti-symmetric stretch vibration of nitro-group in the side-chain of chromophore. 1245 cm^{-1} is attributed to the ether (C–O–C) band of DR-19. These data verified that the imide groups had been introduced to PU backbone. Moreover, the absence of the absorption band at 2270 cm^{-1} corresponding to the characteristic absorption of isocyanate group indicated that all the monomers were consumed.

To examine thermal activity and thermal decomposition characteristics of material, DSC and TGA experiments were carried out on NETZSCH STA449C with the heating rate $10^\circ\text{C}/\text{min}$ under nitrogen, as shown in Figure 4. It can be recognized that the glass transition temperature for PUI was at 196°C , which is much higher than the corresponding side-chain nonlinear optical (NLO) polyurethanes (T_g of PU based on DR-19 and TDI was at about 137°C). The 5% heat weight loss tempera-

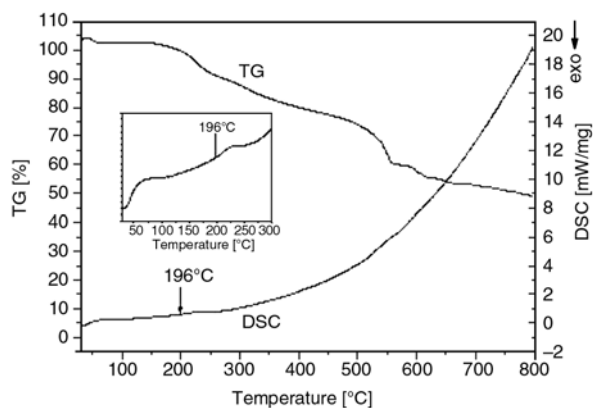


Figure 4. DSC and TGA curves of PUI

ture of PUI was at 229°C. When the temperature increased to 780°C, the mass fraction of PUI was still as high as 50%, indicating the obtained polymer PUI possessed excellent thermal stability. The reason for this was due to the strong hydrogen bonds of the macromolecular chains between polyurethane and polyimide, which formed the physical cross-linkage network among PUI macromolecular chains to alleviate the thermal decomposition of PUI and enhance the thermal stability of this polymer.

3.2. Determination of third-order nonlinear optical property and molecular hyperpolarizability

Theory of the nonlinear optical pointed out that the materials with the central non-symmetric structures possessed the second order nonlinear polarization coefficient, even if the arrangement of the molecular orientation was totally random and the molecule was isotropy, the $\chi^{(3)}$ of the material was not equal to zero. The polymer with delocalized π electron has high third-order nonlinear optical coefficient and fast response speed, so it was possible to be used in the integrated optic, logic optical path and optical computer. Meisser *et al.* indicated that there was direct relationships among the nonlinear optical coefficient $\chi^{(3)}$ (-3ω , ω , $-\omega$, ω), maximum molar absorption coefficient ϵ_{\max} and absorption wavelength λ_{\max} of the conjugated polymer [10]. The third-order nonlinear optical coefficient is defined by the Equation (1):

$$\chi^{(3)} = \frac{\epsilon_{\max}}{\lambda_{\max}^6} \quad (1)$$

The maximum absorption wavelength (λ_{\max}) of PUI was 454 nm in Figure 2. Different contents of PUI in DMF were prepared and the absorbance was determined at 454 nm by Shimadzu UV-240 spectrophotometer, respectively. The working curve was obtained and shown in Figure 5. From Figure 5, the linear regression equation was $y = 32000x + 0.00493$ (y was the absorbance, x was concentration of PUI) and the maximum molar absorbance coefficient (ϵ_{\max}) was 32 000 L·mol⁻¹·cm⁻¹. The correlation coefficient (r) was 0.998 and standard deviation (SD) was 0.664%.

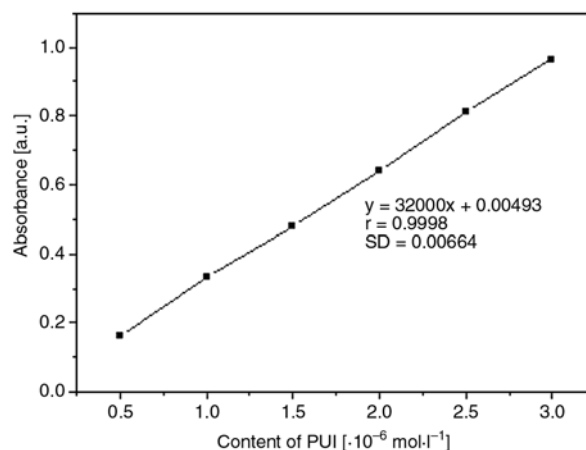


Figure 5. Working curve of PUI

According to the Equation (1), the $\chi^{(3)}$ of PUI was calculated $3.60 \cdot 10^{-12}$ esu. From the data, we could find that the PUI product obtained in this article had a satisfaction third-order nonlinear optical coefficient. Because the diazo bonds connecting with phenyl possessed large π electron conjugated structure, it would increase the conjugated degree of the PUI backbone chain and enhance its third-order nonlinear optical coefficient when introduced to the backbone of the polymer as side-chains. In addition, the push-pull structure in PUI macromolecular increased the conjugated length of the diazo bonds in side-chain increased the electron shift of the whole conjugated system and the third-order nonlinear optical coefficient of PUI polymer. Comparing with the theoretical calculation value of $3.10 \cdot 10^{16}$ molecule/ml, the chromophore density of the prepared PUI measured by the method of working curves was $2.26 \cdot 10^{16}$ molecule/ml, which was close to the former, indicating that the polymerization was according to the stoichiometric ratio. Nonlinear refractive index (n_1) coefficient was obtained from third-order nonlinear optical coefficient and described by Equation (2) [11]:

$$n_1 = \frac{12\pi\chi^{(3)}}{n_{\text{sample}}^2} \quad (2)$$

where n_{sample} is refractive index of PUI ($n = 1.415$). According to this formula (2), nonlinear refractive index coefficient of PUI is $6.78 \cdot 10^{-11}$ esu. Molecular hyperpolarizability (γ) of sample can be calculated and expressed by Equation (3):

$$\gamma = \frac{\chi^{(3)}}{T^4 N_0} \quad (3)$$

where N_0 is the number of molecule per milliliter ($2.26 \cdot 10^{16}$ molecule/ml). T is local field revision factor, it can be expressed by Equation (4):

$$T = \frac{n_{\text{sample}}^2 + 2}{3} \quad (4)$$

According to the formula (4) and (3), T and γ were 1.334075 and $5.03 \cdot 10^{-29}$ esu, respectively. The results indicated that PUI had high third-order nonlinear polarizability.

3.3. Fluorescence characterization of PUI

The fluorescence characters of PUI and model compound DR-19 were determined at excitation wavelength of 300 nm. The Fluorescence spectra were obtained in Figure 6.

It showed that both in the spectrum of PUI and DR-19 there appeared fluorescence peaks and their fluorescence effects were similar, which indicated that the fluorescence effect of PUI was generated from the azobenzene groups in its macromolecular chains. But at the same concentration, the fluorescence intensity of PUI was lower than that of DR-19, which may be a result of the special structure of PUI. In the molecular chain of PUI, there were different length of non-conjugated chains (which came from the $-\text{O}(\text{CH}_2)_2\text{N}-$ in DR-19 and $-\text{HNCCH}_2\text{CNH}-$ in TDI) and definite length of conjugated chains, which forming the un-luminiferous and luminiferous chains of polymer PUI. At the same time, in PUI there existed both small size

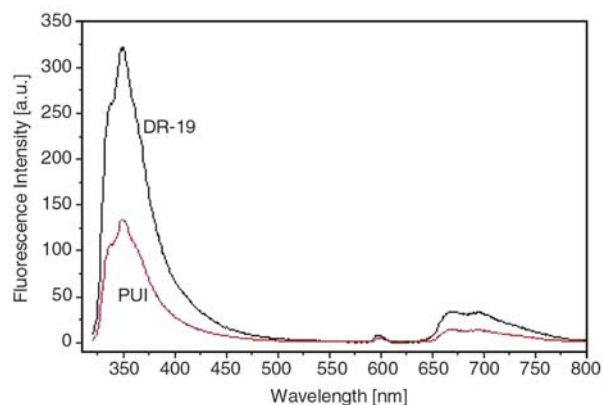


Figure 6. Fluorescence spectra of DR-19 and PUI

and strong stiffness and carbonyl with electron donor groups and electron acceptor of 6FDA, which formed the intramolecular or intermolecular exciplex through the transfer of the electric charges at condition of lighting. So the fluorescence intensity of PUI decreased with the self-quenching of the macromolecules in ground state and excited state when transferring among the molecules [12, 13].

4. Conclusions

We synthesized a novel poly(urethane-imide) (PUI) containing a diazo nonlinear optical chromophore (dispersed red 19) in the side-chain. The determination results of the glass-transition temperature (T_g) and 5% heat weight loss temperature indicated that the material possessed excellent thermal stability. Measurement result of the chromophores density of PUI showed that the polymerization was according to the stoichiometric ratio. The PUI has high third-order nonlinear coefficient and polarizability. Moreover, its fluorescence effect was result from the azobenzene groups in its side-chains. The electron donor and acceptor in polymer formed the exciplex through the transfer of the electric charges at condition of lighting. These results show that PUI polymer is promising materials for nonlinear optical applications.

Acknowledgements

This project was supported by the Natural Science of Jiangsu Province (BK2008247), China Postdoctoral Science Foundation (20070420973), the Jiangsu Planned Projects for Postdoctoral Research Funds (0602037B), Jiangsu Provincial Key Laboratory for Science and Technology of Photon Manufacturing and the Natural Science of Jiangsu Education (08KJB150004).

References

- [1] Qiu F. X., Cao Y. L., Xu H. L., Jiang Y., Zhou Y. M., Liu J. Z.: Synthesis and properties of polymer containing azo-dye chromophores for nonlinear optical applications. *Dyes and Pigments*, **75**, 454–459 (2007).
- [2] Qiu F. X., Da Z. L., Yang D. Y., Cao G. R., Li P. P.: The synthesis and electro-optic properties of polyimide/silica hybrids containing the benzothiazole chromophore. *Dyes and Pigments*, **77**, 564–569 (2008).

- [3] Qiu F. X., Li P. P., Yang D. Y.: Synthesis, characterizations and electro-optical properties of nonlinear optical polyimide/silica hybrid. *Express Polymer Letters*, **1**, 150–156 (2007).
- [4] Fuh A. Y-G., Lin H-C., Mo T-S., Chen C-H.: Nonlinear optical property of azo-dye doped liquid crystals determined by biphotonic Z-scan technique. *Optics Express*, **13**, 10634–10641 (2005).
- [5] Lee M-R., Wang J-R., Lee C-R., Fuh A. Y-G.: Optically switchable biphotonic photorefractive effect in dye-doped liquid crystal films. *Applied Physics Letters*, **85**, 5822–5824 (2004).
- [6] Gnanarajan T. P., Nasar A. S., Iyer N. P., Radhakrishnan G.: Synthesis of poly(urethane-imide) using aromatic secondary amine-blocked polyurethane prepolymer. *Journal of Polymer Science Part A: Polymer Chemistry*, **38**, 4032–4037 (2000).
- [7] Lin M-F., Shu Y-C., Tsen W-C., Chuang F-S.: Synthesis of polyurethane-imide (PU-imide) copolymers with different dianhydrides and their properties. *Polymer International*, **48**, 433–445 (1999).
- [8] Chen J. N., Zhang J. F., Zhu T. Y., Hua Z. C., Chen Q. M., Yu X. H.: Blends of thermoplastic polyurethane and polyether-polyimide: Preparation and properties. *Polymer*, **42**, 1493–1450 (2001).
- [9] Qiu F. X., Xu H. L., Cao Y. L., Jiang Y., Zhou Y. M., Liu J. Z., Zhang X. P.: Nonlinear optical materials: Synthesis, characterizations, thermal stability and electro-optical properties. *Materials Characterization*, **58**, 275–283 (2007).
- [10] Messier J., Kajzar F., Prasad P.: *Organic molecules for nonlinear optics and photonics*. Kluwer Academic Publishers, Dordrecht (1991).
- [11] Jenekhe S. A., Lo S. K., Flom S. R.: Third-order nonlinear optical properties of a soluble conjugated polythiophene derivative. *Applied Physics Letters*, **54**, 2524–2526 (1989).
- [12] Hong Z. Y., Zhao X. J., Ma D. G., Wang D. K., Jing X. B., Wang F. S.: Influence of fluorescence intensity for polymeric structure and chain distance. *Chinese Science Bulletin*, **43**, 588–592 (1998).
- [13] Zhang X. L., Yuan J. F., Qu J. P., Gao Q. Y.: Synthesis of (4-*N,N*-dimethylamine cinnamoylat ethyl) acrylate and its water soluble copolymers and their photochemical property. *Photographic Science and Photochemistry*, **23**, 41–47 (2005).

Characterisation of silicone prepolymers and disparity in results

G. B. Shah*

Applied Chemistry Laboratories (ACL), PINSTECH P. O. Nilore, Islamabad, Pakistan

Received 11 September 2008; accepted in revised form 17 October 2008

Abstract. Liquid hydroxyfunctional polydimethylsiloxanes prepolymers (HOPDMS, Siloprens) with a range of relative molar masses, M_n (25 500–88 000 g/mol) quoted by the supplier have been characterised by a number of techniques such as OH group titration, bulk viscometry, Gel Permeation Chromatography (GPC), and swelling measurements. The resulting molar masses of these prepolymer obtained through these techniques have been compared with one another and that of the values quoted by the manufacturer. Unexpected results of insensitivity of the properties of these prepolymer to the initial molar masses quoted by the suppliers have been observed. It has been found out that these results are dependent upon the type of technique used. The reason for these unexpected results has been discussed in detail and attributed to the multi functionality of the prepolymers, a characteristic not previously suspected or reported.

Keywords: material testing, prepolymers, viscosity average molecular weight, number average molecular weight, molecular weight between crosslinks

1. Introduction

Polymers and prepolymers are usually characterised with a wide range of techniques. These techniques range from molecular weight determination to analytical methods. The molecular weight of a polymer or prepolymer quoted in a different form is dependent upon the techniques used for its determination. Among them the most likely quoted are the number average molecular weight (M_n) and weight average molecular weight (M_w) while a third type of molecular weight referred occasionally is designated as z-average molar mass (M_z).

Usually M_w is greater than the M_n except for an ideal system where uniform molar mass ($M_w = M_n$) is concerned. This difference in the values of M_w and M_z leads to the spread of molar masses i.e. dispersivity ($M_w/M_n > 1$). It is an established fact that M_w is sensitive to high molar masses while the M_n

is affected more with the lower molecular weight. There are quite a large number of methods [1] for determining the average molar mass of a polymer but relatively few for investigating the distribution of that molar mass. The knowledge of the poly dispersivity of a polymer is important to understand the variation in its processing conditions [2–4] and subsequently help in tailoring it according to the requirements.

In the present study liquid hydroxyfunctional polydimethylsiloxane prepolymers having different molar masses (quoted by the manufacturers) were characterised with different techniques and the respective results are compared with one another. The poly dispersivity of the polymer with respect to different techniques has been discussed.

*Corresponding author, e-mail: gbshah.gul@gmail.com
© BME-PT and GTE

2. Experimental part

2.1. Materials

The liquid hydroxyfunctional polydimethylsiloxanes (HOPDMS) prepolymers used were Silopren C1, C2, C5, C18, and C50 supplied by Bayer Ltd. Their respective molecular weights (relative molar masses) (M_n [g/mol]) quoted by the manufacturer [5] were 25 500 (C1), 34 500 (C2), 47 500 (C5), 67 000 (C18) and 88 000 (C50). A rather low molecular weight silicone prepolymer (P100) of viscosity 100 mPa·s supplied by Petrarch Ltd. was also used. The catalyst, dioctyltinmaleate (DOTM) (LT195, M.W 459), was supplied by Lankro Ltd. and the crosslinker vinyltris(ethoxymethoxy)silane (VTEMS A172, M.W 280.4) Union Carbide Ltd., Lithium aluminum dibutylamide was obtained from Lancaster Synthesis Ltd. as 0.16M solution in dimethoxyethane and was diluted to 0.1M before use as a titrant. Gold label anhydrous tetrahydrofuran (THF), 2-naphthol (99 percent pure) and phenylazodiphenylamine were obtained from Aldrich Chemical Co. Analar benzene and anhydrous dimethoxyethane from BDH Ltd. Barium oxide used as a drying agent was obtained from Hopkin and Williams Ltd.

2.2. Hydroxyl (OH) group determination of the prepolymers by titration

Hydroxyl groups determination in silicone prepolymers has been carried out through titration according to an established analytical procedure [6, 7]. About 25 ml of dry THF were placed in a dry 50 ml widemouth conical flask which contained a Teflon covered magnetic stirring bar. A few drops of 0.1 percent (w/v) solution of 4-phenylazodiphenylamine in benzene (indicator solution) were added and the flask was sealed with a rubber septum. A

slow stream of nitrogen dried by prior passage through a tube containing anhydrous CaSO_4 was passed through the flask via a needle through the rubber septum. The magnetic stirrer was started and the hydroxyl groups present were titrated with 0.1M solution of lithium aluminum di-n-butylamine in dimethoxyethane until the colour of the solution changed from yellow to red purple and persisted for 30 sec. Then an accurately weighed sample of the prepolymer (0.3–0.5 g) was syringed into the flask. The titrant was injected drop by drop into the flask via the rubber septum from a one ml syringe graduated in 0.01 ml until the yellow to purple colour change persisted. The weight and volume of the titrant used for titration was noted. The concentration of OH groups was calculated using Equation (1) [6, 7]:

$$\% \text{OH} = \frac{V \cdot 0.017}{W_1} \cdot 100 \quad (1)$$

V in the above equation is the volume [ml] and W_1 the weight [g] of the prepolymer used. The titrant was standardised with dry 2-naphthol (stored over barium oxide) using the above mentioned procedure and the normality (N) of the titrant used was calculated as (Equation (2)):

$$N = \frac{11.8 \cdot W_2}{V \cdot 0.017 \cdot 100} \quad (2)$$

where 11.8 is the %OH group in 2-naphthol and W_2 is the weight [g] of 2-naphthol.

The determinations of moisture content in the various prepolymers were carried out using the Karl Fischer method. The moisture content, converted to OH equivalence ($2\text{OH}/\text{HO} = 1.89$), was subtracted from the total amount of OH groups determined for correction. The titration for each sample was

Table 1. Characterisation data of silicone prepolymers

Prepolymers	M_n (quoted) [5]	M_n from viscometry measurements		GPC Analysis		OH Group determination		\bar{M}_c from swelling measurements
		Barry [13]	Wacker [15]	M_n	M_w	%OH	M_n assuming HOPDMS bifunctional on %OH	
P100	25 000	4 339	7 145	–	–	1.094	2 953	2 250
C1	26 714	31 556	19 967	20 010	58 000	0.162	19 938	8 500
C2	35 850	40 846	25 004	17 130	74 880	0.139	22 014	8 600
C5	49 984	55 407	33 957	27 960	99 130	0.138	23 406	9 000
C18	73 673	74 232	47 749	36 700	133 400	0.105	30 762	11 500
C50	88 000	93 296	64 670	45 161	179 250	0.085	38 000	12 000

repeated three times and the average of these as the %OH groups in the prepolymer chains are given in seventh column of the Table 1.

2.3. Viscosity measurements of prepolymers

The viscosity measurements of the silicone prepolymers were carried out by Haake Rotovisco viscometer. About 10 ml of prepolymer to be tested was poured into the sample cavity to fill to the inside mark. The sample cell was screwed up slowly to the bob. The gear lever was then engaged allowing different speed factors ranging 162–1 corresponding to a shear rate of 2.7–441/sec. The corresponding viscosities (in mPa·s) were then calculated.

2.4. Swelling measurements of crosslinked samples

For swelling measurements, each prepolymer has been cured with various amounts of crosslinker and the \bar{M}_c determined for each cure according to the Flory-Rehner equation (Equation (3)) [8]:

$$\bar{M}_c = \frac{-F_f \rho V_1 v_r^{2/3} v_2^{1/3}}{\ln(1-v_2) + v_2 + \chi v_2^2} \quad (3)$$

where F_f is a factor characterizing the extent to which the deformation in swelling approaches to affine limits. The details of the theoretical values of F_f and that of its use as F_3 in the present case can be found in the previous reports [1, 9, 11–13]. V_1 represents the molar volume of cyclohexane (105.87), v_r is the volume fraction of polymer incorporated into the network (0.95), v_2 the volume fraction of polymer. χ is the cyclohexane polymer interaction parameter (0.42). ρ is the density of the polymer (0.95).

The \bar{M}_c limiting value for each prepolymer was obtained at the inflection point (from which onward the \bar{M}_c values tends to become constant) from the respective plot of \bar{M}_c vs. percent of crosslinker used for curing of that particular prepolymer. The measurement of for C5, using this procedure is given as an example in the form of Figure 1. The detailed procedure for \bar{M}_c measurement is reported previously [9].

2.5. Gel permeation chromatography (GPC)

The gel permeation chromatography for all the prepolymers was carried out by using Shimadzu GPC calibrated with polystyrene standards. The columns used were Shimpack GPC-804, 802 and 802 having dimensions as 8.0 mm i.d. × 30 cm each. The operation temperature was 40°C. Tetrahydrofuran was used as eluent and elution rate was set at 0.5 ml/min. The detection was carried out by refractive index detector.

3. Results

3.1. Characterisation of prepolymers

Table 1 shows some molar masses characterisation data for the HOPDMS prepolymers used in this study. The number average molecular weights (M_n) quoted by the manufacturer [5] are given in the second column. The physical techniques used for determining the molecular weights were bulk viscosity measurements (column 3 and 4), gel permeation chromatography (GPC) analysis (column 5 and 6) and swelling measurement (column 9). The number average molecular weights (M_n) were calculated from the measured viscosities in mPa·s (at a shear rate 24.5 sec) from the following two calibration formulae (Equations (4) and (5)) [14, 15]:

$$\log \eta = 1 + 0.0123 M_n^{0.5} \quad (4)$$

$$\log \eta = 3.08 \cdot \log M_n - 10.06 \quad (5)$$

where η – bulk viscosity of silicone fluid in centi stokes, M_n – number average molecular weight, m – molecular weight of the repeating unit (74) for PDMS.

Equation (4) is the Flory relationship [16] for melt viscosities confirmed for bulk viscosities of Polysiloxanes by Barry [14].

The Equation (5) is an empirical equation developed by Wacker-Chemie GmbH which is claimed [15] to give ‘best fit’ relation between melt viscosity and number average molecular weight.

The fifth column gives the number average molecular weights (M_n) and the sixth column provides weight average molecular weights (M_w) determined from the GPC analysis. The polydispersity ranges from about 3 for C1 up to 4 for C50. The OH groups present in the polymer chain were measured by titrating the prepolymer with lithium aluminum

n-butylamide. The percentage of water present in the prepolymer was measured by the Karl Fisher method and for correction subtracted from the total OH groups. The %OH groups for the corresponding prepolymers can be seen in the seventh column of the Table 1. If it is assumed that all the prepolymers are bifunctional, the molecular weights (M_n) based on the experimentally determined values of %OH have been calculated (column 8) using Equation (6):

$$M_n = \frac{34 \cdot 100}{\%OH} \left[\frac{100 - \%cyclics}{100} \right] \quad (6)$$

where %cyclics are percentage of soluble siloxanes that ranges from D_3 to D_8 . The sol fraction for each weighed sample was obtained by extraction with cyclohexane. The weighed samples were put in cyclohexane for 15 days. During this period the solvent was changed once to facilitate the extraction of soluble materials. After removing the solvent, the specimens were dried to constant weight under vacuum at room temperature. The sol fraction for each sample was calculated. The values of sol fraction (about 5% for all the Siloprenes except that for C2 where it was 10%) obtained from each fully cured prepolymer network were used as %cyclics in Equation (6).

The limiting values of \bar{M}_c obtained from the swelling measurements for each prepolymers are provided in the ninth column. These \bar{M}_c values represent the molecular weight between successive junctions when all the OH groups have satisfactorily reacted. The \bar{M}_c value have been obtained at the inflection points (from which onward the \bar{M}_c values tends to become constant) from the plot of

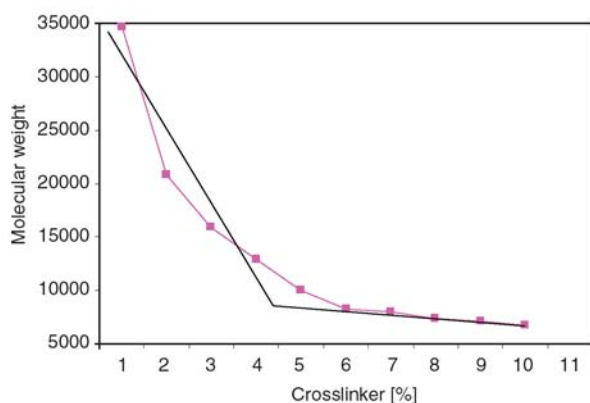


Figure 1. Variation of molecular weight between junctions for C5 with % crosslinker

\bar{M}_c values vs. percent of crosslinker used for curing the corresponding prepolymer. The \bar{M}_c determination at the inflection point for C5 is shown in Figure 1. The limiting values for Wacker prepolymer (viscosity 50 Pa·s) networks obtained as above from swelling measurements were found to be the same as that of for \bar{M}_c the C50 networks.

Comparing the molecular weights, it is clear that M_n values from the viscosity calibration Equation (4) approximate to the Bayer quoted values for M_n . The M_n values from GPC though consistent with that obtained from the OH determination differed not only from the quoted values but also from \bar{M}_c . All the values of M_n were much higher than the corresponding \bar{M}_c and for the prepolymers used (C1–C50) in this study, the differences ranged 3–7 folds.

4. Discussion

4.1. Difficulties in characterisation of prepolymers

The paucity of OH groups on the polymer chains and the nature of spectroscopic methods such as IR (infrared) and NMR (nuclear magnetic resonance) have made it difficult to characterise the prepolymers used in this study by this technique. The results of characterisation of prepolymers by methods such as GPC, OH group titration, bulk viscosity and swelling measurements with the exception of viscosity measurements do not agree with the manufacturer's quoted number average molecular weights (Table 1).

The dissimilarity between the various M_n values determined for the prepolymers used can be attributed to: the diverse nature, sensitivity, accuracy and limitation of the different experimental techniques used. The GPC separates molecules according to their effective size; it may not adequately distinguish between branched and linear polymers of the same molecular weight [17]. With the HOPDMS analysis the pendant OH group present along the chain will presumably make it impossible for the GPC to differentiate this chain from that of a linear chain without this group. The OH group titration gives the number of functional groups per specific amount of polymer or prepolymer without any indication about their molecular weight distribution. For linear polymer, it is possible to assume that the total number of chain ends is twice the number of

polymer molecules. However if branching exist, then this assumption gives erroneous results in respect of estimating the number average molar mass.

The viscosity measurements for all the prepolymers were carried out at different shear rate range of 2.7–441/sec. During these measurements, each of the materials behaved almost like Newtonian fluid. However, the molecular weights for each material was calculated for the viscosities determined at on shear rate i.e. 24.5/sec so that comparison can be made between them. The melt viscosity though used for M_n determination is also sensitive to weight average molecular weight [17]. The different M_n for each prepolymer (Table 1) obtained using independent viscosity calibration equations reflects the uncertainty relating melt viscosity to the number average molecular weight. Thus the results of the molecular weight determination through these different techniques would not be expected to be consistent. The similarity of the quoted [5] M_n and that calculated through viscosity measurement (using Equation (4)) when compared with that from the other techniques showed disparities. It is likely that the quoted number average molecular weights are in fact the average molecular weights obtained through viscosity measurements (using Equation (4)); they therefore are misleading. The manufacturer's information seemed to imply that the prepolymer samples were essentially terminally bifunctional in OH and moreover search of the published literature never revealed any reference to multifunctionality in this type of silicone prepolymers. The \bar{M}_c values of the silicone polymer networks crosslinked with low amounts of crosslinker or catalyst were somewhat near to the M_n from the GPC analysis and OH group titration. However, as reported [9, 10, 18], these networks

are partially cured and so these values represent the networks where the OH groups have not sufficiently reacted.

Stoichiometric amounts of crosslinker calculated on the basis of molar masses of the prepolymers assuming bifunctionality, does not cure the material. On the other hand the stoichiometric amounts of crosslinker calculated on the \bar{M}_c basis corresponding theoretically to the point where all the OH groups have reacted gives fully cured polymer networks. Comparing the values of \bar{M}_c (Table 1) for each prepolymer network, it is surprising that with the exception of P100 they vary so little, bearing in mind the large variation in molecular weight of the silicones from which they were prepared. The values of M_n obtained through OH determination which is comparatively smaller than the Bayer quoted values support this view. If the prepolymers were strictly bifunctional, the M_n from the OH determination should have been equal to the quoted number average molecular weights. In fact, the molecular weights determined from the OH determinations are in agreement with the values from GPC but are higher than the \bar{M}_c .

In order to determine the number of functional groups per chain, each molecular weight (M_n) in turn was divided by the \bar{M}_c values. This data is presented in Table 2. Assuming the OH group titration and the \bar{M}_c data on the materials reliable, the functionality of the prepolymer was calculated as $(M_n/\bar{M}_c)+1$. These values are given in the last column of the Table 2. The number of functional groups calculated in this way for all the silicone prepolymer (last column of Table 2) suggests that irrespective of the prepolymer the ratio of the OH groups per unit chain length is approximately constant.

Table 2. Molecular weight of various prepolymers in multiple of M_c

Prepolymers	M_n (quoted) [5]	M_n from viscometry measurements		GPC analysis		M_n from %OH	\bar{M}_c	Functionalities* (M_n/\bar{M}_c)+1
		Barry [13]	Wacker [15]	M_n	M_w			
P100	–	1.930	3.175	–	–	1.38	2 250	2.31
C1	3.14	3.712	2.349	2.35	6.824	2.47	8 500	3.35
C2	4.17	4.750	2.907	1.99	8.707	2.84	8 600	3.56
C5	5.55	6.156	3.773	3.11	11.01	2.74	9 000	3.60
C18	6.41	6.455	4.152	3.19	11.6	2.82	11 500	3.67
C50	7.33	7.775	5.389	3.76	14.94	3.33	12 000	4.17

*Based on the OH titration (M_n) and \bar{M}_c

5. Conclusions

In view of the method of preparation of the silicone prepolymer from chloro silanes and the difficulty of separating dichloro and trichloro silanes due to the close boiling points i.e. 70, 66°C, it follows that the preparation of solely linear hydroxy terminated bifunctional PDMS is unlikely and that irrespective of the molecular weight of the prepolymers the number of silanol groups per unit chain length may not differ significantly. For example, the presence of one mole of trichlorodimethylsilane during the preparation of polydimethylsiloxanes will decrease the degree of polymerisation to only 200 on the completion of reaction [19] and the resulting polymer will have pendant groups or branching.

The unexpected result was the insensitivity of the properties to the initial molar mass of the polymers from which the networks was derived. The reason for this was the multifunctionality of the prepolymers, a characteristic not previously suspected or reported.

Whilst there is this molecular uncertainty it is the \bar{M}_c values which represent the actual structure of the cured silicone elastomers and which dictate the properties of the polymer network under stress conditions. It is for this reason that the respective \bar{M}_c values must be used for the interpretation of the results of any mechanical properties of the polymer networks.

References

- [1] Wake W. C., Tidd B. K., Loadman M. J. R.: Analysis of rubbers and rubber-like polymers. Applied Science Publishers, London (1983).
- [2] Baijal M. D.: Application of metallic membrane filters in the clarification of styrene-butadiene rubber solutions for gel permeation chromatography. Analytical Chemistry, **44**, 1337–1338 (1972).
- [3] Barrere M., Ganachaud F., Bendejacq D., Dourges M. A., Maitre C., Henery P.: Anionic polymerization of octamethylcyclotetrasiloxane in miniemulsion. II Molar masses analyses and mechanism scheme. Polymer, **42**, 7239–7246 (2001).
- [4] Kazmierski K., Hurduc N., Sauvet G., Chojnowski J.: Polysiloxanes with chlorobenzyl groups as precursors of new organic-silicone materials. Journal of Polymer Science Part A: Polymer Chemistry, **42**, 1682–1692 (2004).
- [5] Product brochure of Bayer. Bayer AG, Germany (1983).
- [6] Kellum G. E., Uglum K. L.: Lithium aluminum dibutylamide as a direct acidbase titrant for determination of silanols. Analytical Chemistry, **39**, 1623–1627 (1967).
- [7] Smith A. L.: Analysis of silicones. Wiley, New York (1974).
- [8] Flory P. J., Erman B.: Theory of elasticity of polymer networks. 3. Macromolecules, **15**, 800–806 (1982).
- [9] Shah G. B., Winter W.: Effect of bimodality on tear properties of silicone networks. Macromolecular Chemistry and Physics, **197**, 2201–2208 (1996).
- [10] Shah G. B.: Aspects of the polycondensation of hydroxyfunctional polydimethylsiloxanes. PhD Thesis, UWCC (UK) (1990).
- [11] Flory P. J., Gordon M., McCrum N. G.: Statistical thermodynamics of random networks [and discussion]. Proceedings of the Royal Society of London. Series A, Mathematical and Physical Sciences, **351**, 351–380 (1976).
- [12] Flory P. J.: The elastic free energy of dilation of a network. Macromolecules, **2**, 119–122 (1979).
- [13] Flory P. J.: Theory of elasticity of polymer networks. The effect of local constrain on junctions. Journal of Chemical Physics, **66**, 5720–5729 (1977).
- [14] Barry A. J.: Viscometric investigation of dimethylsiloxane polymer. Journal of Applied Physics, **17**, 1020–1024 (1946).
- [15] Private Communication Wacker-Chemie GmbH: The relationship between molecular weight and bulk viscosity. pp. 1–3, 20th September (1988).
- [16] Flory P. J.: Viscosities of linear polyesters. An exact relationship between viscosity and chain length. Journal of the American Chemical Society, **62**, 1057–1070 (1940).
- [17] White J. R., Campbell D.: Polymer characterisation physical techniques. Chapman and Hall, London (1989).
- [18] Shah G. B.: Bimodality and increased amount of crosslinker enhances tensile properties of silicone networks. e-Polymers, no. 113 (2007).
- [19] Mark H. F., Tobolsky A. V.: Physical chemistry of high polymeric systems. Interscience, New York (1950).